Winter 1-31-2023

Electrochemical Sensors and Biosensors of Biomarkers and Therapeutic Agents Detection

Mahmoud Abdelhakem
mahmoud.ayman@aucegypt.edu

The American University in Cairo
الجامعة الأمريكية بالقاهرة

Graduate Studies

Electrochemical Sensors and Biosensors of Biomarkers and Therapeutic Agents Detection

A Thesis Submitted by

Mahmoud Ayman Saleh Abdelhakem

to the

Nanotechnology Program

2022-08-23

in partial fulfillment of the requirements for the degree of Master's of Nanotechnology

Declaration of Authorship

I, Mahmoud Abdelhakem, declare that this thesis titled, "Electrochemical Sensors and Biosensors of Biomarkers and Therapeutic Agents Detection" and the work presented in it are my own. I confirm that:

- This work was done wholly or mainly while in candidature for a research degree at this University.
- Where any part of this thesis has previously been submitted for a degree or any other qualification at this University or any other institution, this has been clearly stated.
- Where I have consulted the published work of others, this is always clearly attributed.
- Where I have quoted from the work of others, the source is always given. With the exception of such quotations, this thesis is entirely my own work.
- I have acknowledged all main sources of help.
- Where the thesis is based on work done by myself jointly with others, I have made clearexactly what was done by others and what I have contributed myself.

Signed:

Mahmoud Ayman Saleh Abdelhakem

Date:

2022-08-08

Abstract

Electrochemical sensing is a pioneering tool amongst all other sensing techniques even though it had been started in early 20th century. Due to their cost efficacy, accuracy, and real-time measurement, electrochemical sensing has been utilized in a vast of biomedical applications in therapeutic drug monitoring and biomarker detection. This thesis work concerned the monitoring of three therapeutic agents in spiked plasma, urine, dosage form, and interstitial skin fluid with high specificity and accuracy. Two of our sensing platforms utilized nanomaterials for sensing (sensors) of Cilostazol and Velpatasvir utilizing α-MnO_2-V_2O_5 (metal oxide nanorods) and NH_2-MIL-53 (Aluminum-based metal organic frameworks), respectively. Nanomaterial-based sensors are optimal for electrochemically active therapeutic agents due to their cost-effectiveness and non-laborious preparation, which was the case for Cilostazol and Velpatasvir. However, for vancomycin that is electrochemically inactive and has very high priority to be monitored due to its efficacy against methicillin resistant *Staphylococcus Aureus* and its high toxicity, an advanced level of biosensor was utilized for its detection that is minimally invasive. Aptamers have been utilized due to their low cost of preparation compared to other biorecognition molecules, and their capability to generate signal upon binding to the target molecule that is associated to the attached methylene blue to its 3' end. All of our sensors possessed a wide range of linearity, high reproducibility, high sensitivity, and low limit of detection.

Acknowledgement

My appreciation for my Advisor, Prof. Nageh Allam, for his guidance, patience, and feedback, which are beyond words. I could not have made this journey without his provided generous knowledge and experience. Additionally, without the kind funding provided by the American University in Cairo and University of Waterloo, these projects would not have been possible.

I also appreciate the support of my host professor at the University of Waterloo, Dr. Mahla Poudineh. Also deserving of praise are my lab mates in both universities who have influenced and inspired me.

I should not forget to mention my family, particularly my parents. Their confidence in me has sustained my motivation and upbeat attitude throughout this process. I also want to dedicate my thesis to my deceased sibling, Ahmad, for the good time we spent together.

List of Contents

List of Figures

List of Abbreviations

List of Tables

List of Equations

Chapter 1 Introduction

1.1 Therapeutic drug monitoring as a challenge

Therapeutic drug monitoring (TDM) could be defined as the measurement of drug levels in body fluids for the purpose of improving the prescribing procedures in case of adequate medical interpretation[1–3]. Another definition that can be found in the literature is that TDM is defined as the individualization of drug administration to maintain constant levels of drug concentration in plasma within the therapeutic window of the intended drug[3,4]. The main purpose of TDM has been to maximize the efficacy and safety of a particular therapeutic agent by utilizing the knowledge of pharmaceutics, pharmacokinetics, and pharmacodynamics[4–8]. This is considered as an enormous step toward the individualization of drug regimens in order to maximize the patient benefit through personalized dosing[9].

TDM concept emerged in the 1960s in a clinical study that showed that there is a correlation between plasma concentration of phenytoin in several epileptic patients with seizure control and drug toxicity[10]. In 1967, Baastrup and Schou have made a clinical study showing the levels of lithium in plasma of psychotic patients and psychosis management[11]. Then in the 70s, there were many papers focusing on the effect of plasma levels of drugs on the incidence of toxicity and determining the therapeutic ranges of drugs in plasma[12]. Afterward, TDM has been used for many purposes to maximize the therapeutic efficacy of treatment through assessing the plasma level of the drug while minimizing its adverse effects since plasma level is a better indicator for the kinetic profile of the drug better than monitoring dosage[13]. The reasons why monitoring plasma levels of a drug is better than monitoring dosage include[13]

1- Better correlation exists between the therapeutic effect of a drug and plasma level than between dosage and effect.

2- Pharmacokinetic parameters can be thoroughly understood from the monitoring of plasma levels of drugs, including absorption (bioavailability), distribution, metabolism and excretion that differ from person to person and from ethnicity to ethnicity.

3- The development of reliable and easy to use drug monitoring assays (sensors).

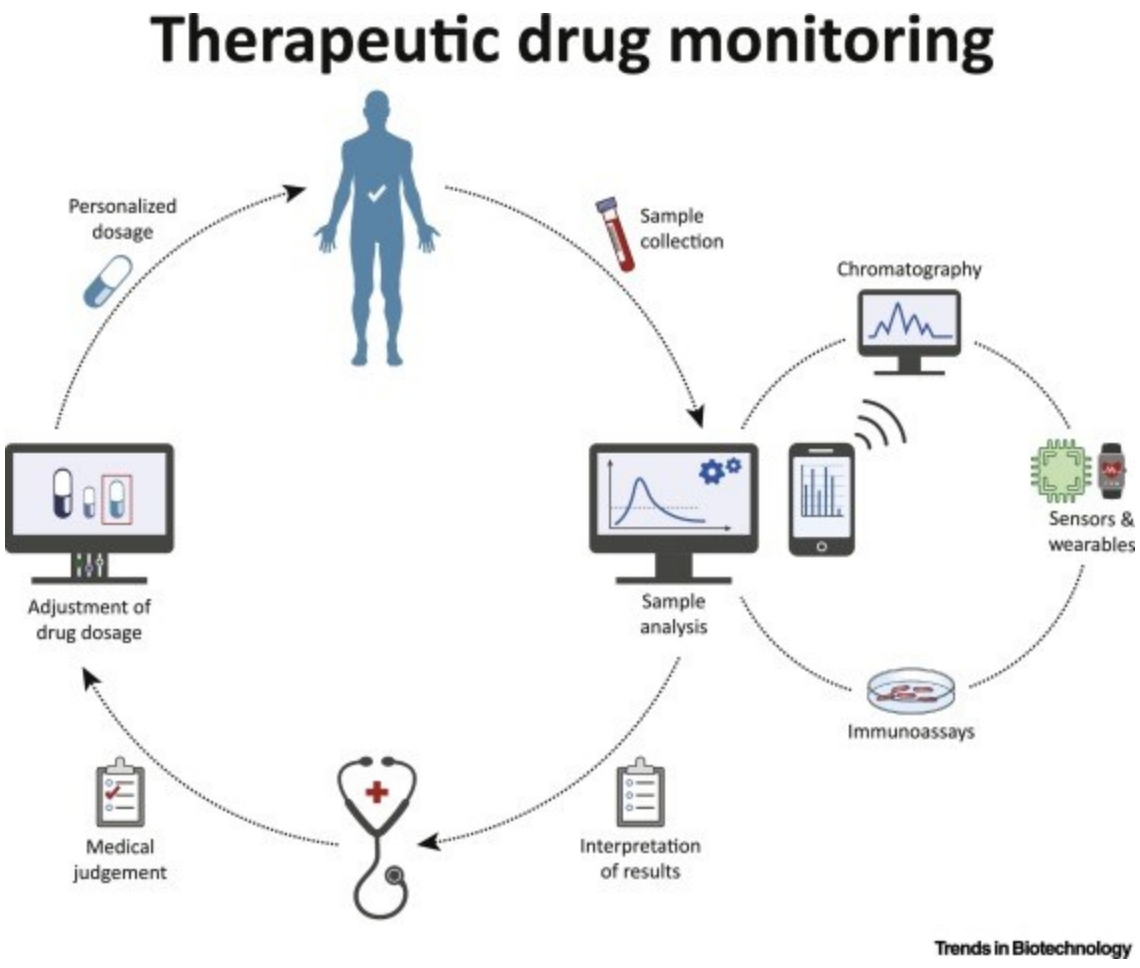

Figure 1.1 Graphic illustration of the means of therapeutic drug monitoring and its role in the medical decisions[14]

1.2 Biomarkers monitoring as another challenge

The term biomarker is short for "biological marker" that can be defined as cellular, biochemical, and molecular compound (that includes genetic and epigenetic) that can be measured in various systems in the body, including cells, tissues and/or body fluids[15]. Henceforth, according to this definition, diagnosis of these biomarkers is indeed an important step in the clinical and biomedical field as they are considered as signs of normal or abnormal body activity [15]. It can be also referred to medical sigs or symptoms that that can indicate a medical condition, which can be measured precisely and reproducibly[16]. The term of biomarker has emerged in the 70s of the last century when there were many debates about the usage of biomarkers to predict the prognoses in a major trial of terminal diseases, including cancer and cardiovascular disease[17]. The levels of a biomarker in biological systems varies constantly with the levels of the activity or progression degree of the disease, as usually the biomarker is an intermediate component of molecular or cellular pathway that is involved in a biological process[16].

1.3 Electrochemical sensors as a solution

Sensors are devices that measure biological and chemical reactions through inducing a signal that is proportional to the analyte concentration in the redox reaction. They are involved in pivotal applications, including detection and monitoring of diseases, drug monitoring, detection of pollutants, detection of micro-organisms, and detection of biomarkers in body fluids (blood, urine, saliva and sweat)[18]. As shown in Figure 1.2, the components of biosensors are illustrated and they are[18]:

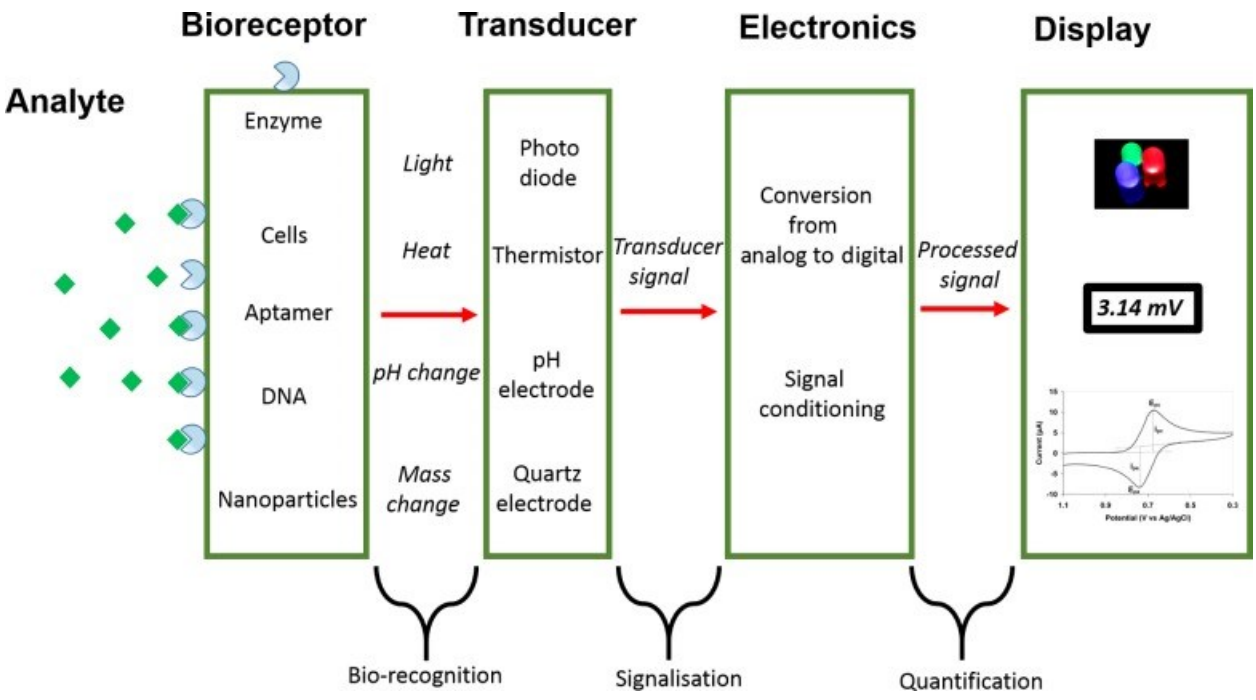

Figure 1.2 Illustration of the sensor components [18]

a- Analyte: the substrate of interest that needs to be detected.

b- Bioreceptor (only in biosensors): the biomolecule that specifically recognises the analyte of interest and also is known as the bioreceptor, this includes antibodies, enzymes and aptamers. The process of the bioreceptor binding to the analyte is called biorecognition.

c- Transducer: the transducer is the element that produces energy upon biorecognition. This energy can be measured optically or electrically, and this signal is proportional to the amount of analyte bound to the bioreceptor.

d- Display: the display is a system that can generate signals or numbers that can be interpreted by the analyst. Usually, it is a combination of hardware and software that generates the results in a user-friendly way.

The history of sensors can be traced back to 1906 when M. Cremer proved that there is a proportional link between the concentration of the acid in a liquid and the potential that is obtained from the other side of a glass membrane[19]. Then, the concept of pH was introduced in 1909 by Sorensen et al. ant the first pH electrode sensor was invented by Hughes et al. in 1922[20]. Then, the first immobilization of the invertase enzyme on aluminum hydroxide and charcoal substrate was done by Griffin and Nelson between 1909 and 1922[21,22]. Afterward, the first biosensor that looked like the sensors that we know nowadays was developed in 1956 that detects oxygen depletion by C. Clark et al[23]. Clark electrode that was the reason that Clark was renown of the father of biosensors. This was followed by his development of the first amperometric enzyme sensor[23] for the detection of glucose in 1962 that was followed by the development of a potentiometric sensor for urea detection by Guilbault *et al.* in 1969[24]. Then the first sensor that was released to market was developed by Yellow Spring Instruments in 1975 and since then the field of sensors became the point of interest for many laboratories so that only between 2005 and 2015 there were over 84000 reports indexed under the topic of biosensors[18].

1. Characteristics of a sensor

In order to have an optimized sensor system, some properties have to be possessed by the sensor system including [18]:

a- **Selectivity**: it is considered to be the most pivotal property of a sensor system. It can be defined as the ability to detect the analyte of interest in the presence of other admixtures and contaminants. Biosensors are considered better than sensors in this point since the, for example, antigen-antibody reaction is so specific that it only happens between the immobilized antibody and the specific antigen.

b- **Reproducibility**: it is the capability of a biosensor to provide the same response for the same experimental set-up. Usually, it is linked to the precision and accuracy of the signal transducer and the electronics part of the sensor where precision is the capability of the sensor to provide the same result in every measurement, and accuracy if the capability to provide a mean value that is close to the true value when multi-measuring a sample. Hence, reproducibility is the reliability and robustness of the sensor to any interferent.

c- Stability: it refers to how susceptible it is to environmental disturbances around the biosensing system. A biosensor under measurement may experience a drift in its output signals as a result of these disruptions. This may result in a concentration measurement inaccuracy and compromise the biosensor's precision and accuracy. In applications where a biosensor needs lengthy incubation periods or ongoing monitoring, stability is the most important component to rely on. Sometimes the reaction of electronics and transducers may be temperature-sensitive, which could affect a biosensor's stability. To achieve a steady response from the sensor, proper tuning of the electronics is necessary. The degree to which the analyte attaches to the bioreceptor—the affinity of the bioreceptor—can also have an impact on stability. High affinity bioreceptors promote the analyst's covalent or strong electrostatic connection, which -in turn- strengthens a biosensor's stability. The degradation of the bioreceptor over time is another element that has an impact on a measurement's stability.

d- Sensitivity: The limit of detection (LOD) or sensitivity of a biosensor is the lowest concentration of analyte that it can detect. A sensor is necessary in a number of medical and environmental monitoring applications to confirm the existence of traces of analytes in a sample at analyte concentrations as low as ng/ml or even fg/ml. For instance, prostate cancer is linked to blood levels of the prostate-specific antigen (PSA) of 4 ng/ml, for which doctors

recommend biopsy procedures. As a result, sensitivity is thought to be a key characteristic of a biosensor.

e- **Linearity**: In a mathematical equation, y=mc, where c is the analyte concentration, y is the output signal, and m is the sensitivity of the biosensor, linearity is the property that demonstrates the accuracy of the measured response to a straight line for a set of measurements with various analyte concentrations. The resolution of the biosensor and the range of analyte concentrations under test can both affect the biosensor's linearity. The smallest change in an analyte's concentration necessary to cause a change in the biosensor's response is known as the resolution of the biosensor. A good resolution may be needed depending on the application, as the majority of sensor applications need not only analyte detection but also monitoring of analyte concentrations over a broad operating range. The range of analyte concentrations for which the biosensor response alters linearly with the concentration is referred to as the "linear range," which is another phrase related to linearity.

1.4 Transdermal biosensing utilizing polymeric microneedles

Transdermal biosensing analyzes interstitial fluid (ISF), the fluid found underneath of skin and in the spaces around cells and has been introduced as an ideal candidate for non- or minimally invasive biosensing[25]. Compared to other peripheral biofluids like saliva, sweat, and tears, interstitial fluid (ISF) is notably rich in soluble bioanalytes such proteins, peptides, metabolites, and nucleic acids and demonstrates a strong correlation with blood[26–30]. The absence of clotting factors in ISF also allows for prolonged continuous measurements[31]. Various non- and minimally invasive methods have been used for ISF extraction, including suction blisters, reverse iontophoresis, microdialysis, ultrasound, and microneedles (MNs)[31]. Among these approaches, MN-assisted ISF extraction has recently garnered considerable attention because of its simplicity

of use and the potential to integrate diagnostics [31]. MN arrays physically penetrate through the stratum corneum to access and extract the ISF [31]. Different types of MNs have been fabricated for ISF extraction, for example, porous MNs employ capillary force; hollow MNs extract ISF based on negative pressure, and hydrogel-based MNs (HMNs) employ material absorption property [31].

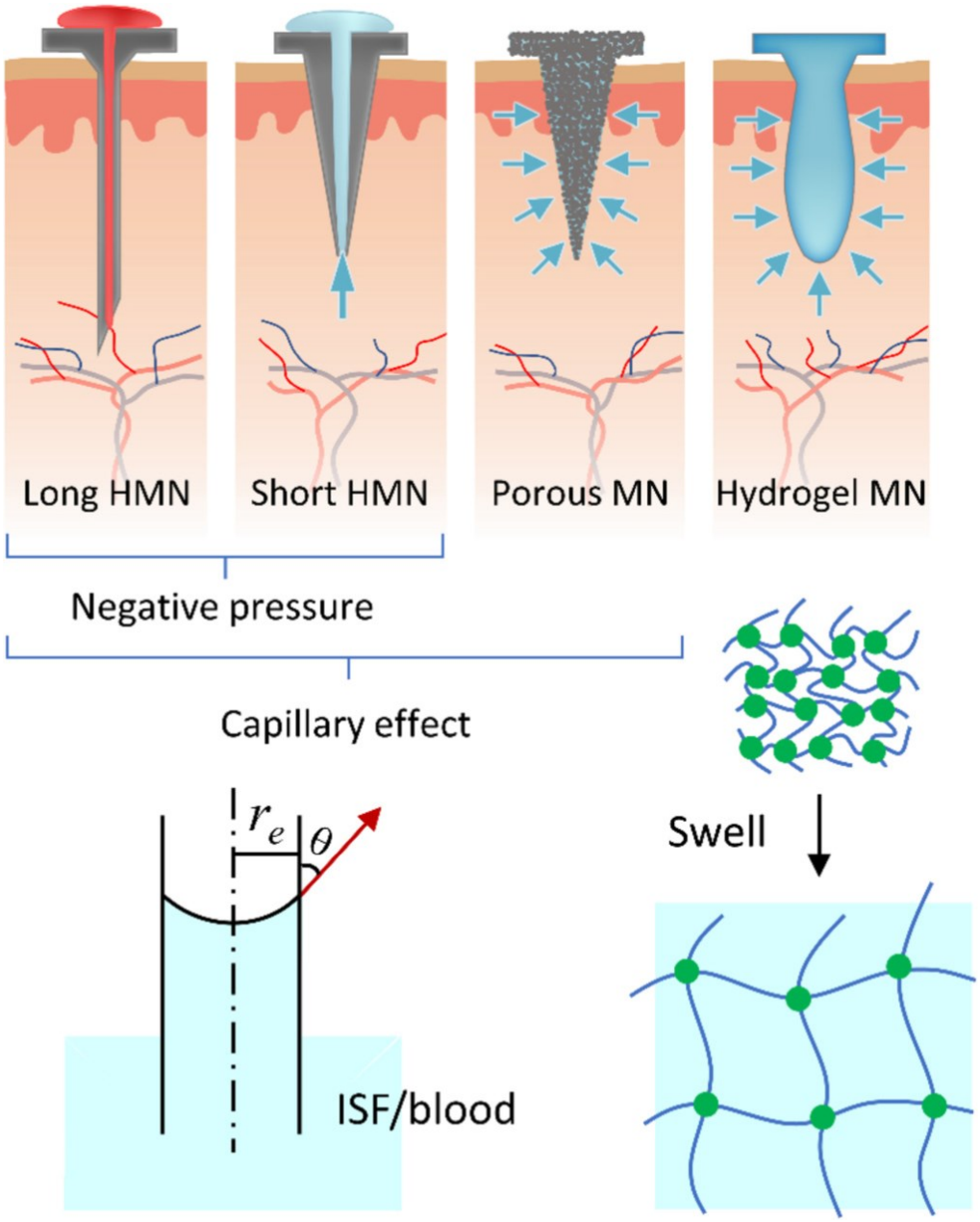

Figure 1.3 Various types of microneedles utilized in transdermal sensing[32]

MN-based biosensors have been also developed for on-needle detection of specific target analytes. These assays utilize solid and coated MNs that act as the device electrodes for electrochemical measurement. Recently, gold MNs functionalized with aptamer probes have been reported for the measurement of therapeutic drugs[33]. Although using aptamer probes has expanded the capability of on-needle sensing beyond redox active analytes, the use of solid metal MN creates biocompatibility issues with the electrodes as well as their fabrication process is complicated and costly. Additionally, they cannot extract fluids, which limits their capability for sensing low abundance target molecules. Off-needle MN biosensors directly extract ISF for post-processing and analysis. A major disadvantage of these systems is the need for multiple extractions for enabling serial and/or semi-continuous measurements. In these applications, hollow MNs are used to extract ISF with low extraction volume, limited biocompatibility, and a potential risk of MN clogging due to tissue curing[34]. HMNs are a viable alternative to hollow needles with the capability to extract a higher volume of ISF into their swellable matrix[35]. The transdermal HMN arrays are compact, easy to use, readily accessible, and painless; do not require peripheral accessories; and are expected to improve patient compliance. In addition, their fabrication is simple and inexpensive and does not require complex facilities, thus, overcoming limitation of other MN systems[35]. HMNs have recently shown a great potential for diagnostics where the extracted ISF is used for off-site detection of different analytes[35]. Presently, HMN arrays have been developed for in-situ glucose and pH measurement[36]. To date, HMNs have not been exploited for on-needle, on-site sensing of other clinically relevant biomolecules, such as drug molecules with narrow therapeutic windows.

1.5 Objectives and Scope of the Thesis

This thesis has two main objectives. First, we aim to modify carbon paste electrode (CPE) to enhance the selectivity, sensitivity, stability, reproducibility and linearity of the electrochemical CPE electrodes towards the detection of pharmaceutical therapeutic agents, Cilostazol and Velpatasvir, in plasma, urine, and pharmaceutical dosage forms. For this purpose, we developed two nanomaterials of different types, MnO2-V2O5 and NH2-MIL-53(Al) metal organic framework (MOF).

Second, we aim to produce a wearable electrochemical aptasensor that can detect vancomycin levels in ISF continuously with a minimal invasive way via polymeric microneedles. **Chapter 2:** Provides a background about the electrochemical sensing techniques that can be used for sensing applications.

Chapter 3: Provides a literature review about the utilization of various materials and biomolecule modifications for the detection of biomarkers and pharmaceutical therapeutic agents.

Chapter 4: Provides a literature review about the utilization of various materials and biomolecule modifications for the detection of biomarkers and pharmaceutical therapeutic agents.

Chapter 5: Provides a literature review about the utilization of various materials and biomolecule modifications for the detection of biomarkers and pharmaceutical therapeutic agents.

Chapter 6: Provides a literature review about the utilization of various materials and biomolecule modifications for the detection of biomarkers and pharmaceutical therapeutic agents.

Chapter 2 Scientific background

2.1 Types of biosensors according to signal transduction

According to signal transduction methods, biosensors can be integrated to five categories[37]:

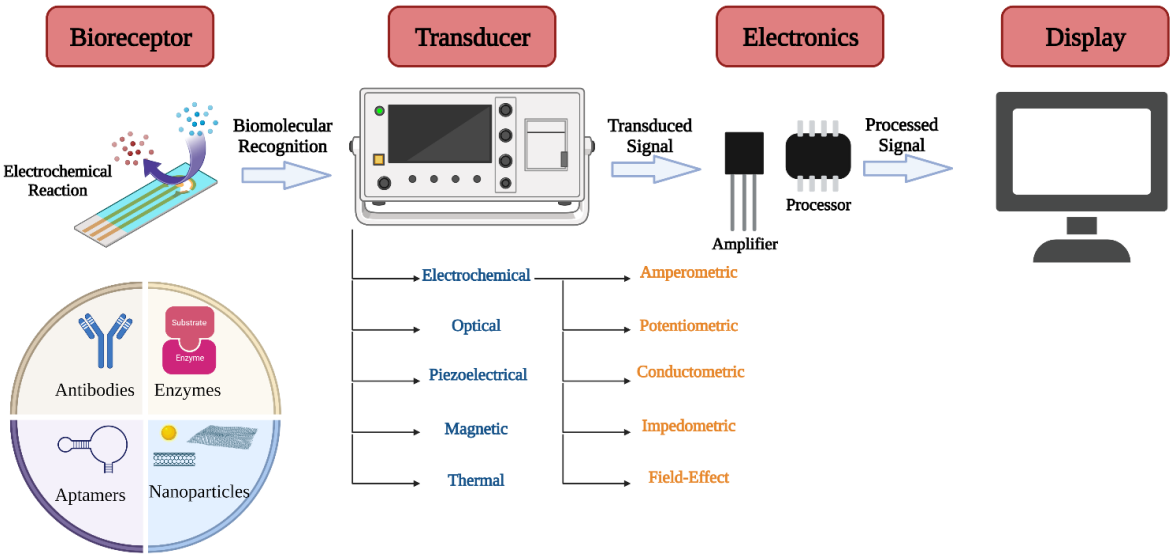

Figure 2.1 Main parts of a biosensor system[38].

1- **Electrochemical sensors:**

The term "electrochemical sensors" refers to a class of very significant sensors whose response is a result of an interaction between electricity and chemistry. The three main categories of electrochemical sensors are conductimetric, potentiometric, and amperometric. The sensors that measure electrical resistance, impedance, or admittance are known as conductimetric ones. The amperometric sensor response pertains to measuring electrical current, whereas the potentiometric sensor response relates to measuring voltage. In essence, a chemical environment is what these sensors react to. Chemical species like gases (O_2, CO, CO_2, H_2S, NO, NO_2, etc.), protons (pH), humidity, or biological amounts like glucose, cholesterol, enzymes, antibodies, proteins, etc. are

examples of typical measurands. It is noteworthy to note that these sensors are frequently referred to as "bio-electrochemical sensors" by academics working in the domains of biology and medicine due to the numerous biological uses for these sensors in humans, animals, and plants[39].

2- **Optical sensors:**

A small analytical instrument called an optical biosensor combines an optical transducer system with a biorecognition sensing element. An optical biosensor's primary goal is to provide a signal that is proportional to the concentration of a material being analysed (analyte). Enzymes, antibodies, antigens, receptors, nucleic acids, entire cells, and tissues can all be used by the optical biosensor as biorecognition components. The interaction of the biorecognition element with the analyte is detected using the evanescent field close to the biosensor surface via optical waveguide interferometry, surface plasmon resonance (SPR), and evanescent wave fluorescence[40].

3- Magnetic sensors

By sensing changes in magnetic characteristics or magnetically induced effects such changes in coil inductance, resistance, or magneto-optical properties, magnetic biosensors use paramagnetic or super-paramagnetic particles, or crystals, as a technique of detecting biological interactions. The particles employed in magnetic biosensors have a diameter that ranges from nanometers to microns and are coated with a bio-receptor such an antibody or nucleic acid strand. The physical characteristics of the particles change when they interact with the target; this could be related to size or movement. Coils, GMR devices, Hall Effect devices, and other optical and imaging techniques are some of the technologies used to detect the particles in a magnetic biosensor. The ability of a magnetic biosensor to manipulate paramagnetic particles in a magnetic field to bring them to a sensor surface where biological interactions take place and enable quick detection of a target accelerates the binding interactions[41].

4- Piezoelectric sensors:

A material's capacity to generate voltage when mechanically stressed is referred to as piezoelectricity or the piezoelectric effect. A sensor component called a piezoelectric platform or piezoelectric crystal operates on the theory that oscillations alter when a mass is bonded to the surface of the piezoelectric crystal[42].

5- Thermal sensors:

Thermometric biosensors take advantage of heat absorption or evolution, which is a fundamental characteristic of biological reactions. The reaction medium's temperature changes as a result of this. The extent of the reaction (for catalysis) or the structural dynamics of the biomolecules in the dissolved state were calculated in previous studies on calorimetry by directly monitoring the change in heat. However, the use of this technology in biosensors resulted in the creation of thermometric apparatus. These primarily gauge variations in fluid temperature that occur after an appropriate substrate reacts with the mounted enzyme molecules[43].

2.2 Electrochemical biosensors

Electrochemical sensors existed over when M. Cremer proved that there is a proportional link between the concentration of the acid in a liquid and the potential that is obtained from the other side of a glass membrane[19] in 1906 (as aforementioned in chapter 1). The most extensively studied and utilised biosensors are electrochemical ones, which operate on the electrochemical characteristics of the analyte and transducer. High levels of sensitivity, selectivity, and detection are displayed by electrochemical biosensors. This biosensor produces detectable electrochemical

signals in the form of voltage, current, impedance, and capacitance as a result of an electrochemical reaction between the bioreceptor and analyte on the transducer surface[38,44,45].

2.3 Electrochemical cell

The electrochemical sensor generates electrical signals like current, voltage, or system conductivity using the electrochemical reaction between the sensitive elements and the detected materials. The linear relationship between the measured substance's concentration and the electrical measured signal is considered to be the main sensing function. One of the most significant varieties of electrochemical sensors is the current-type sensor. The counter electrode, reference electrode, and working electrode detection system form the foundation of the current-type electrochemical sensor, as in Figure 2.1. On the surface of the working electrode, a redox reaction occurs between the substance being tested and the sensitive material that results in changing the current[46].

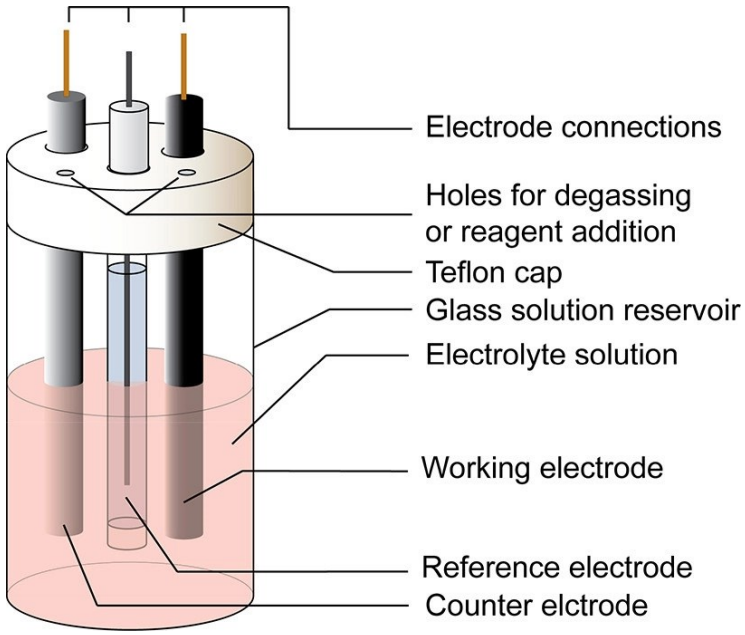

Figure 2.2 The components of an electrochemical cell[47]

2.4 Electrochemical sensing technique

In (bio-)electrochemistry, the reaction under study would typically either produce a measurably large current (amperometric), a measurably small potential or charge accumulation (potentiometric), or noticeably small change in the conductivity of a material between electrodes (conductometric)[48]. Other electrochemical detection methods are also mentioned, including impedimetric (which measures impedance, including resistance and reactance) [49,50]and field-effect[51], which use transistor technology to measure current as a result of a potentiometric effect at a gate electrode. Here, all of these measurement methods will be discussed, along with a few literature sources that use versions of these methods.

1. Amperometric sensors:

An electrochemical sensor can be called an amperometric device when it continuously measures the current produced by the oxidation or reduction of an electroactive species during a biochemical reaction[52]. The simplest amperometric biosensors, in which a current is generated in proportion to the oxygen concentration, is considered to be Clark oxygen electrodes. The reduction of oxygen at a platinum working electrode in comparison to an Ag/AgCl reference electrode at a specific potential is used to measure the current from the reaction[23]. So, the main principal behind amperometric detection is that the current of the reaction is measured at a fixed potential that is defined as, amperometry. In contrast, voltammetry is the measurement of current during a controlled variation of potential. The peak current value that is measured in the electrochemical reaction is directly proportional to the bulk concentration of the electrochemical species[53–55]. Herein, the various types of amperometric techniques will be discussed.

a- Chronoamperometry:

Chronoamperometry is a different amperometric method that involves applying a square-wave potential to the working electrode and measuring a steady state current as a function of time[56]. The expansion or contraction of the diffusion layer at the electrode causes changes in the current. Nernst first proposed the idea of a diffusion layer, which states that there is a thin, stationary layer of solution in contact with the electrode surface. Diffusion regulates the transfer of analyte from the bulk solution of higher concentration to the electrode as the local analyte concentration drops to zero at the electrode surface. As a result, there is a gradient of concentration away from the electrode surface. Convective transfer keeps the analyte concentration in the bulk solution at a value of c_0.

Thus, the Cottrell equation[57,58], which is depicted in equation 1, and this chronoamperometric technique are related. It describes the current-time dependence for planar electrode linear diffusion control. The Cottrell equation relates the current I to the analyte concentration (c_0), the Faraday constant (F), the number of transferred electrons per molecule (n), the electrode area (A), the diffusion coefficient (D), the time (t), and the electrode area. The Cottrell equation states that the rate of analyte diffusion to the electrode determines the current.

$$I = nFAc_0\sqrt{\frac{D}{\pi t}} \qquad \text{Equation 2:1}$$

b- Voltammetric techniques

Voltammetry is a type of electro-analytical amperometric technique that measures the current produced when a potential is changed in order to determine information about an analyte. Voltammetry comes in a variety of forms, including polarography (DC Voltage)[59], linear sweep,

differential staircase, normal pulse, reverse pulse, differential pulse, and even more[60,61], because there are numerous ways to change a potential while measuring the induced current. We will only mention the Square Wave Voltammetry (SWV) technique as it has been extensively used in our literature.

SWV

2. Potentiometric sensors

When no current or very little current flows between the working and reference electrodes in an electrochemical cell, potentiometric devices measure the accumulation of a charge potential at the working electrode [62–64]. Potentiometry, then, tells us about the ion activity during an electrochemical reaction [65]. The Nernst equation, where E_{cell} stands for the observed cell potential at zero current, governs the relationship between concentration and potential for potentiometric measurements, as in equation 4. The electromotive force, or EMF, is another name for this. R is the universal gas constant, T is the absolute temperature in degrees Kelvin, n is the charge number of the electrode reaction, F is the Faraday constant, and Q is the ratio of the ion concentration at the anode to the ion concentration at the cathode[66]. E^{o}_{cell} is a constant potential contribution to the cell.

$$EMF\ or\ E_{cell} = E^{0}_{cell} - \frac{RT}{nF} \ln Q \qquad \text{Equation 2:2}$$

Direct potentiometry is the use of the Nernst equation to directly measure the analyte ion concentration [67]. Currently, ion-selective electrodes (ISE) are frequently used to achieve the lowest detection limits for potentiometric devices. The detection limit is analyte-specific by definition, and current devices have limits of detection that range from 10^{-8} to 10^{-11} M. Potentiometric sensors

are useful for measuring low concentrations in small sample volumes because they ideally have the advantage of not affecting the sample chemically. Currently, there is a fairly small range of ions for which low detection limits are feasible, and these ions lack significant analytes like nickel, manganese, mercury, and arsenate ions. In the review by Bakker et al. [65], extensive details about potentiometry and their limit of detection (LOD) are provided.

3. Conductometric sensors

The ability of an analyte (such as electrolyte solutions) or a medium (such as nanowires) to conduct an electrical current between electrodes or reference nodes is measured by conductometric devices. Even though conductimetric devices can be thought of as a subset of impedimetric devices, methods for assessing capacitance changes utilizing electrochemical impedance spectroscopy are well-described in literature. The majority of the time, conductometric devices have been closely linked to enzymes because an enzymatic reaction can change the ionic strength and, consequently, the conductivity of a solution between two electrodes. Therefore, enzymatic reactions that result in changes in the concentration of charged species in a solution can be studied using conductometric devices [68]. The applicability of such enzyme-based conductometric devices for biosensing is constrained by the variable ionic background of clinical samples and the requirement to measure small conductivity changes in media of high ionic strength [69]. Another strategy is to keep a close eye on how an electrode's conductance changes when, for example, enzymes or complementary antibody-antigen pairs are immobilised on the electrode surface.

The rapid advancement of semiconductor technology and sensor integration with microelectronic devices, such as FET devices, have enabled the development of multi-analyte conductance biosensors and conductive polymer-based devices [70,71]. Conductometric immunosensors combined with nanostructures, particularly nanowires, are now receiving more attention for biosensing [72,73].

There are examples of successful development of these devices for practical application, such as drug detection in human urine and pollutant detection in environmental testing [74], even though conductometric sensing has not been widely adopted as it could be [75]. In conductometric biosensors for toxicity analysis, whole cells have also been used as a biorecognition component by immobilising the cells to a transducer of interdigitated electrodes [76].

4. Impedimetric sensors

The earliest electrochemical impedance spectroscopy articles were published in 1975 [77]. One can measure the resulting current response I by applying a small, sinusoidally varying potential U [61,78]One can determine the complex impedance of the system, which is the sum of the real and imaginary impedance components, as a function of frequency by varying the excitation frequency f of the applied potential over a range of frequencies (i.e. angular frequency w). Therefore, as shown in Equation 5[79,80], EIS combines the analysis of both real and imaginary components of impedance, namely electrical resistance and reactance.

$$Z\,(jw) = \frac{U\,(jw)}{I\,(jw)} = Z_r(w) + jZ_i(w); w = 2\pi f \qquad \text{Equation 2:3}$$

IS possesses the ability to study any intrinsic material property or specific processes that could influence the conductivity/resistivity or capacity of an electrochemical system. Therefore, Electrochemical Impedance Spectroscopy (EIS) is a useful tool in the development and analysis of materials for biosensor transduction, such as the study of polymer degradation. For example, by coating conductive electrodes with insulating polymers and then introducing this to an enzymatic reaction, the direct or indirect degradation of the polymer coating can be studied. If during the reaction existing free ions are able to penetrate into the polymer, the insulating nature of the polymer would be compromised and result in modified impedance characteristics of the

transducing element [81,82]. Utilizing electrochemical EIS to describe the formation of a hydrogen peroxide Horseradish Peroxidase (HRP) biosensor is a recent example [83]. Impedance techniques can be used to track changes in electrical characteristics brought on by biorecognition activities occurring at the surfaces of modified electrodes, electrochemical sensing, or both. Protein immobilisation and antibody-antigen interactions on the electrode surface, for instance, can cause changes in the conductance of the electrode and be measured [61,79,84,85].

5. Field-Effect Transistor (FET)

An electric field is used to control the conductivity of a channel, or a region depleted of charge carriers, between two electrodes, or the source and drain, in a semiconducting material, to create a FET. By changing the electric field potential at a third electrode known as the gate relative to the source and drain electrodes, the conductivity can be controlled. The presence of a sufficient positive or negative potential at the gate electrode would either attract or repel charge carriers (such as electrons) in the conduction channel, depending on the configuration and doping of the semiconducting material. This would either fill or empty the charge carrier depletion region, forming or deforming the conducting channel's actual electrical dimensions. The conductance between the source and drain electrodes is regulated by this. An FET switches between the conductive and non-conductive states in linear mode when the drain-to-source voltage is significantly lower than the gate-to-source voltage. An FET can also function as a constant-current source and is frequently employed as a voltage amplifier in saturation mode. The gate-to-source voltage in this mode controls the amount of constant current. FET devices are frequently used in the developing field of electrochemical biosensing because they are preferred for weak-signal and/or high impedance applications[86,87].

2.5 Theory behind nanoparticles and biorecognition molecules in electrochemical sensing

Electrochemical sensors and biosensors have made extensive use of a variety of nanoparticle types, including metal, oxide, semiconductor, and even composite nanoparticles. The basic roles of nanoparticles can be broadly categorised as: 1) immobilising biomolecules; 2) catalysing electrochemical reactions; 3) enhancing electron transfer; 4) labelling biomolecules; and 5) acting as reactant. These nanoparticles play different roles in various electrochemical sensing systems based on their distinctive properties[88].

1. Biorecognition molecules immobilization

Nanoparticles can strongly adsorb biomolecules due to their high surface free energy and large specific surface area, which is a key factor in the immobilisation of biomolecules in biosensor construction. In general, biomolecules may frequently become denaturized and lose their bioactivity when they are adsorbed directly onto the exposed surfaces of bulk materials. However, because nanoparticles are biocompatible, when such biomolecules are adsorbed onto their surfaces, they can still be biologically active. Considering that the majority of nanoparticles are charged, they can electrostatically adsorb biomolecules of various charges. Some nanoparticles can immobilise biomolecules through interactions besides the typical electrostatic one. For instance, it has been suggested that gold nanoparticles can immobilise proteins by forming covalent bonds with their amine groups and cysteine residues [89,90]. All examples for biorecognition molecules will be discussed in chapter 3.

2. Catalysis of Electrochemical Reactions

There are many nanoparticles with excellent catalytic properties, particularly metal nanoparticles. By adding catalytic nanoparticles to electrochemical sensors and biosensors, it is possible to reduce the overpotentials of many analytically significant electrochemical reactions and even realise the reversibility of some redox reactions that, at conventional, unmodified electrodes, are irreversible. For instance, a sensitive NO microsensor was created by modifying a platinum microelectrode with gold nanoparticles, in which the latter catalyse the electrochemical oxidation of NO with a decrease in overpotential of about 250 mV [91]. At electrodes modified with dense gold nanoparticle films, the catalytic oxidation of NO can also be seen [92]. Selective electrochemical analysis could be accomplished based on the selective catalysis of nanoparticles. Based on the catalytic effect of gold nanoparticles on the ascorbic acid oxidation, Ohsaka and colleagues [93] developed an electrochemical sensor for the selective detection of dopamine in the presence of ascorbic acid. As a result, the ascorbic acid oxidation overpotential was reduced and the ascorbic acid and dopamine oxidation potentials were effectively separated, enabling selective electrochemical detection. More detailed examples will be mentioned in chapter 3.

3. Enhancement of Electron Transfer

A crucial step in the creation of third-generation enzyme electrodes is the electrical contact of redox enzymes with electrodes. Since the active centres of enzymes are surrounded by remarkably thick insulating protein shells, which prevent electron transfer between electrodes and the active centres, enzymes typically lack direct electrical communication with electrodes. However, because nanoparticles, mostly metal nanoparticles at nanoscale dimensions, have conductivity properties that make them suitable for enhancing the electron transfer between the active centres of enzymes

and electrodes acting as electron transfer “mediators” or “electrical wires”[88]. More detailed examples will be mentioned in chapter 3.

4. Labeling Biomolecules

The development of sensitive electrochemical biosensors involves the labelling of biomolecules like DNA, antigen, and antibody with nanoparticles, which is becoming more and more significant. The amount or concentration of analytes can be identified based on the electrochemical detection of the nanoparticles that have been used to label the biomolecules. These biomolecules can maintain their bioactivity and interact with one another. Stripping voltammetry is a very effective electrochemical analytical 0technique for measuring trace metals, so dissolving the nanoparticle labels—mostly metal and semiconductor nanoparticles—and measuring the dissolved ions with it represents a general electroanalytical procedure[94]. More detailed examples will be mentioned in chapter 3.

5. Nanoparticles Acting as Reactant

The development of sensitive electrochemical biosensors involves the labelling of biomolecules like Deoxyribonucleic Acid (DNA), antigen, and antibody with nanoparticles, which is becoming more and more significant. The amount or concentration of analytes can be identified based on the electrochemical detection of the nanoparticles that have been used to label the biomolecules. These biomolecules can maintain their bioactivity and interact with one another. Stripping voltammetry is a very effective electrochemical analytical technique for measuring trace metals, so dissolving the nanoparticle labels—mostly metal and semiconductor nanoparticles—and measuring the dissolved ions with it represents a general electroanalytical procedure[94]. More detailed examples will be mentioned in chapter 3.

Chapter 3 Literature Survey

3.1 Point of care sensor detection of therapeutic agents and biomarkers

Based on rapid diagnostics, intelligent data analysis, and statistical informatics analysis, the development of sophisticated and miniaturised devices for sensing a wide range of biological molecules has emerged as a crucial strategy for the real-time diagnosis of various diseases and effective management of disease progression. Because the target analytes recognised by these devices are proteins, enzymes, antibodies, DNA/RNA probes, and microorganisms, which can be detected with high sensitivity, accuracy, and low detection limits, the fabrication of smart devices based on bio-nanomaterials is thought to be the result of a transdisciplinary effort from the materials science to the medical field [95]. Depending on the biochemical process involved in recognition, the bio-detection system can be either a bio-catalytic or a bio-affinity-based system: In the first scenario, the bioreceptor (proteins, enzymes, or cells) engages in a catalytic reaction with the analyte, whereas in the second scenario, an equilibrium is reached as a result of a particular binding mechanism between the bioreceptor (aptamer, antibody), and the analyte [96]. The biosensors can be divided into electrochemical, piezoelectric, magnetic, optoelectronic, and thermal types based on the transduction pathways. Nanostructures, which are frequently incorporated into the (bio)sensor by attachment to a suitably modified platform, are related to the concept of nano(bio)sensors. The excellent properties of nanoparticles and nanomaterials make them ideal for designing sensing systems with improved performance. By customising their size and morphology, they can be integrated into transducers by attachment to a suitable modified platform, resulting in (bio)sensors with higher sensitivity and faster response times. Due to their exceptional combination of biocompatibility, surface area, and conductivity, hybrid materials and nanocomposite structures made of metallic NPs, combined with specific conductive polymers and

a modified electrode, have been developed for electrochemical sensing [97,98]. For signal processing on a smartphone, the output of the sensing nano-platform can be connected to wireless devices. As a result, these nano-devices could be used to monitor a person's health when implanted in the body. According to the European Commission, a nanomaterial is "a naturally occurring, incidental, or manufactured material containing particles, in an unbound state, as an aggregate, or as an agglomerate, and for 50% or more of the particles in the number size distribution, one or more external dimensions is in the size range 1 nm-100 nm." The number size distribution threshold of 50% may occasionally be replaced by a threshold between 1% and 50% when justified by issues with the environment, human health, safety, or competitiveness[99].

3.2 Sensors

Electrochemical sensors are systems that transduce electrochemical reactions into analytical signals. They are widely favored over other techniques of sensors owing to their cost-efficacy, real-time measurements, and straight forward procedures[100]. According to the signal transduction, there are five kinds of electrochemical sensors conductive, potentiometric, impedimetric, amperometric, and voltametric[101]. Out of these five electrochemical techniques, both voltametric and amperometric are the most popular ones in literature[102].

Herein, we will discuss the categories of sensors based on the catalyst nanoparticles.

1. Metals and metal derived materials

3.2.1.2 *Metal nanoparticles*

Noble metal nanoparticles, especially gold, silver, and platinum nanoparticles, are the most popular metallic nanoparticles used in sensing owing to their spectacular surface and interface features in the nanoscale that improves their biocompatibility and signal transduction in comparison to their absence[103,104].

A. Gold nanoparticles (AuNPs)

Due to their capability to form highly stable nanoparticles with different aspect ratios, that can provide higher surface areas, with straight forward manner, they are considered to attain interests of the biomedical field researchers over the last three decades[105,106]. Gold nanoparticles has been used for various therapeutic drugs and biomarkers as a catalyst and redox mediator, including glucose[107–113], dopamine[114–119], uric acid[114,120–126], bisphenol[127], nitrites[128–130], epinephrine[131–134], and ascorbic acid[118,120,126,135–139] in addition to some drugs as etoposide, epirubicin[140], flutamide[141], nilutamide[142], irinotecan[143], topotecan[144] (anticancer drugs), diclofenac[145–147], indomethacin[148], aspirin[149,150], ibuprofen[151,152], ketoprofen[151], acetaminophen[153] (non-steroidal anti-inflammatory drugs (NSAID)), hydrochlorothiazide[154], amlodipine[155], timolol[156], trazocin[157,158], Captopril[159], atenolol[160], sotalol[161], betaxolol[162] (antihypertensive drugs), tramadol[163–166], codiene[167–169], Morphine[170–172] (Narcotics)… etc.(antifugal)

B. Silver nanoparticles (AgNPs)

AgNPs have made a great impact for biomedical sensor applications due to their good conductivity, their ability of amplifying signals, and spectacular biocompatibility. Over the last two decades they have been extensively used for the detection of several biomarkers and drugs. AgNPs have been used to detect biomarkers and drugs as well, such as glucose[173–180], hydrogen peroxide[174,178,181–191], dopamine[192–196], epinephrine[197] and serotonin[198]. Drugs that were determined by AuNPs include, doxorubicin[199], adriamycin[200], flutamide[201], imatinib[202], epirubicin[203], 5-fluorouracil[204] (anticancer drugs), ibuprofen[205–208], diclofenac[209], acetaminophen[210–213] (NSAID), propranolol [214](antihypertensive drug)

3.2.1.3 *Metal oxides nanoparticles*

Transitional metal oxides nanoparticles have, including iron oxide, manganese oxide, titanium oxide, copper oxide, zirconium oxide, cobalt oxide, nickel oxide, tungsten oxide, silver oxide, and vanadium oxide, were extensively used in sensors due to their spectacular electrochemical and photochemical properties[215]. Herein, we will discuss titanium and iron oxide being two of the most used metal oxides.

A. Iron oxide

Iron oxides, especially magnetite (Fe_3O_4) nanoparticles have been extensively studies in sensors due to its excellent conduction at room temperature that is attributed to the rapid electron transfer between Fe^{+3} and Fe^{+2} in magnetite nanoparticles[216]. Iron oxides have proven to possess high sensitivity towards biomarkers and drugs in electrochemical sensors, such as glucose [217–222], cholesterol[222], dopamine [223–227], hydrogen peroxide [228–232], uric acid[233,234], epinephrine[235,236], and nitrate[237]. In addition, some drugs were determined including metformin[238], glicalazide [239](antidiabetic), doxorubicin[240–243], methotrexate[244–247], raloxifene[248], tamoxifene[248] (anticancer), diclofenac[249–252], acetaminophen[253–256], aspirin [257](NSAID).

B. Titanium dioxide

Titanium NPs possess high potential as a modified of electrochemical sensors owing to their low cost, high conductivity, biocompatibility, and high stability in harsh chemical conditions against corrosion[258,259]. Titanium dioxide nanoparticles has also proven efficiency of improving the catalysis of sensors and enzyme sensors through the availability of numerous numbers of active sites for chemical reaction[260,261]. It has served as a perfect catalyst for the detection of some biomarkers such as glucose[262–270], choleterol[271–274], dopamine[275–282], uric acid[283–286], ascorbic

acid[283,284,287–293], hydrogen peroxide[294–296], epinephrine[297–301], and serotonin[302,303]. In addition to its wide use in catalytic electrochemical sensing of some drugs, such as timolol[304], propranolol[305](antihypertensive drugs), paracetamol[306–310], diclofenac[311,312], and piroxicam[313](NSAID), dacarbazine[314](anticancer).

https://www.sciencedirect.com/science/article/pii/S2666523921000180

3.2.1.4 *Metal organic frameworks (MOFs)*

MOFs are crystalline porous slid materials that has attracted huge research interests in the last decade[315]. Their highly crystalline structure emerges from the coordinate bonds that self-assembles the metal ions with organic ligands tat results in shaping a network like structure that can in one-, two- or three-dimensional structures[316]. In addition to their exceptional porosity and large surface area, they have other advantages, including thermal stability, modifiable surface properties, and tunable chemical functionalities[317]. Due to their spectacular features, they constituted a pivotal role in various research fields, including gas adsorption[318], sensors[319], drug delivery[320], and catalysis[321–323].

Several MOFs were used for the detection of glucose, including zeolitic imidazolate framework 8 copper MOF@ZIF-8[324] and bimetallic Cu@Ni organic framework[325], hydrogen peroxide, including Ni(II)-Based MOF[326],graphene@HKUST-1[327], copper oxide nanoparticles @ZIF-8[328], uric acid, including bimetallic zeolitic imidazolate frameworks (BMZIFs) based on ZIF-8 and ZIF-67[329], Cu-BTC MOF[330], hierarchical core−shell MOF[331], and Ni-MOF[332], dopamine, including hierarchical core−shell MOF[331]. In addition, some drugs with different categories were also determined using MOFs, such as captopril[333,334], amlodipine and losartan[335], propranolol[336], and nifedipine[337](antihypertensive drugs), acetaminophen[338–340], ibuprofen[341], and

diclofenac[341](NSAID), idarubicin[342], doxorubicin[343], imatinib[344], nilutamide[345], gemcitabine [346](anticancer).

3.3 Biosensors

Biosensors are the devices that implements a biological recognition molecule, including enzymes, antibodies, aptamers, ssDNAs, for the generation or inhibition of signal that is indicative for a biomarker, DNA, RNA, protein, or drug through fixing them on the surface of the electrode. This signal is detected recorded and transmitted using the electronic components of the biosensor system. The biosensor system is composed of an (a) analyte, (b) biological recognition molecule, (c) transducer, (d) electronics and (e) display, as shown in Figure 2.1[347].

Herein, we will discuss the categorization of electrochemical biosensors according to the type of the biorecognition molecule.

1. Antibodies

Antibodies are the most used biorecognition molecules in biosensors. They are naturally released by immune systems of vertebrates as a defensive mechanism when exposed to a foreign or toxic substances. They are produced by B-cells that contributes to the immune system of a human body, which contains around one trillion B-cells. The antibodies are Y-shaped immunoglobulins, each arm of them contains heavy chain (~55 kDa) and light chain (~25kDa) antibody that are connected by sulfide bonds. The morphological structure of an antibody is constituted from a constant region (that constitutes the lower part of an antibody) and a variable region (upper part of antibody). The upper part of an antibody is the part responsible for binding with an antigen[348].

Usually, sensors that possess antibodies are called immunosensors and they are usually used for the detection of proteins and antigens (large molecules) and herein we will mention the biomarkers only. Immunosensors have been used in the detection of proteins, such as B-amyloid[349–356] and tau [357–359]proteins that are used in early Alzheimer disease diagnosis, and enzymes, such as the detection of insulin levels[360–363] for the diagnosis of diabetes mellitus diagnosis.

2. Enzymes

Electrochemical enzyme-based sensors constitute a large category of biosensors that combines the ultra-high selectivity and sensitivity towards the targeted analyte. Enzymes are selective catalysts which interacts with the substrate to form a product and the electrons involved in the reaction are measured through amperometry[364]. The enzymes utilized in this type of biosensors are either oxidases or dehydrogenases that utilizes coenzymes in the oxidation reaction of substrates such as (NAD^+, $NADP^+$, NADH, NADPH, ATP FAD, FADH), as in first generation enzyme sensors, mediators (ferricyanide and ferrocene, although, methylene blue, phenazines, methyl violet, alizarin yellow, Prussian blue... etc.), as in second generation enzyme sensors which limits the oxygen dependency, or a nano scale wiring element (redox polymer that entraps the enzyme) that permits direct electron transfer between the electrode and the substrate, as in third generation enzyme sensors which eliminates the need of oxygen in the reaction[365].

Amongst the oxidases utilized in electrochemical enzyme sensors are oxidases that were used for the detection of glucose[366–369], ethanol[370–373], and lactate[371,374–376], while dehydrogenases were used in the detection of β-hydroxybutyrate[377] (ketone bodies).

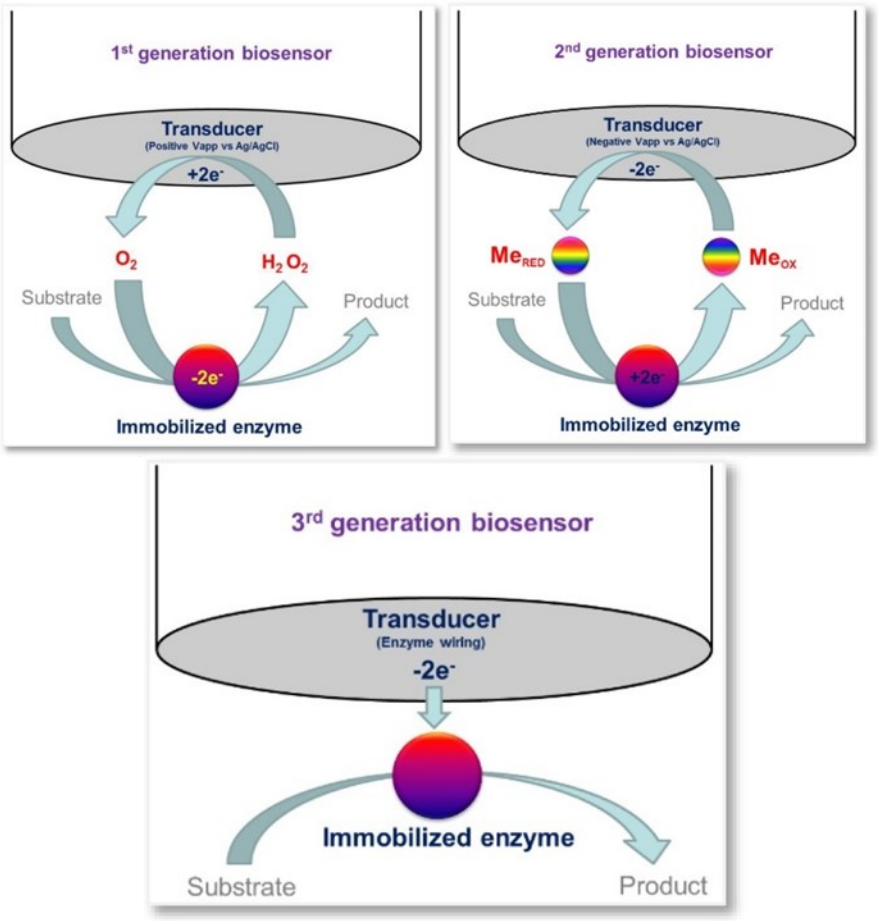

Figure 3.1 The difference between the three generations of enzyme sensors[378]

3. Aptamers

Biosensors that utilize aptamers as the biorecognition moieties are called aptasensors. Aptasensors were first introduced for literature in 2004 for the detection of thrombin[379]. Aptasensors possess a wide range of merits over other previously mentioned biosensor types since it offers high stability, flexibility of design, and cost-efficiency. Amongst these merits is the extremely high affinity and specificity of aptamers towards their targets that can be equivalent to antibodies and can be produced against non-toxic and non-immunogenic targets, their affinity and sensitivity towards targets can be customized (unlike antibodies), they are highly resistant to denaturation and

degradation (unlike enzymes), and their easiness of synthesis and modification chemically in addition to their storage stability makes them the top choice for research[380,381].

Electrochemical aptasensors have been utilized in the detection of biomarker proteins, including Alzheimer tau [382,383] and β-amyloid[384–388] protein biomarkers, heart failure troponin I [389–393] and C-reactive protein[394–397] biomarkers, and lung cancer biomarker epidermal growth factor receptor (EGFR) [398–400]that is distinctive for metastatic lung disease. In addition, aptasensors can also be used for small structure molecules, drugs or biomarkers, regarding their electrochemical activity or inactivity. For example, diclofenac[401], cocaine[402], tetracycline[403] and vancomycin[404].

Chapter 4 Experimental Materials and Methods

4.1 Materials and methods for sensors of therapeutic agents Velpatasvir (CTL) and Cilostazol (CTL)

4.1.1 *Materials for detection of VLP and CTL*

Manganese chloride hexahydrate, MnCl2.6H2O (99.8%, Sigma Aldrich), Vanadyl sulfate hydrate, V(O)SO4.XH2O (99.9 %, Alfa Aesar), sodium hydroxide, NaOH (99.9 %, Alfa Aesar), ethanol C2H5OH, (99.0 %, Loba Chemie) 2-Aminaterephthalic acid (99.0%, Sigma Aldrich), AlCl3.6H2O (99.0%, Sigma Aldrich), Salicylaldehyde (98.0%, Sigma Aldrich), acetic acid (≥99%, Sigma Aldrich), bromine (≥99.99%, Sigma Aldrich), ethanol (99.5%, Sigma Aldrich). All chemicals and reagents were used as received without any purification process.

NODCR kindly supplied CTL and VLP drug substance. The dosage form experiments were conducted using Pletaal® (Otsuka) tablets containing 100.0 mg of drug. Graphite power with a particle size of less than 50 μm3 were obtained from Aldrich. Paraffin oil (Merck Co. Germany) was used as the base liquid for carbon paste electrode. The fresh human plasma was provided by (VACSERA, Cairo, Egypt). Britton-Robinson buffer (BRB) was prepared by mixing 0.04 M (of the final volume) acetic acid, 0.04 (of the final volume) Phosphoric acid, with an appropriate amount of NaOH in order to have the desired pH from 2.0 -9.0.

4.1.2 *Apparatuses utilized in the detection and characterization*

The electrochemical properties of the sample were analyzed by Bio-logic 300 electrochemical workstation. A platinum wire electrode from BAS (USA) was used as the counter electrode. The experiment potentials were calibrated with respect to Ag/AgCl (3.0 M NaCl) reference electrode from BAS (USA). A Hanna HI-5522 pH meter (Hanna instruments, Egypt). All the

electrochemical experiments were conducted at an ambient temperature of 25$_o$ C. Impedance spectroscopy were conducted at a range of 100 mHz to 100 kHz. Scanning electron microscopy (SEM) measurements were conducted using a JSM-6700F scanning electron microscope (Japan Electro Company). FT-IR spectra was measured using IR-Affinity -1 Fourier Transform Infrared Spectrophotometer (Shimadzu, Japan). XRD data and crystalline phases were determined using an X-ray diffractometer (XRD) on an X'Pert Pro MRD with a copper source at a scan rate (2□) of 1os-1. Sigma Plot 14.0 was used for all statistical data.

4.1.3 Methods of catalyst material synthesis

a. Synthesis of α-MnO_2-V_2O_5 nanocomposite: -

α-MnO_2-V_2O_5 nanocomposite was synthesized as follows: 1.0 g of $MnCl_2.9H_2O$ and 0.9 g of V(O)SO4.XH_2O were dissolved in 50.0 mL distilled water. At room temperature and under vigorous stirring condition a homogeneous solution was obtained then 100.0 ml 0.4 M of NaOH solution was slowly added. After stirring for 2 hours, the resulting precipitate was washed twice with distilled water then by ethanol before being dried at 60^o C overnight. The prepared sample was annealed at 500 ºC for 2 hr with 5 ºC/min. After the annealing process, a black powder of α-MnO_2-V_2O_5 nanocomposite was collected.

b. Synthesis of 5-bromo-salicylic acid(5-BSA)-NH_2-MIL- 53(Al)

Synthesis of NH_2-MIL- 53(Al) was conducted on three stages as following:

1- Synthesis NH_2-MIL- 53(Al)

A certain amount (3.75 g) of 2-Aminaterephthalic acid (NH2-H2BDC) and Sodium hydroxide (NaOH) were dissolved in deionized water (DI) and ultra-sonicated for 10 minutes. Another certain amount of AlCl3•6H2O (5.00 g) is dissolved in 20 ml DI and mixed with the other solution

using a magnetic stirrer for 24 hours in room temperature. After seven cycles of centrifugation and elution, a faint yellow colloidal material is obtained. Afterwards, the elucidated material is vacuum dried at 150^{O} C for 24 hours to remove residual water and obtain NH_2-MIL- 53(Al) MOF[405].

2- Synthesis of 5-Bromo Salicylaldehyde

Salicylaldehyde (1.22 g, 0.01 mol) was suspended in acetic acid (15 mL) in a flask and was cooled in an ice bath. To this solution bromine in acetic acid (25% vol., 6.4 mol) was added slowly drop by drop with constant stirring. The mixture was stirred to get a clear solution. After complete addition of bromine, the stirring was stopped, solution was allowed to solidify. The solid mass was filtered, washed repeatedly with water to remove excess of bromine and recrystallized from alcohol to get white crystalline solid. M. P.: 105O C., Yield: 80%[406].

3- Synthesis of *5-BSA-NH_2-MIL- 53(Al)*

5-bromo salicylaldehyde (5-BSA) Sensor was synthesized following the synthesis method described in the preceding literature with slight modifications[407,408]. 1.50 gm of NH_2-MIL- 53(Al) was finely grinded and added to a solution of 5-bromo salicylaldehyde acid (0.50 g) in 40 ml ethanol, the mixture was sonicated for 30 min then stirred for 6 h at 80°C.The process was repeated several times to ensure the successful covalently attachment. The bale red crystals of 5-BSA Sensor were filtered and washed with abundant ethanol. Eventually, this sensor was dried at 70 °C for 5 h and transferred to be grinded well. The resulting product was named 5-BSA sensor.

4.1.4 Drug stock solution

A stock sample solution of CTL of 1.0 x 10^{-3} M of CTL (MWT = 369.69 g/mol) and VLP (MWT = 883.02 g/mol) was prepared daily by dissolving 18.47 mg of CTL and 44.15 mg of VLP

in 50 ml 96.0% ethanol HPLC grade (Sigma-Aldrich) in a volumetric flask. Working solution was prepared by adding a proper amount of drug stock solution in 9ml of BRB of a defined pH to obtain the desired concentration. These solutions have a stability of a week in a refrigerator of a 4º Celsius temperature.

4.1.5 Recommended experimental procedures

Before conducting any voltammetric measurements, the modified α-MnO_2-V_2O_5/ CPE and 5-BSA/ CPE were scanned using SWV in the potential range of 0.0 - 1.2 V at a scan rate of 100 mv. s^{-1} in BRB of 7.0 pH until an electrochemical response was obtained. Afterwards, the modified electrode was transferred into another cell containing BRB of 7.0 pH and the required amount of CTL and VLP, and a square wave voltammogram is recorded in the potential range of 0 - 1.2 V at a scan rate of 100 mV. s^{-1}. In order to obtain a relatively high and sharp peaks, the values of 40 mV and 3 ms were chosen for pulse amplitude and pulse width, respectively.

For the calibration procedure, aliquots of CTL and VLP were added to 9.0 ml of drug in order to obtain a concentration range of 5 x 10^{-8} to 1 x 10^{-3} M of CTL and 1.00 x 10^{-8} to 1.00 x 10^{-3} M of VLP. The pulse amplitude, pulse width and scan rate were used as aforementioned.

Determination of LDP by SWV analytical procedure was validated according to International Conference on Harmonization (ICH) guidelines, concerning linearity, range, accuracy, and precision

4.1.6 Material Characterization

Panalytical Empyrean X-ray Diffractometer using copper CuKa radiation (λ= 0.15406 nm) in the range of 5º to 80º with a step size 0.03 was used to investigate. The phases and crystallinity

of the as-prepared nanocomposite. Fourier transform infrared spectroscopy (FTIR) measurements were carried out with a BRUKER Vertex 70 FTIR spectrometer. The morphology and elemental analysis of resulted materials were identified using field emission scanning electron microscopy (FESEM, Zeiss SEM Ultra 60, 5 kV) and energy dispersive X-ray (EDX), respectively.

4.1.7 Verification of sensors in plasma, urine and dosage form

a- Analysis of plasma samples for CTL and VLP

Fresh plasma samples were collected from a healthy individual before the experiments. 10 µl of the supernatant were added to 4.50 ml of pH 7.0 BRB with different volumes of CTL and VLP stock solution in order to reach the desired concentration. The solution was transferred to an electrochemical cell to be analyzed without any further pre-treatments.

b- Analysis of pharmaceutical formulations for CTL

Five tablets of Pletaal® 100.0 mg were weighed and ground. The calculated amount of the powder containing a defined amount of drug is added to 25.0 ml of ethanol in. Then, ethanol was added to the flask to reach 25.0 ml and dissolved using a vortex mortar. The solution was filtered using 0.45µm filter paper then the elucidated I_p was calibrated.

c- Analysis of urine samples for VLP

Fresh urine samples were collected from a healthy individual before the experiments. 10 µl of the supernatant were added to 4.50 ml of pH 7.0 BRB with different volumes of VLP stock solution in order to reach the desired concentration. The solution was transferred to an electrochemical cell to be analyzed without any further pre-treatment.

4.2 Materials and methods for apta-sensors of therapeutic drugs vancomycin (VCM)

4.2.1 Microneedles (MNs) fabrication

The VCM system integrates hydrogel microneedles with VCM aptamer modified flexible gold electrodes for biorecognition and capturing of VCM in ISF that provides accurate and reliable simulation of plasma levels in a minimally invasive method [409–411]. For the synthesis of our microneedles, we utilized 10% conjugated DAHA hydrogel that was synthesized by synthesizing dopamine-hyaluronic acid polymer (DAHA) using 1-Ethyl-3-(3-dimethyl aminopropyl) carbodiimide (Sigma-Aldrich) and N-hydroxy succinimide (EDC/NHS) (Sigma-Aldrich) coupling reaction based on our well-established protocol. The DAHA was synthesized with different DA constitutions in the product confirmed by UV. Increasing the solution's pH to 8 causes the linkage of the carbon atoms of benzene rings together covalently and the formation of DA-DA conjugate sites, thus a chemically crosslinked polymeric structure was fabricated. The DAHA hydrogel was then molded into a microneedle array by a negative polydimethylsiloxane (PDMS) mold that was then centrifuged at 7000 rpm for 5 minutes and then left to dry in a desiccator for 24 hours before use.

4.2.2 Thiolated aptamer modification of flexible screen-printed gold electrode

For electrochemical cleaning, as indicated in Plaxco et al. literature, we cleaned the electrode surface through Cyclic voltammetry (CV) scanning in 0.5 M NaOH from -0.35 to -1.35 V with a scan rate of 1 V/s, for 40 cycles, and E step 0.01 V until the shape of the CV scans become steady and are not showing any visible peaks to remove any naturally occurring thiols**.** Afterwards, both oxidation and reduction chronoamperometric steps were done in 0.5 M H_2SO_4, respectively. Then the electrode is scanned through CV for 20 cycles for the potential window of -0.35 to 1.5 V, E step 0.01 V, with a scan rate of 0.1 V/s in 0.5 M H_2SO_4.[412]

We utilized 5’ thiol modified VCM aptamer (sequence is provided below) with 3’ methylene blue reporter, which was reported in Plaxco et al. literature in our study[413]. For the modification of our electrode with the aptamer 1 µL of 100 µM of 5’ thiol modified VCM aptamer (IDT, Coralville, US) was mixed with 1 µl of (1000X molar ratio) 10 mM of Tris (2-carboxyethyl) phosphine (TCEP) (Sigma-Aldrich), that is equivalent to 1000X molar ratio of the aptamer, and left in dark for 2-3 hours to allow the reduction of disulfide bonds of the 5’ thiol for activation prior to reaction with the gold surface of the electrode. The complete reduction of thiol bonds is indicated hen the bluish color of the solution turns into complete invisible. Then the aptamer is diluted to 1 µM with 1X PBS (Sigma-Aldrich) with 2 mM $MgCl_2$ reaching a final volume of 100 µl.

VCM Aptamer. SH -5-CGAGG GTACC GCAAT AGTAC TTATT GTTCG CCTAT TGTGG GTCGG-3-MB

The electrode was left in solution for 8 hours to react with 5’ thiol modified VCM aptamer with 3’ methylene blue reporter an then dried with nitrogen and transferred into freshly prepared 2 mM 6- Mercaptohexanol (MCH) solution to passivate any unoccupied surface area by aptamers for 5 hours in dark. The electrode is taken and gently rinsed with 1X PBS with 2 mM $MgCl_2$ to remove any excess 6-MCH.

4.2.3 Agarose phantom gel preparation

The agarose phantom gel was prepared using the protocol of our previous work[33] by mixing 120 mg agarose (Sigma-Aldrich) with 10 ml of PBS with 2 mM $MgCl_2$ and heated until boiling in a beaker and stirred until the mixture becomes clear and the amount of vancomycin from the stock solution of 1 mM is added whenever the temperature of the beaker becomes lower than 40 ^{0}C. Afterward, the agarose is covered by a very thin layer of parafilm to mimic the epidermis[34].

4.2.4 Porcine skin Preparation

Porcine skin patches were prepared by cutting small pieces of pig ear skin, the patches are then washed with DI and soaked in PBS with 2 mM $MgCl_2$ solution with the desired concentration for 24 hours prior to measurements. The skin patches are then taken away from the solution and dried with paper wipes to remove external moisture of the skin

4.2.5 VCM detection using the gold rod electrode (in solution)

For the in vitro electrode characterization in solution, we scanned both the flexible gold electrode and the gold electrode utilizing Utilizing the signal-on frequency that was proven using the gold electrode, that is 100 Hz for square wave voltammetry (SWV), the electrode was scanned between 0 and -0.5 V with a step potential of 0.001 V and amplitude of 0.025 V using Palmsens potentiostat.

4.2.6 VCM detection in agarose hydrogel and porcine skin:

For the in vitro and ex vivo electrode characterization in agarose hydrogel and porcine skin, we scanned both the flexible gold electrode and the gold electrode utilizing Utilizing the same aforementioned conditions using CHI 1040 potentiostat.

Chapter 5 Results and Discussion

5.1 MnO_2-V_2O_5 nanorods for the detection of the antiplatelet prodrug agent Cilostazol in pharmaceutical formulations

The experimental part, including the reagents, apparatus, and the followed procedures to synthesize, characterize, and electrochemically determinate CTL using α-MnO_2-V_2O_5 NRs along with the methodology used to analyze plasma and dosage form samples, is listed in the supporting information. **Figure 1** illustrates the used procedures.

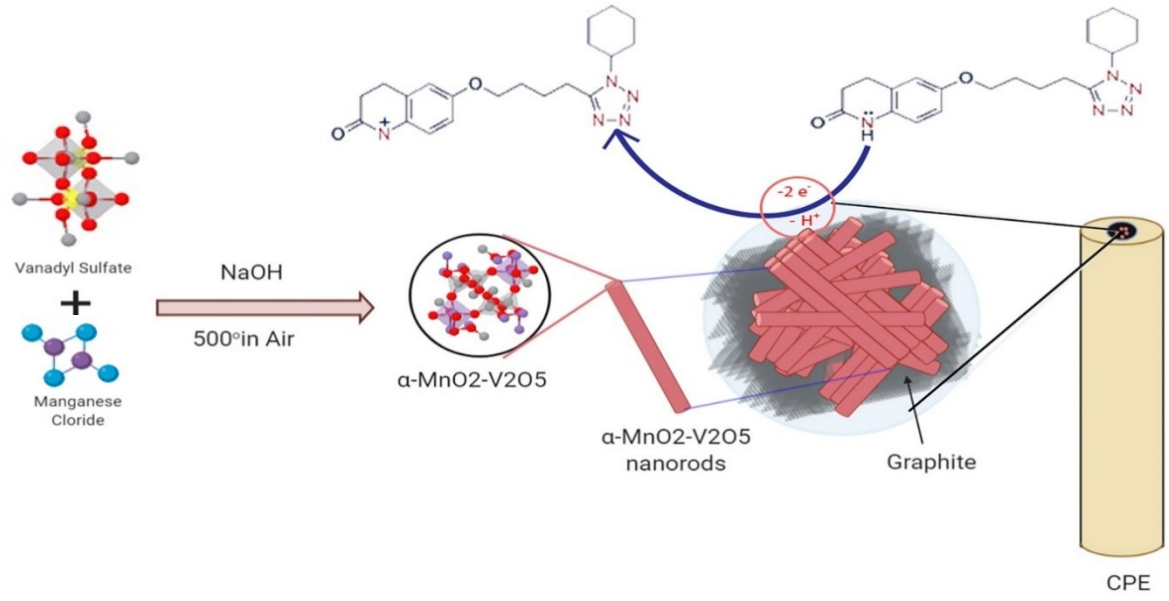

Figure 5.1 Illustration of the preparation of the α-MnO_2-V_2O_5 nanocomposite, detection of CTL, and the involved oxidation mechanism.

5.1.1 Surface and electrochemical characterization of the fabricated sensors

The morphology of the synthesized α-MnO_2-V_2O_5 nanocomposite shown in Figure 5.2a reveals a successful formation of nanorods that are ca. 68.5 nm in diameter. Furthermore, the EDX scan was used to investigate the elemental composition of the nanocomposite. Figure 5.2b displays the EDX and mapping results of the prepared nanocomposite, revealing the coexistence of V, Mn, and

O, which are uniformly distributed. The atomic presents of the O, Mn, and V were found to be 58.41, 32.93, and 6.66, respectively.

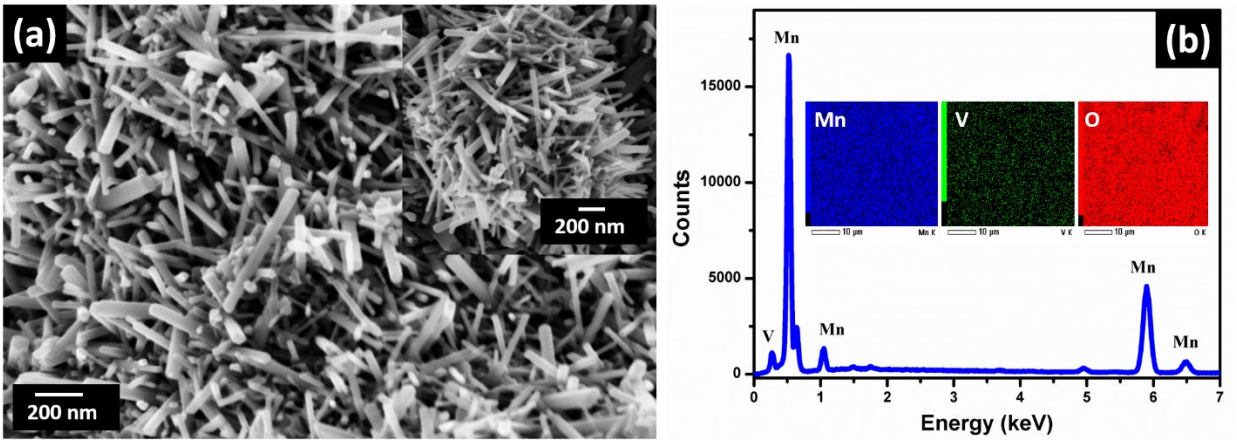

Figure 5.2 (a,b) Low and high magnification FESEM images of the prepared α-MnO_2-V_2O_5 nanocomposite, and (c) EDX spectra and mapping of the O, Mn, and V elements.

To investigate the crystal structure of the as-prepared nanocomposite and its chemistry, the X-ray diffraction spectra were recorded. Figure 5.3 shows the XRD pattern of the annealed α-MnO_2-V_2O_5 nanocomposite and their references with multiple characteristic peaks at 2θ = 12.781º, 18.112º, 32.538º, 41.932º, 49.848º, 56.354º, 60.255º, 65.059º, 69.666º, and 72.675º which are related to the diffraction from the (1 1 0), (2 0 0), (1 0 1), (3 0 1), (1 4 1), (6 0 0), (2 5 1), (0 0 2), (5 4 1), and (1 3 2) crystal faces of tetragonal α-MnO_2, respectively with a space group: I4/m (JCPDS card no. 04-007-2142) with interplanar distances (d) of 6.92, 4.89, 2.75, 2.15, 1.82, 1.63, 1.53, 1.43, 1.35, 1.3 Å, respectively. In addition, the XRD pattern exhibits two strong peaks at 28.776º and 38.050º, which could be related to the (2 1 0) and (3 0 0) plans, respectively of orthorhombic V_2O_5 with space group: PE (JCPDS card no. 00-053-0538)[414] with interplanar distances (d) of 3.10 and 2.36Å, respectively. Moreover, Fourier transform infrared (FT-IR) spectroscopy was used to investigate the functional groups in the synthesized α-MnO_2-V_2O_5 nanocomposite. Figure 5.3 shows the stretching band of surface hydroxyl group (surface-OH) and

adsorbed water molecules (H-O-H) at 3420 cm^{-1} and 1629 cm^{-1}, respectively. The vibrations band of Mn-O bond appeared at 520 cm^{-1} [415]. The peak centered at 695 cm^{-1} is assigned to the V–O–V stretching mode, as shown in Figure 5.4.

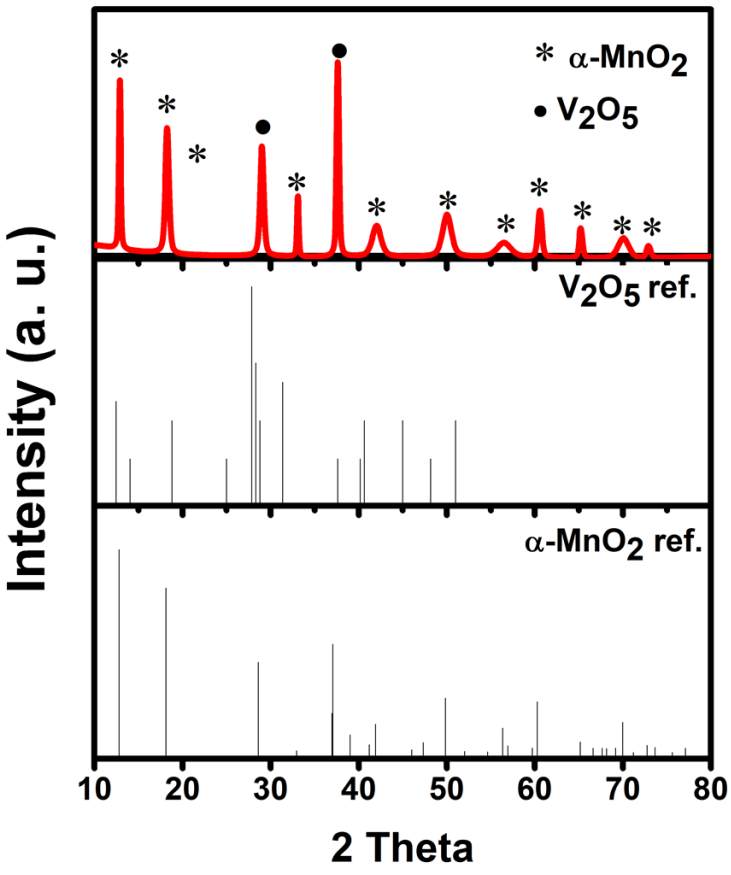

Figure 5.3 XRD pattern of the prepared nanocomposite α-MnO_2-V_2O_5 and their reference.

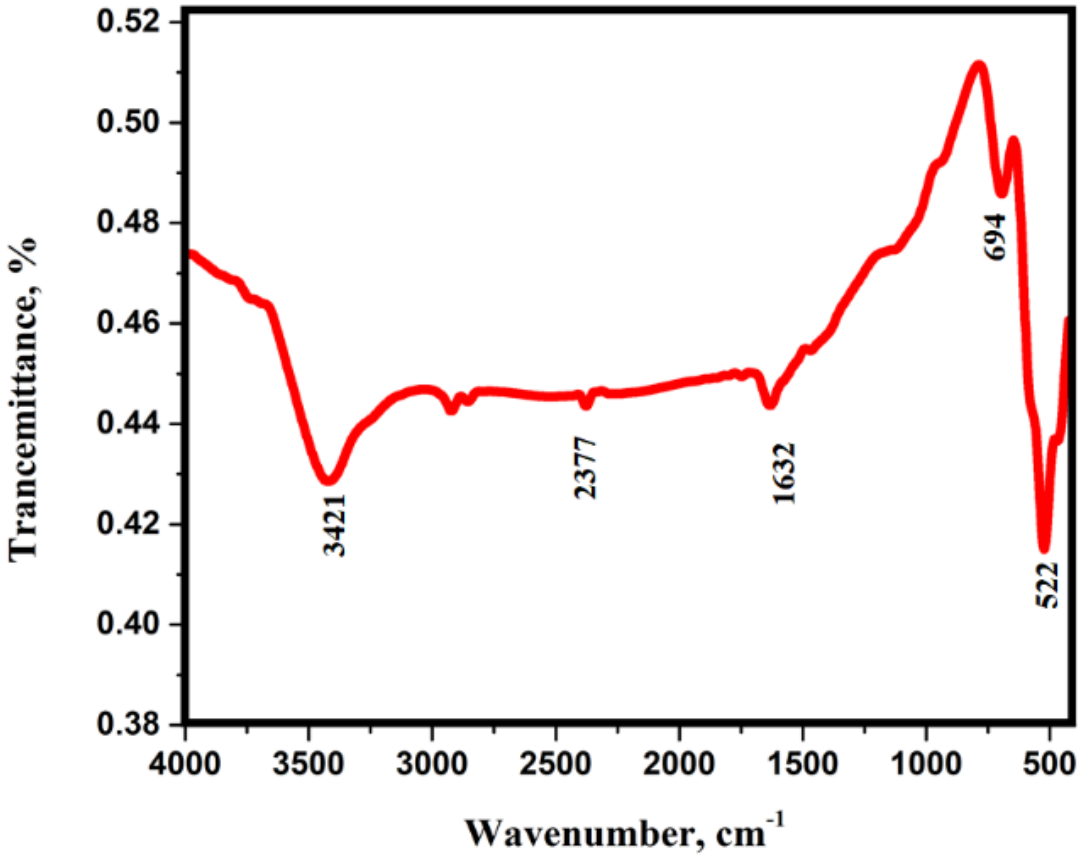

Figure 5.4 the FT-IR spectra of the prepared nanocomposite α-MnO2-V2O5.

5.1.2 Electrochemical performance

Square wave voltammetry (SWV) was used to investigate the electrochemical behavior of bare CPE against α-MnO_2-V_2O_5 NRs-modified CPE platforms for the sensing of CTL in BR buffer of 7.0 pH using 0.10 mM of CTL, Figure 5.5a There are no detectable anodic or cathodic peaks in the absence of CTL, which indicates electrochemical inactivity of the utilized sensor platform in the working potential window. For bare CPE, the anodic oxidation peak current of CTL was 24.99 µA at 756.02 mV. Upon the use of α-MnO_2-V_2O_5 NRs, the peak current of the anodic oxidation

was drastically increased to 65.88 µA at 748.08 mV, revealing the facile oxidation of CTL. Before forming the composite, the oxidation occurred at the beak current of 38.11 µA for α-MnO_2 and 54.54 µA for V_2O_5, which indicates the superiority of the formed composite in the catalysis of the reaction. Thus, α-MnO_2-V_2O_5 NRs/CPE can be utilized for the sensitive lower potential detection of CTL. Furthermore, α-MnO_2-V_2O_5 NRs/CPE has shown to possess the highest electrochemical activity towards CTL, good conductivity, and a high rate of electron transfer. The electroactive surface area of the prepared α-MnO_2-V_2O_5 NRs/CPE sensor platform was estimated by cyclic voltammetry by using a 5.0 x10^{-3} M $K_3Fe(CN)_6$ in 0.10 M KCl and recording the current vs voltage peak at various scan rates, using the Randles-Ševčík equation for a quasi-reversible reaction as in equation 5.1[416]:

$$I_p = 2.65 \times 10^5 n^{\frac{3}{2}} A D^{\frac{1}{2}} C \nu^{\frac{1}{2}}$$

Equation 5:1

where I_p is considered as the peak current, n is the number of electrons involved in the electrochemical anodic oxidation, D is the diffusion coefficient, C is the redox probe concentration, A is the electrochemical surface area of the electrode, and ν is the applied scan rate. The D value for $K_3Fe(CN)_6$ is 7.6 x 10^{-6} cm^2 s^{-1}.[417] From the slopes of the I_p vs. $\nu^{1/2}$ plot and using Eq. 5.1, the electrochemical surface area was estimated to be 31.67 and 66.69 cm^2 for CPE and α-MnO_2-V_2O_5 NRs/CPE, respectively.

Utilizing the electrochemical impedance spectroscopy, many electrochemical properties of the material can be explored, including the kinetics of the reaction, the mass transport, and the charge transfer coefficient as shown in Figure 5.5b. These measurements were conducted in a 1:1 solution of 5.0 mM $K_3Fe(CN)_6$ and 0.1 M KCl. Note that the charge transfer resistance at the electrode interface (R_{CT}) can be estimated from the diameter of a semi-circle in the high-frequency regime.

Henceforth, the proposed material enhanced the charge transfer at the modified electrode compared to α-MnO_2, V_2O_5, and bare CPE counterparts as analyzed by Nyquist plots. Upon fitting the data, the R_{CT} of the semi-circle was estimated to be 5857 Ω at the CPE, which was decreased to 800 Ω for the α-MnO_2-V_2O_5 NRs-modified CPE. Before the formation of the composite, the R_{CT} of the semi-circle was 1670 Ω for the V_2O_5 NPs and 3135 Ω for α-MnO_2 NPs, Which indicated the enhanced conductivity of the formed composite in comparison to the parent two metal oxides. Thus, the EIS data are in agreement with the SWV findings, revealing that α-MnO_2-V_2O_5 NRs possess better electron conduction than the bare electrode due to its interactive nature. Using square wave voltammetry, the electrochemical activity of α-MnO_2-V_2O_5 nanocomposite/ CPE was compared to bare CPE in 1.0 mM $K_3Fe(CN)_6$ in 0.1 M KCl solution. As illustrated in Figure 5.5c, the oxidation peak for α-MnO_2-V_2O_5 nanocomposite/ CPE was 3.95 times higher than that of bare CPE. Moreover, the use of α-MnO_2-V_2O_5 nanocomposite enhanced the electron transfer on the surface of the electrode, as the peak separation (E_{Pa}-E_{Pc}) was enhanced from 405 mV in α-MnO_2 NPs to 160 mV in α-MnO_2-V_2O_5 indicating the enhanced electron transfer in the formed composite[418].

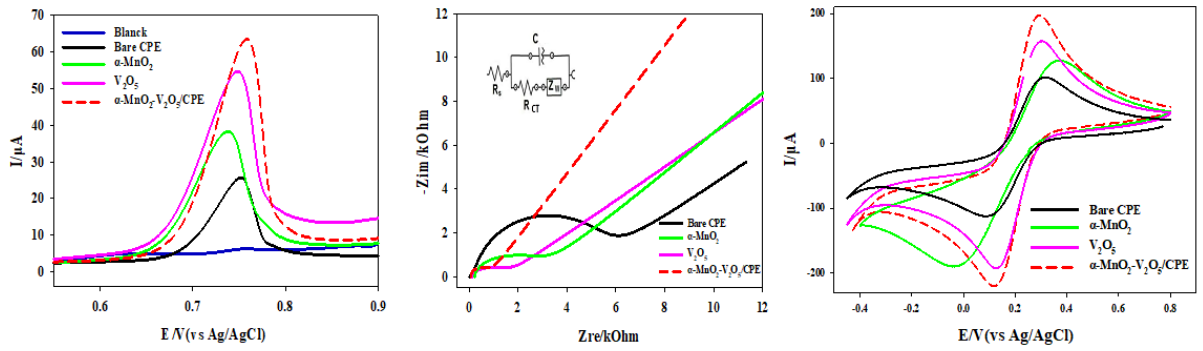

Figure 5.5(a) Square wave voltammogram of 0.10 mM of CTL in BR Buffer (pH 7.0) at the scan rate of 100.00 mV s^{-1}, (b) impedance in 1.0 mM $K_3Fe(CN)_6$ in 0.10 M KCl, and (c) cyclic voltammograms of 5.00 x10^{-3} M $K_3Fe(CN)_6$ in 0.1 M KCl at the scan rate of 100.00 mV s^{-1} showing a comparison between bare CPE, α-MnO_2, V_2O_5, and α-MnO_2-V_2O_5/CPE.

5.1.3 Effect of pH

The effect of pH of the electrolyte of on the electrochemical anodic oxidation of CTL was studied using square wave voltammetry in the pH range of 2.0- 10.0 as shown in Figure 5.6 Upon increasing the electrolyte pH, there was a notable negative shift in the peak potential, which can be ascribed to the dependence of the reaction on the protonation-deprotonation process during the electrochemical oxidation of CTL, in accordance with Nernst equation[419]. Upon increasing the pH gradually from 2.0- 10.0 using BRB buffer, the anodic oxidation peak increased gradually until pH 7 then decreased due to the poor solubility of CTL in alkaline pH. Therefore, pH 7 was used for further investigation of CTL as it gives the highest anodic oxidation peak and it mimics the physiological pH of the blood. Analysis of the voltammetric response in terms of the peak potential (E_p) manifests a linear relationship with the change of the electrolyte pH as: E_p (V) = 0.9907- 0.0297 pH, (R^2 = 0.9958). As the pH of the electrolyte increased, the voltammetric profile changes accordingly. Furthermore, the best line fit of data (29.7 mV per unit pH at 25 ºC) is following the Nernstian behavior, which indicates that the electrochemical oxidation reaction involves two protons and one electron transfer as suggested in Figure 5.1.

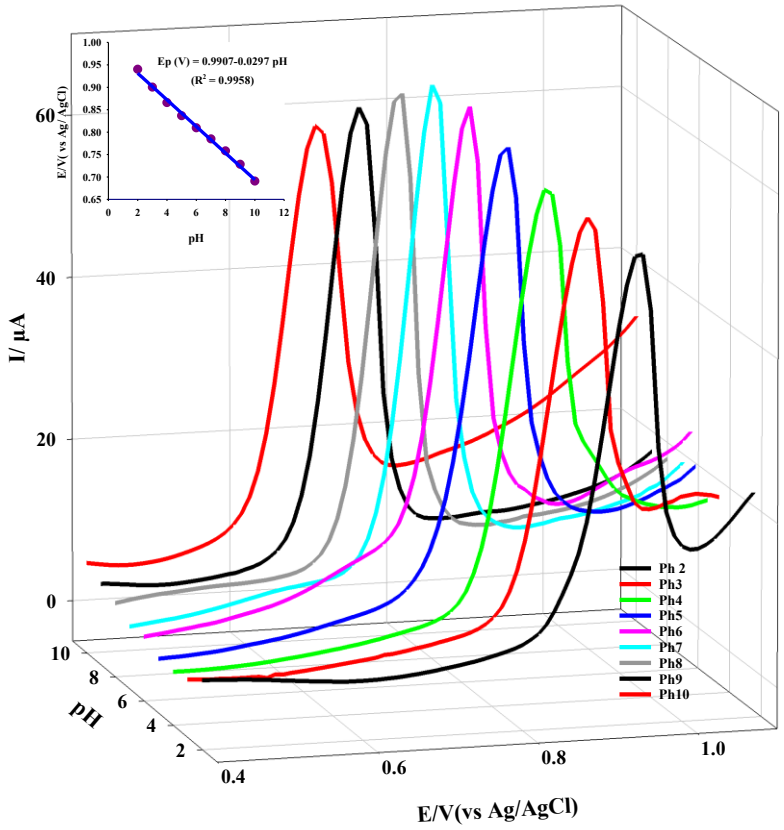

Figure 5.6 Square Wave Voltammograms of 0.10 mM CTL at different pH values using α-MnO_2-V_2O_5 nanocomposite and a Scan rate of 0.1 V s^{-1}. The inset shows a plot of the anodic peak potential of CTL versus pH change.

5.1.4 Effect of scan rate

The influence of scan rate on the electrochemical anodic oxidation mechanism of 0.1 mM CTL on α-MnO_2-V_2O_5 nanocomposite/CPE is investigated. The irreversible electrochemical oxidation was obvious as the peak potential (E_p) becomes more shifted towards the positive value at lower scan rates. A linear relationship was obtainable by plotting the peak current (I_p) against the square root of the scan rate ($v^{1/2}$): I_p (µA) = 6.5029 $v^{1/2}$+ 2.4716 µA, where the correlation factor equals 0.9990, Figure 5.7a. The linear relationship indicates that the anodic oxidation process is a diffusion-controlled process. A direct proportionality was found between log I_p and log v in the range of 10 – 200 mV s^{-1} as: log I_p (µA) = 0.4943 mV s^{-1} + 0.8431 µA, see Figure 5.7b.

Note that the slope was less than 0.5, which indicates that the electrochemical oxidation is a diffusion-controlled process, revealing the sufficiency of using α-MnO_2-V_2O_5 NRs[420]. The results imply that the electrochemical oxidation reaction of CTL on α-MnO_2-V_2O_5/CPE is a diffusion-controlled process. Furthermore, the peak potential shifts towards the positive direction as we increase the scan rate, which indicates the kinetic limitation in the reaction between the drug and the electrode surface[421].

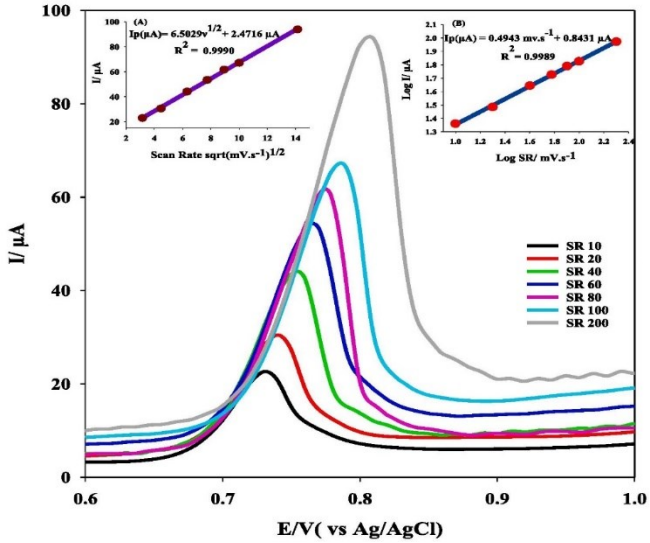

Figure 5.7 Square wave voltammograms of 0.10 mM CTL in pH 7.0 BR buffer using α-MnO_2-V_2O_5 nanocomposite/CPE sensor recorded at various scan rates (10–200 mV s^{-1}). Insets: (A) a plot of peak current vs. scan rate and (B) a plot of log I_p and log ν.

5.1.5 Analytical performance and method validation

The accredited guidelines of the International Conference on Harmonization (ICH) for validation of analytical methods were adopted for the validation of the proposed sensing protocol[422]. Square wave voltammetric studies were implemented using α-MnO_2-V_2O_5 nanocomposite/CPE surface in BR buffer of pH 7.0 containing different concentrations of CTL. The calibration curve was constructed by considering the pivotal practical range, based on the

normal tablet concentration of CTL in its pharmaceutical formula, in order to achieve accuracy, precision, and linearity. The square wave voltammograms (SWVs) are illustrated in Figure 5.8 along with the calibration plot (inset of Figure 5.8). SWV of α-MnO_2-V_2O_5 nanocomposite/CPE electrode in B–R buffer at a scan rate of 100 mV s^{-1} solution (pH 7.0) containing different concentrations of CTL showed a calibration range of 1.11×10^{-7} to 2.7×10^{-5} M CTL, see **Table 5-1**. The analytical characteristics of the proposed sensor platform show oxidation peak currents of CTL using α-MnO_2-V_2O_5 nanocomposite/CPE, which are dependent on the concentration of CTL in the electrolyte. The peak currents exhibited a linearity over the concentration range of 1.11×10^{-7} to 2.7×10^{-5}M (I_p (μA) = 1.6315 μM + 4.8569 μA, R^2 = 0.9986). Moreover, the limit of detection (LOD) of this platform was estimated using the equation 5.2, where SD is the standard deviation of the peak currents of CTL oxidation for a number of trials (n) that is equal to 5, and x is the slope of the calibration curve. The calculated LOD was 2.482×10^{-8} M. The limit of quantification (LOQ) was calculated using the equation 5.3, which was found to be 8.265×10^{-8} M.

$$LOD = \frac{3\,SD}{x}$$

Equation 5:2

$$LOQ = \frac{10\,SD}{x}$$

Equation 5:3

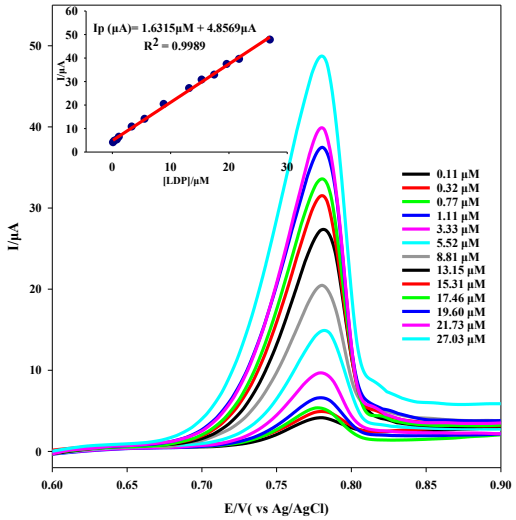

Figure 5.8 Square wave voltammogram for various concentrations of CTL (0.11 - 100 μM) in pH 7.0 of BR buffer at the scan rate of 100 mV s^{-1} using α-MnO_2-V_2O_5 nanocomposite /CPE while the inset shows the calibration curve of CTL in pH 7 of BR buffer.

Table 5-1. Analytical parameters for the determination of CTL in B-R buffer pH 7.0 using α-MnO_2-V_2O_5 nanocomposite /CPE via the proposed SWV method.

Analytical parameter	**SWV method**	
	Standard	Plasma
Linear concentration range (M)	1.11×10^{-7}– 2.70×10^{-5}	3.33×10^{-7} - 1.70×10^{-5}
Intercept (μA)	4.8569	6.2908
Slope (μA μM^{-1})	1.6315	1.5306
Standard deviation of intercept (μA)	0.064	0.043
Standard deviation of slope (μA μM^{-1})	0.051	0.065
Coefficient of determination (R^2)	0.9989	0.9999
LOD (M)	1.17×10^{-8}	2.07×10^{-6}
LOQ (M)	8.265×10^{-8}	6.89×10^{-6}

The repeatability of the adopted method was assured by analyzing the sample five times using its pure form. As shown in **Table 5-1**, the RSD values assure the good reproducibility of our proposed electrochemical platform. Consequently, in order to determine the mean precision of the method, the same procedures were repeated within five consecutive days as can be seen in **Table 5-1**, which indicates good values for the developed sensor. Moreover, plasma samples of CTL were tested in order to investigate the applicability of the proposed platform. Henceforth, a calibration curve of the elucidated current against the CTL concentration in plasma was constructed as illustrated in Figure 5.9 The plasma calibration curve exhibited a straight line in the range of 0.33×10^{-7} - 2.70×10^{-5} M with $R^2 = 0.9999$, achieving LOD and LOQ of 2.07×10^{-7} M and 6.89×10^{-7} M, respectively (undetectable in urine). Thus, it is crystal clear from these results that a wide concentration range of CTL can be determined using the SWV method.

5.1.6 Reproducibility and stability of α-MnO_2-V_2O_5 NRs Nanocomposite.

The reproducibility of the proposed sensor platform was assessed using five electrodes as proposed in the experimental part. The Relative standard deviation of the peak current is 1.95 % for 1.00×10^{-4} M CTL, revealing a good reproducibility of the fabrication procedure. The repeatability of the proposed electrode was examined by performing the experiment 5 times for the electrochemical determination of the same solution concentration (1.00×10^{-4} M CTL). The RSD of the I_p was calculated to be 1.41 %, indicating excellent repeatability of the sensor platform. The paste was stored with exposure to air for three weeks and the oxidation peak achieved 99.20% of its original response in 1.00×10^{-4} M CTL. Thus, the sensor is appropriate for routine analysis of CTL.

5.1.7 Interference studies

The selectivity of the suggested sensor platform to CTL was assessed by the presence of uric acid that is considered an abundant molecule in the human body. Both uric and ascorbic acids are normally existing metabolites within urine and plasma, which can interfere with the detection of the drug electrochemically[423]. The use of α-MnO_2-V_2O_5 nanocomposite helped in the appearance of the uric acid peak in comparison to bare CPE. The square wave voltammogram showed well-defined and separated oxidation peaks of ascorbic acid, uric acid, and CTL at 340.06, 589.96, and 749.29 mV, respectively. Other substances that are present within pharmaceutical formulations and can interfere with the determination of CTL were investigated electrochemically, including magnesium stearate, stearic acid, talc powder, potassium sorbate, methylcellulose, povidone-iodine, starch, colloidal silicon oxide, croscarmellose, mannitol, gums, dextrin, inulin, pectin, agar, carboxy-methyl cellulose, titanium dioxide, and microcrystalline cellulose that exist as excipients in the pharmaceutical formulations in addition to some cations that include Cu^{2+}, Zn^{2+}, Mn^{2+}, Mg^{2+}, and Na^{+}. These materials were assessed in the presence of 10 μM in BRB of pH 7. None of these excipients were found to interfere with the electrochemical detection of CTL in solution with a tolerance limit of less than ± 5.0% for each excipient.

5.1.8 Analytical application

Using the standard addition method, various CTL concentrations were electrochemically detected, see **Table 5-2**. The recovery percentages for the detection of CTL in both dosage form and plasma samples are denoting a good precision of the proposed platform. The experimental results indicate that the sensor platform has excellent potential for the detection of CTL in both dosage form and plasma samples, as could also be seen in Figure 5.9.

Table 5-2 Application of SWV for the determination of CTL in plasma and dosage form.

Pharmaceutical formulations	Amount added (μM)	Amount found (μM)	Recovery%
Pletaal® (100mg/tab)	0.22	0.22	99.26
	0.77	0.76	99.73
	5.50	5.51	100.22
	13.15	12.92	98.32
	17.46	17.31	99.18
	21.73	21.82	100.45
	27.027	26.65	98.62
Mean ± S.D			99.40±0.78
Plasma	0.33	0.33	100.33
	0.44	0.45	102.12
	8.80	8.78	99.81
	13.15	13.20	100.37
	17.46	17.28	98.96
	21.73	21.63	99.53
	27.027	27.00	99.91
Mean ± S.D			100.15±0.99

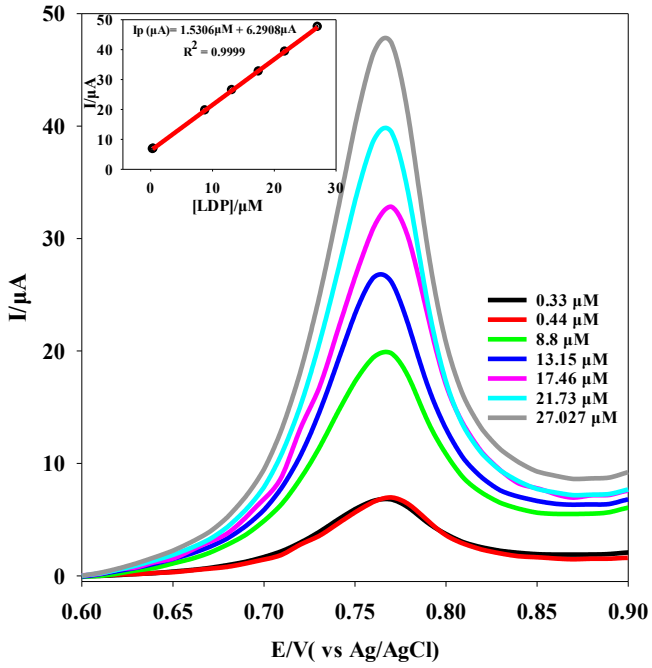

Figure 5.9 Square wave voltammogram for various concentrations of CTL in spiked plasma samples (0.33 - 100 μM) in pH 7.0 of BR buffer at the scan rate of 100 mV s^{-1} using α-MnO_2-V_2O_5 nanocomposite /CPE while the inset shows the calibration curve of CTL in spiked plasma samples in pH 7 of BR buffer.

5.1.9 Previous studies

In comparison to previous studies, there was only one report on the electrochemical sensing of CTL. Our method reported a wider range of detection with a wider linearity, a lower limit of detection, and quantification on the surface of the modified electrode in comparison to the previously reported method, see **Table 5-3**. Moreover, our method is considered to be much cheaper and enjoys a simpler preparation method.

Table 5-3 Comparison between previous reports and our findings.

Methods	Electrode	Modifier	pH	LWR	Detection limit	Verification in real samples	Ref.

CV/SWV	GCE	Bismuth NPs/ MWCNTs	2.5	2.16×10^{-6} – 3.51×10^{-5} M	2.057 μM	Plasma/dosage form	38
SWV/EIS	CPE	α-MnO_2-V_2O_5 NRs	7.0	1.11×10^{-7} – 2.70×10^{-5} M	0.248 nM	Plasma/dosage form	This study

5.2 Sensitive Determination of SARS-COV-2 and Anti-Hepatitis C Virus Agent Velpatasvir Enabled by Novel Metal-Organic Frameworks

The surface amine groups were sacrificed to modify the surface of the parent MOF via the reaction of 5-bromosalicylaldehyde ligand with the amino groups, resulting in the formation of salicylidene (R–N=C–$C_6H_4OH(Br)$) moiety as a bidentate ligand, Figure 5.10.

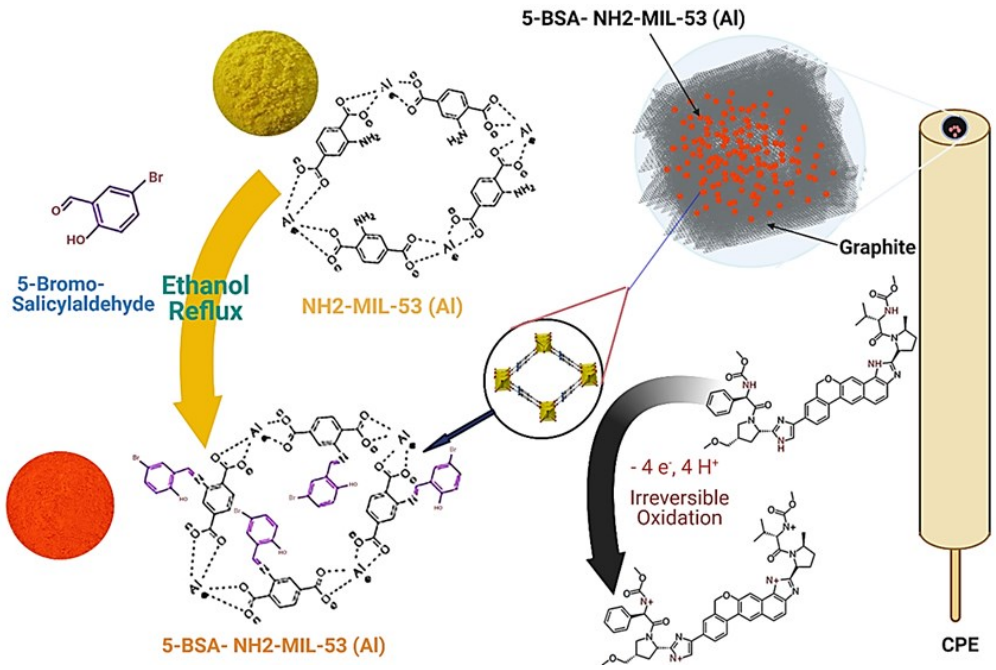

Figure 5.10 Schematic of the preparation of 5-BSA-NH_2-MIL- 53(Al) and the suggested oxidation mechanism of VLP.

5.2.1 Surface and electrochemical characterization of the fabricated sensors

Figure 5.11a,b depicts the FESEM images of NH_2-MIL-53(Al) and 5-BSA-NH_2-MIL-53(Al), respectively. The images reveal a sheet-like with a mean side length of ~118±2 nm. Note that the addition of 5-bromosalicylaledhyde does not result in a profound change in the morphology of the material. To elucidate the crystal structure and phase purity of the NH_2-MIL-53(Al) MOF and 5-BSA-NH_2-MIL- 53(Al) materials, x-ray diffraction (XRD) spectra were recorded as depicted in Figure 2c. The XRD spectra of both NH_2-MIL-53 (Al) and 5-BSA-NH_2-MIL- 53(Al) indicate similar peaks at 2θ = 8.8°, 10.5°, 15.08°, 17.5°, 20.2°, and 26.4° [424–426]. Hence, 5-BSA-NH_2-MIL- 53(Al) and NH_2-MIL-53(Al) possess the same crystalline structure with no change upon imine formation. However, the broadness of the XRD peaks of NH_2-MIL-53(Al) reveals a smaller crystallite size.[47]

The BET adsorption isotherm of NH_2-MIL-53(Al) depicted in Figure 2d reveals type IV isotherm. The steep increase upon increasing the relative pressure in the low-pressure region indicates microporous structure [427,428], while the hysteresis loop in the high-pressure region reveals mesoporous characteristics [429,430]. The BET surface area of NH_2- MIL-53(Al) was estimated to be 794 $m^2.g^{-1}$, which is decreased to 652 $m^2.g^{-1}$ for the 5-BSA-NH_2-MIL- 53(Al) counterpart, revealing the preservation of free -NH_2 within the NH_2-MIL-53(Al). The non-local density functional theory (NLDFT) method was used to determine the cumulative pore volume of 5-BSA-NH_2-MIL- 53(Al) and NH_2-MIL-53 (Al). Comparatively, the pore volume of the prepared 5-BSA-NH_2-MIL- 53(Al) (1.111 cm^3/g) was found to be lower than the parent NH_2- MIL-53(Al) MOF (1.407 cm^3/g). This decrease in both the surface area and pore volume is indicative of the successful post-synthetic imine formation. The pore radius as estimated from the BJH model for 5-BSA-NH_2-MIL- 53(Al) and NH_2-MIL-53(Al) were found to be 1.89 and 1.99 nm, respectively. Therefore, the micropore diameters of the 5-BSA-NH_2-MIL- 53(Al) and NH_2-MIL- 53(Al) seem to be distributed within this range. The FTIR spectra (Figure 5.11) of both 5-BSA-NH_2-MIL-53(Al) and NH_2-MIL-53(Al) reveal -NH_2 symmetric and asymmetric stretches of NH_2-BDC ligand at 3492 and 3384 cm^{-1} [431]. However, the peaks at 3501 and 3384 cm^{-1} assigned to the N-H were diminished in the case of 5-BSA-NH_2-MIL- 53(Al), indicating the formation of the imine group upon the reaction of the amine of the NH_2-BDC ligand with the aldehyde group of the 5-formylsalicylaldehyde ligand [431,432].

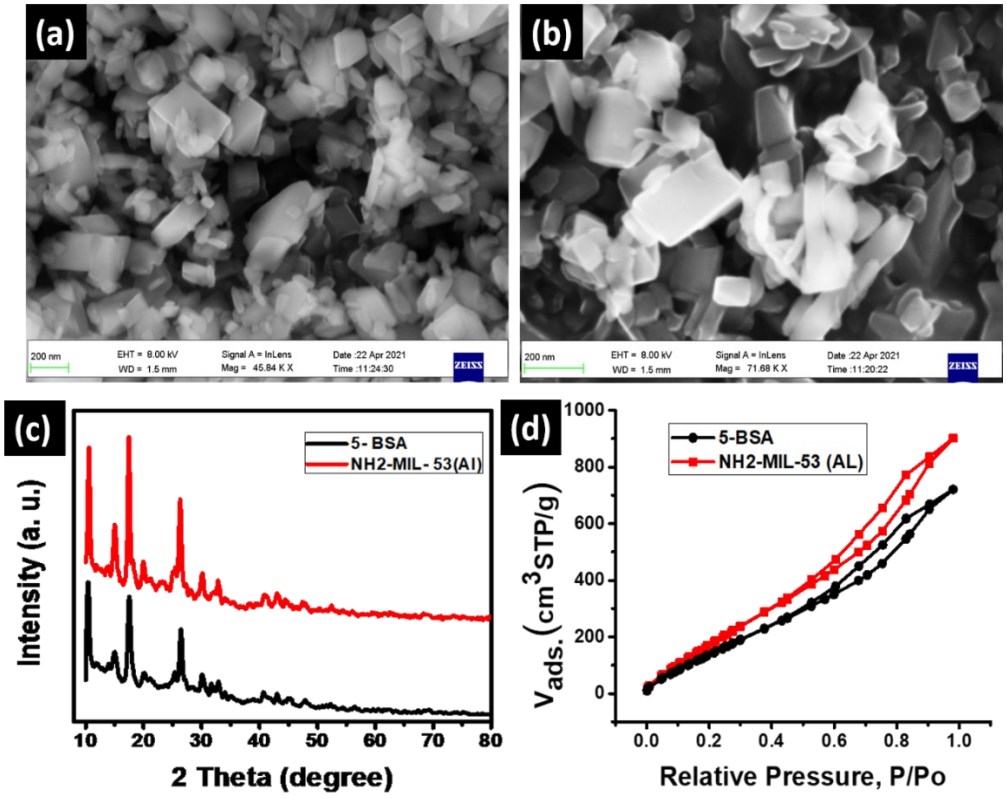

Figure 5.11FESEM images of (a) NH_2-MIL-53 (Al) and (b) 5-BSA-NH_2-MIL- 53(Al), (c) XRD of both NH_2-MIL-53(Al) and 5-BSA-NH_2-MIL- 53(Al), and (d) BET adsorption-desorption isotherms of NH_2-MIL-53(Al) and 5-BSA-NH_2-MIL- 53(Al).

5.2.2 Electrochemical performance

The square wave voltammetry (SWV) technique was utilized to elucidate the electrochemical performance of bare CPE compared to 5-BSA-NH_2-MIL- 53(Al) -modified CPE for the electrochemical oxidation of VLP in Britton-Robinson Buffer (BRB) pH 7.0 using 1.0×10^{-3} M VLP, Figure 5.12 a. Neither anodic nor cathodic beaks were detected in the absence of VLP, which demonstrates that our sensor platform has no electrochemical activity in the working potential window. For the unmodified CPE, the I_p of the electrochemical oxidation of VLP was 14.03 µA at 8820 mV, which is greatly increased to 36.12 µA at 8226 mV upon the modification of bare CPE with 5-BSA> This enhancement in I_p reveals the facile oxidation of VLP on the

modified electrode, revealing the necessity of using 5-BSA-NH_2-MIL- 53(Al) for the sensitive lower potential detection of VLP.

The electrochemically active surface area of the 5-BSA-NH_2-MIL- 53(Al)-modified CPE was estimated from the Cyclic Voltammogram (CV) using the Randles-Ševčík equation (Equation 5.1). For a quasi-reversible reaction in a 1:1 solution of 1.0×10^{-3} M $K_3Fe(CN)_6$ and 0.10 M KCl and recording the current was elucidated vs peak potential at various scan rates [416].

where I_p is the peak current, n is the number of electrons involved in the electrochemical anodic oxidation, D is the diffusion coefficient, C is the redox probe concentration, A is the electrochemical surface area of the electrode, and v is the applied scan rate. The D for $K_3Fe(CN)_6$ was taken as 7.6×10^{-6} $cm^2 .s^{-1}$ [416]. The electrochemically active surface areas of the bare CPE and the 5-BSA-NH_2-MIL- 53(Al)-modified CPE were 0.067 and 0.338 cm^2 as calculated from the slopes of the I_p vs $v^{1/2}$ graphs.

Utilizing the electrochemical impedance spectroscopy (EIS) diagrams (Figure 5.12 b), reaction kinetics, mass transport, and charge transfer coefficient through the electrode surface were inspected using a 1:1 solution of 1.0×10^{-3} M $K_3Fe(CN)_6$ in 0.1 M KCl. Note the quasi-circle in the high-frequency window, where the diameter of the semi-circle enables the estimation of the charge transfer resistance at the electrode/electrolyte interface (R_{CT}). The Nyquist plot reveals a Warburg-type equivalent circuit model. Thus, modifying the CPE with the proposed MOF enhances the charge transfer compared to the unmodified CPE. Upon fitting, the R_{CT} of the bare CPE was found to be 4400 Ω that was sharply decreased to 1541.13 Ω upon modification with 5-BSA-NH_2-MIL-53(Al), which can be attributed to the large surface area of the MOF and its interactive nature that enhances electron transfer. Moreover, the electrochemical activity of bare CPE was compared to that of 5-BSA-NH_2-MIL- 53(Al)/CPE electrode in a 1:1 solution of $1.0 \times 10^{-}$

^{3} M $K_3Fe(CN)_6$ in 0.1 M KCl as illustrated in Figure 5.12 c. The anodic peak current value of the 5-BSA-NH_2-MIL- 53(Al)/CPE electrode was almost five multiple times that of bare CPE. Furthermore, the use of 5-BSA-NH_2-MIL- 53(Al)/CPE decreased the peak separation ($E_{p\ anodic}$-$E_{p\ cathodic}$) significantly from 0.32 to 0.17 V in comparison to bare CPE, revealing enhanced electron transfer [418]. Therefore, 5-BSA-NH_2-MIL- 53(Al) has a good catalytic activity towards the electrochemical oxidation of VLP, good conductivity, and a high rate of electron transfer.

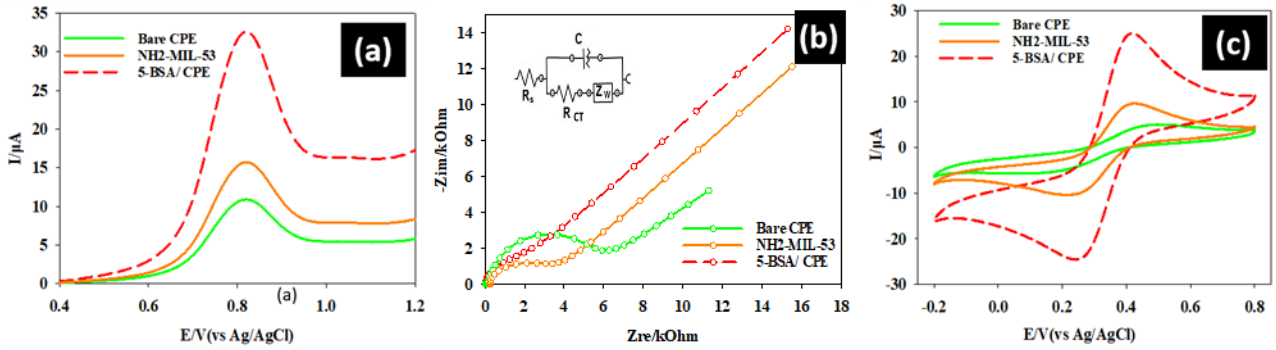

Figure 5.12 (a) square wave voltammograms (SWV) of 0.1 mM of VLP in BR Buffer (pH 7.0) at the scan rate of 0.1 V.s^{-1}, (b) impedance plots at a scan rate of 0.1 V.s^{-1} in 1.0 mM K_3Fe $(CN)_6$ in 0.1 M KCl, and (CV of 1.0 mM K_3Fe $(CN)_6$ in 0.1 M KCl at the scan rate of 100 mV.s^{-1}.

5.2.3 Effect of pH

The effect of pH on the electrochemical anodic oxidation of VLP was assessed in the pH range of 2.0 to 10.0 as shown in Figure 5.13. Upon varying the pH of the solution from 2-10, the peak potential was shifted towards the zero potential, indicating the protonation-deprotonation electrochemical reaction of VLP [419]. Plotting the peak potential (E_p) versus the buffered solution pH, the voltammetric response of VLP can be assessed as E_p (V) = 1.2703-0.0598 pH, (R^2 = 0.9990). It was found that the slope of the obtained linear relationship is near to the known Nernstian value of a one electron-one proton electrochemical oxidative reaction, as indicated in Figure 5.13, which is 59.0 mV per pH unit at ambient temperature. Utilizing the Nernestian

behavior of VLP electrochemical oxidation, the suggested mechanism of oxidation is depicted in Figure 5.10.

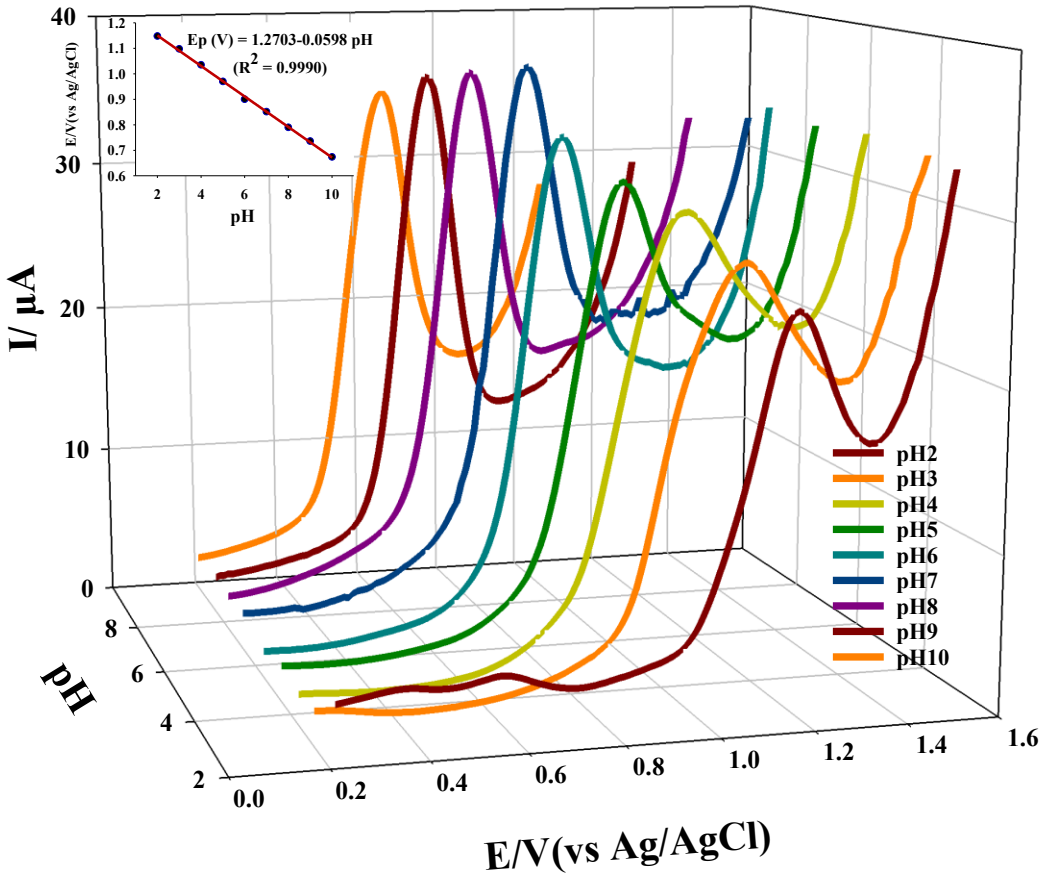

Figure 5.13 SWV of 0.1 mM of VLP at different pH values of BRB buffer using 5-BSA-NH_2-MIL-53(Al) at a scan rate of 0.1 $V.s^{-1}$. The inset linear graph shows the linear relationship between the solution pH and the peak potential (E_p).

5.2.4 Effect of scan rate

The effect of scan rate on the electrochemical anodic oxidation of VLP was also investigated using 5-BSA-NH_2-MIL- 53(Al)/CPE, Figure 5.14. Upon increasing the scan rate, the peak potential (E_p) is shifted into more positive values, indicating an irreversible electrochemical

behavior of VLP. A linear relationship was obtained by plotting the peak current (I_p) versus the square root of the scan rate ($\nu^{1/2}$) in the range of 0.010 – 0.100 Vs^{-1}. This indicates a diffusion-controlled process, as in equation I_p (μA) = 4.4194 $\nu^{1/2}$ (mV/s) + 2.7671 μA, R^2 = 0.9986, as illustrated in Figure 5.14, a. Furthermore, the slope of the relation between the algorithm of scan rate and the measured current was less than 0.5, log Ip (μA) = 0.4529 mVs^{-1}+ 0.7638 μA, R^2 = 0.9981, which supports the point that the anodic oxidation process is diffusion-controlled one, as in Figure 5.14, b. All of these findings necessitate the use of CPE modified with 5-BSA-NH_2-MIL-53(Al).

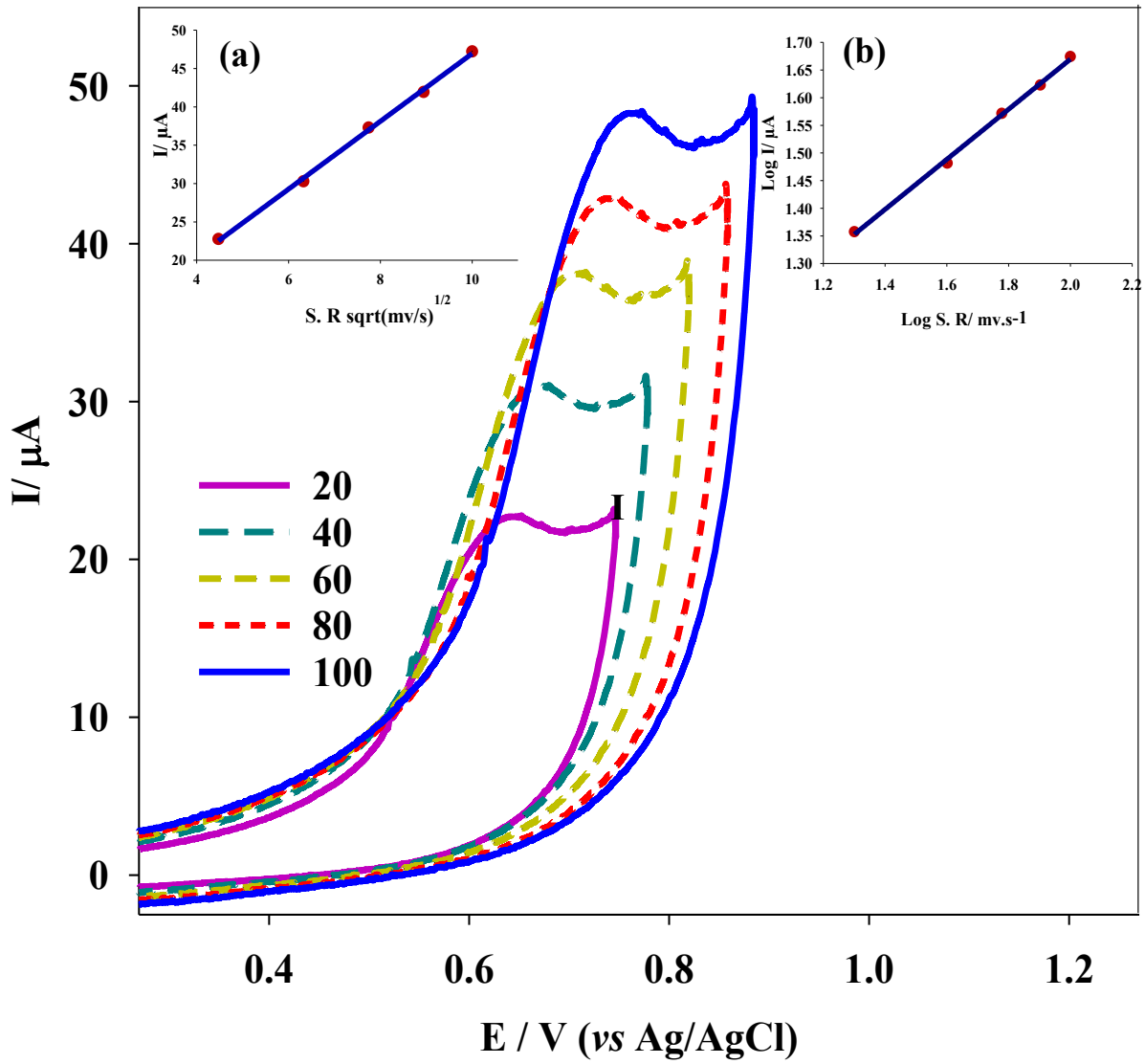

Figure 5.14 CV of 0.10 mM VLP at pH 7.0 using 5-BSA-NH_2-MIL- 53(Al)/CPE in a wide scan rate (0.010- 0.200 $V.s^{-1}$). Insets: (A) a plot of peak current vs. the square root of scan rate, and (B) a plot of the algorithm of peak current vs. the algorithm of scan rate.

5.2.5 Analytical performance and method validation

The proposed sensing protocol is optimized based on the accredited system of the International Conference on Harmonization (ICH) [422]. SWV scans using 5-BSA-NH_2-MIL-53(Al)/ CPE in Britton-Robinson Buffer of pH 7.0 containing several dilutions of VLP were

performed and analyzed. To achieve linearity, accuracy, and precision, the calibration curve was established taking into consideration the practical range of VLP in normal tablet concentration. The SWVs of these dilutions are shown in Figure 5.15. At a scan rate of 0.1 $V.s^{-1}$, VLP showed two linear behaviors based on its concentration in BRB. In the range of $1.11 \times 10^{-6} – 1.11 \times 10^{-7}$ M, the regression equation is I_p (μA)= 4.9059 C μM + 3.7830 μA, R^2 = 0.9954, while in the range of $1.11 \times 10^{-7} – 25.97 \times 10^{-6}$ M, the regression equation is I_p (μA)= 0.8388 C μM+ 8.2987 μA, R^2 = 0.9954. The main cause for the decrease in the slope of the second linear range of higher concentrations is the increase of the required energy for anodic stripping in addition to the ohmic drop in such high levels of VLP [135]. Furthermore, the limit of detection (*LOD*) and limit of quantification (*LOQ*) were calculated to be 8.776×10^{-9} and 2.924×10^{-8} M, respectively, as in equation 5.2 and 5.3.

where SD is the standard deviation of I_p of VLP anodic oxidation for 5 trials and x is the slope of the calibration curve.

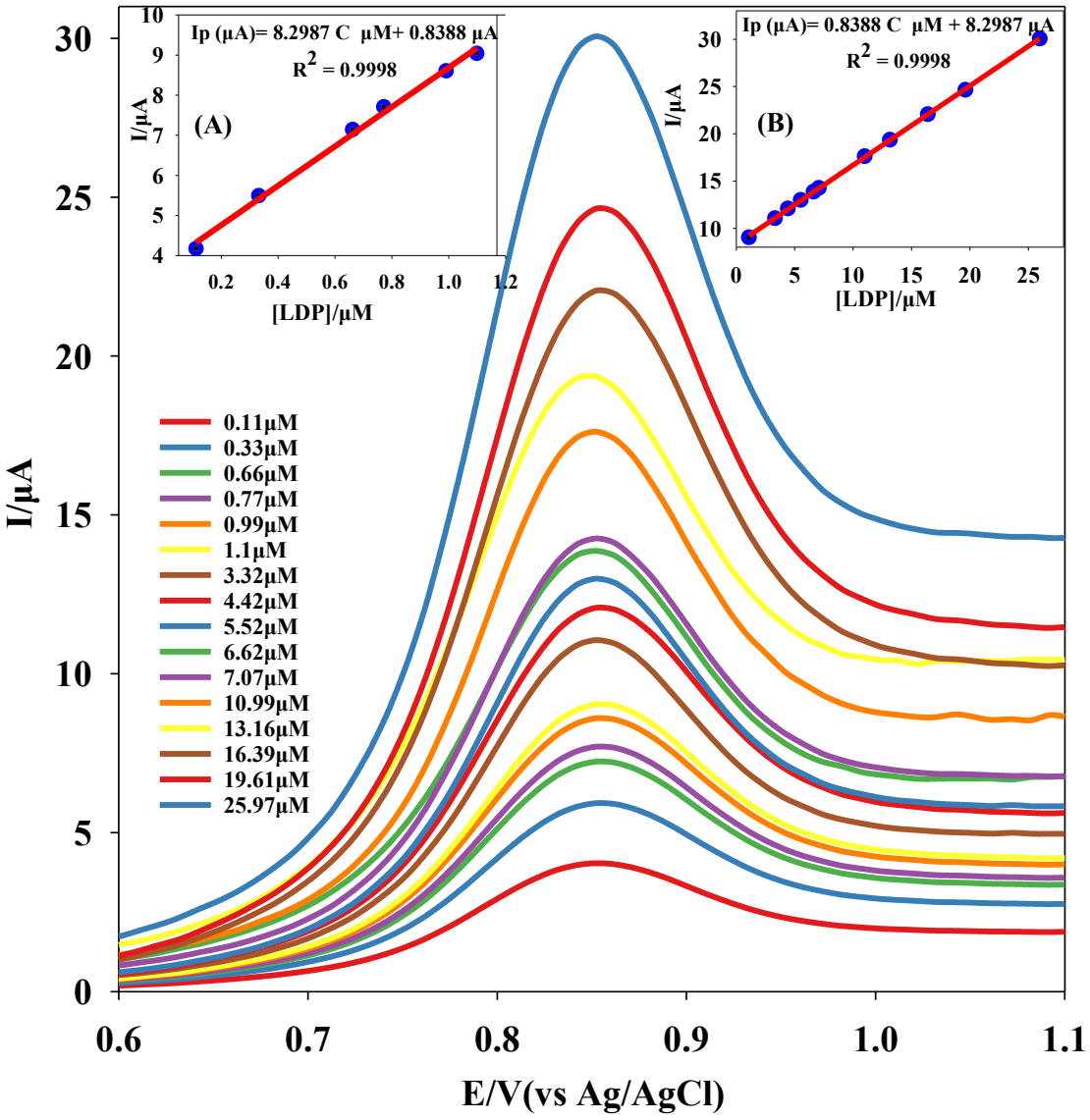

Figure 5.15 SWV of several dilutions of VLP (25.97 - 0.11 µM) in pH 7.0 Britton-Robinson buffer utilizing 5-BSA-NH_2-MIL- 53(Al)/ CPE sensor at a scan rate of 0.1 $V.s^{-1}$. The inset illustrates the plot of the peak current as a function of concentration in the range of 1.11 × 10^{-6} – 1.11 × 10^{-7} and 1.11 × 10^{-7} – 25.97 × 10^{-6} M.

5.2.6 Reproducibility and stability of α-MnO_2-V_2O_5 NRs Nanocomposite.

A sensor platform should possess three important characteristics, repeatability, storage stability, and reproducibility. Repeatability was tested by using the same electrode for 10 consecutive SWV scans against 0.10 mM VLP in pH 7.0 BRB and the relative standard deviation (RSD) was found

to be 2.47%, as in Figure 5.16a. Stability analysis was evaluated by storing the electrode at ambient temperature after scanning it in similar conditions and repeating the SWV scanning every week for 4 weeks as in Figure 5.16b. Reproducibility was examined by plotting the I_p for 7 CVs of different freshly prepared electrodes, as in Figure 5.16c, where the RSD was found to be 1.21%.

5.2.7 Analytical application

Utilizing the serial dilution method, vast concentrations of VLP in spiked plasma and urine samples have been determined electrochemically and compared to the added concentration in **Table 5-4.** The proposed 5-BSA-NH_2-MIL- 53(Al)/ CPE sensor reveals a good precision via the recovery results, which showed no apparent changes from the added values. According to the electrochemical studies, the sensor can determine VLP concentrations in plasma and urine samples, as shown in Figure 5.16.

Table 5-4 Application of SWV for the determination of VLP in plasma and urine samples.

Sample	Standard amount added (M)	Amount found (M)	Apparent recovery%
Plasma	1.11×10^{-7}	$1.08 \times 10^{-7} \pm 0.09$	102.78
	7.77×10^{-7}	$7.88 \times 10^{-7} \pm 0.08$	101.53
	1.11×10^{-6}	$1.13 \times 10^{-6} \pm 0.04$	98.23
	7.07×10^{-6}	$7.09 \times 10^{-6} \pm 0.08$	99.71
	16.40×10^{-6}	$16.37 \times 10^{-6} \pm 0.06$	100.18

	25.97×10^{-6}	$26.02 \times 10^{-6} \pm 0.10$	100.20
Urine	1.11×10^{-7}	$1.12 \times 10^{-7} \pm 0.07$	99.10
	7.77×10^{-7}	$7.68 \times 10^{-7} \pm 0.05$	98.87
	1.11×10^{-6}	$1.07 \times 10^{-6} \pm 0.09$	103.73
	7.07×10^{-6}	$7.12 \times 10^{-6} \pm 0.04$	99.29
	16.40×10^{-6}	$16.44 \times 10^{-6} \pm 0.10$	99.75
	25.97×10^{-6}	$26.10 \times 10^{-6} \pm 0.07$	100.05

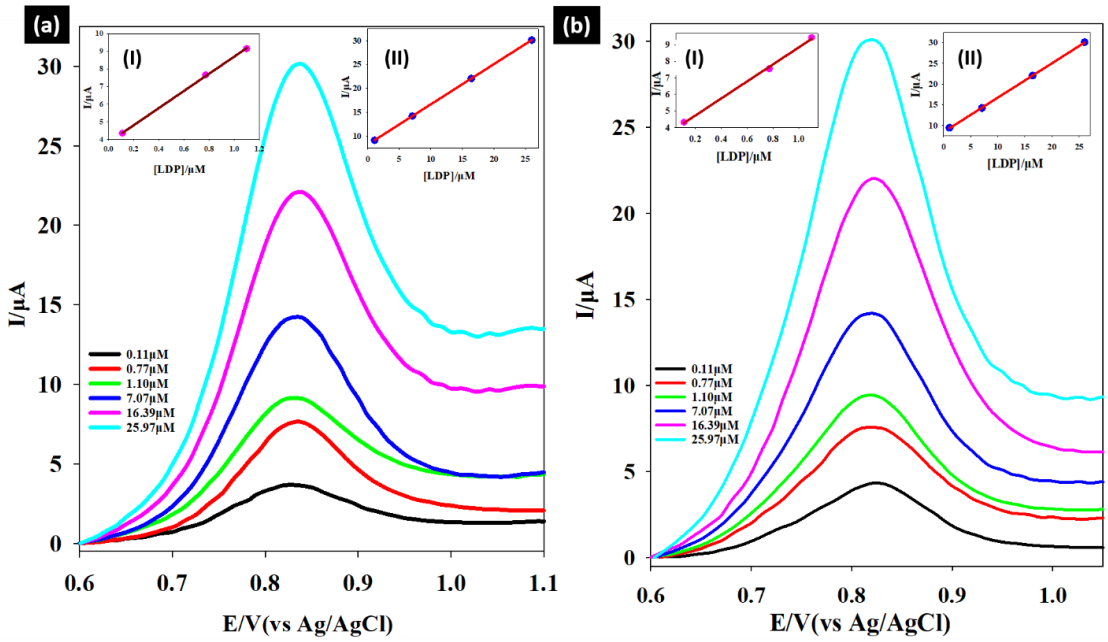

Figure 5.16 SWV for serial dilutions of VLP spiked (a) plasma samples and (b) urine samples 25.97 - 0.11 μM in pH 7.0 Britton-Robinson buffer utilizing 5-BSA-NH_2-MIL- 53(Al)/ CPE sensor at a scan rate of 0.1 $V.s^{-1}$. Insets illustrate the plot of the peak current as a function of concentration in the range of $1.11 \times 10^{-6} - 1.11 \times 10^{-7}$ and $1.11 \times 10^{-7} - 25.97 \times 10^{-6}$ M.

The selectivity of the proposed 5-BSA-NH_2-MIL- 53(Al)/ CPE sensor was determined in the presence of ascorbic acid as one of the prevalent elements in the plasma that can interfere with the electrochemical determination of some therapeutic elements[423]. The utilized 5-BSA-NH_2-MIL-53(Al)/ CPE sensor illustrated the ability to determine both ascorbic acid and VLP in the same pH 7.0 Britton-Robinson buffered solution as two separate peaks at 0.35 V and 0.85 V, respectively, as shown in Figure 5.17. Other excipients that are commonly used during tablet manufacturing and can interfere with VLP determination have been determined electrochemically in the presence of 1.0 mM of VLP at pH 7.0 Britton-Robinson buffered solution separately, as shown in Figure 5.17. Note that none of the tested materials obviously interfered with the detection of VLP in solution with a tolerance limit of less than ± 5.0% for each separate excipient. Therefore, we report a cheap and simple method for the electrochemical determination of VLP.

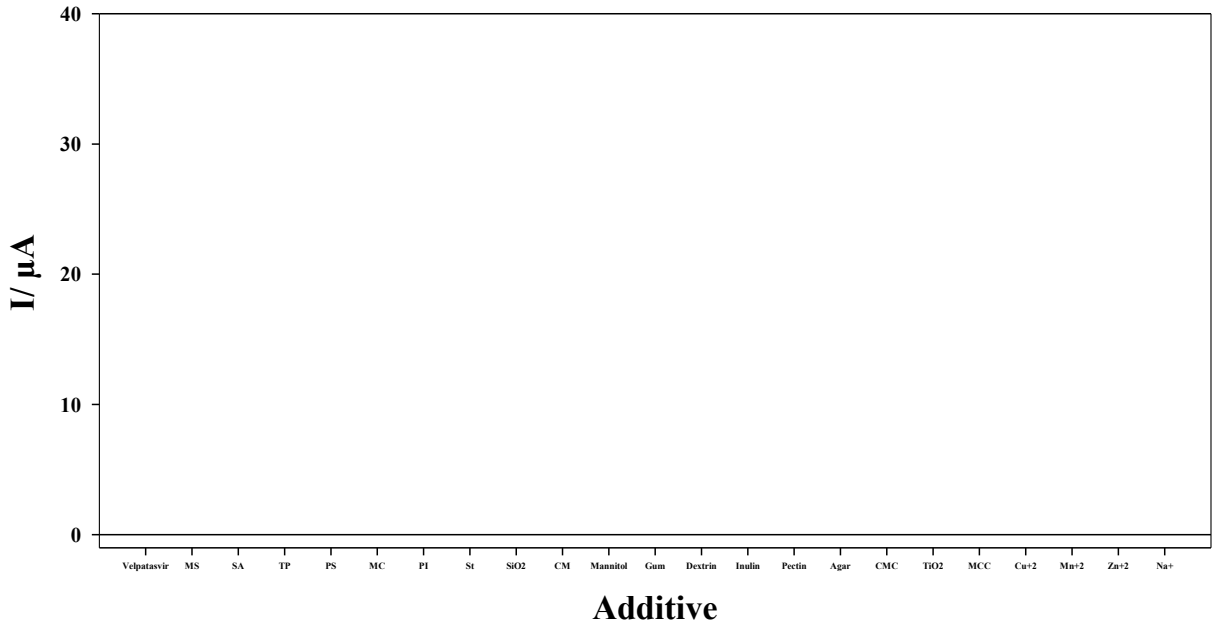

Figure 5.17 Obtained I_p of SWV of 0.10 mM VLP mixture with the most used excipients at pH 7.0 using 5-BSA-NH_2-MIL- 53(Al)/CPE at a scan rate of 0.1 $V.s^{-1}$.

5.3 VCM-Tracker apta-sensor for the detection of vancomycin

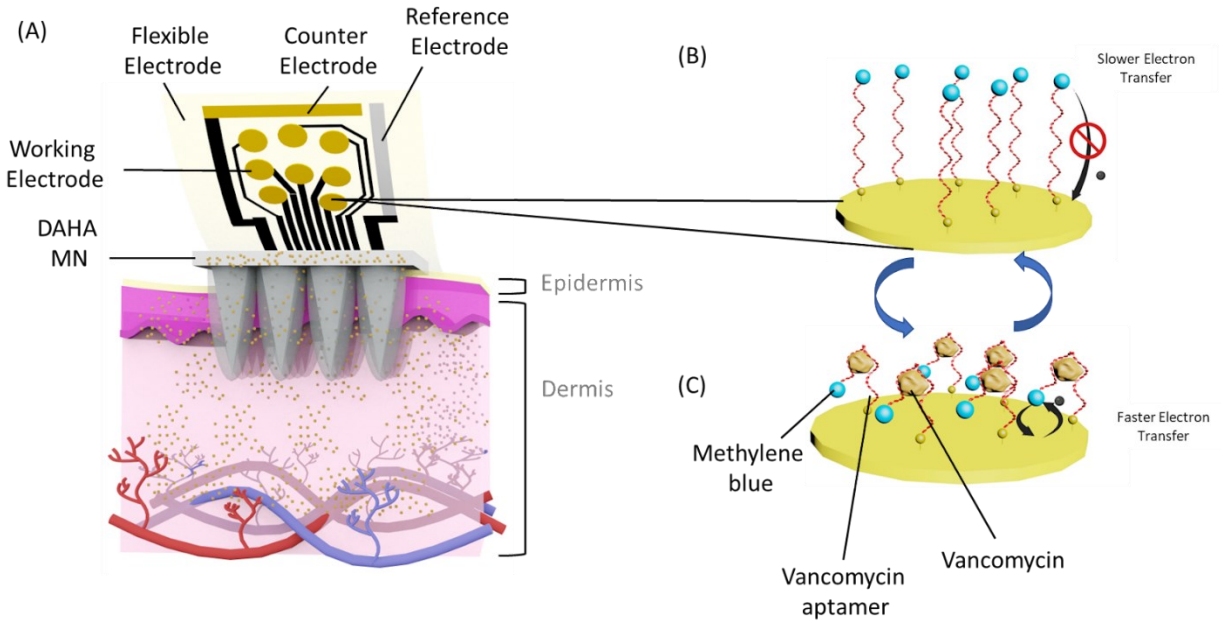

*Figure 5.18 Overview of the VCM-Tracker. (**A**) An illustration of VCM detection using DAHA-HMNs and flexible electrodes. HMNs penetrate into the dermis and VCM diffuses into the patch's needles where it can be measured by the flexible electrode. The flexible electrodes are composed of gold working and counter electrode, and silver/ silver chloride reference electrode. (**B**) the kinetics of the reduction reaction of aptamer-MB redox mediator in the absence of VCM and (**C**) in the presence of VCM.*

5.3.1 Vancomycin detection using flexible electrodes

First, we validated the VCM detection using the selected aptamer on gold rod as a working electrode. Square wave voltammetry (SWV) scans of various frequencies (10- 100 Hz) were conducted for six different concentrations (0.2, 1.0, 3.0, 10.0, 50.0, 100.0, 200.0 µM) to elucidate the effect of various frequencies and concentrations upon the change of the peak current I_p of the electrode. Due to the dependency of the electron transfer rate on the folding of aptamer upon binding to the target, as shown in Figure 5.19A, the current response of VCM aptamer is a function of SWV frequency change, which produces three unique responses upon binding to the target,

signal-on, signal-off, and non-responsive[57,58]. As it appears in the Figure 5.19B from the concentration-signal response for the range of 2 x 10^{-4} µM to 200 µM, 100 Hz is considered to be the Signal-On frequency, 10 Hz is considered to be the Signal-Off frequency, and 30 Hz appears to be the non-response frequency. The same data using 100 Hz as the main frequency of the calibration was used to illustrate a calibration plot, as in Figure 5.19C and its inset. From this plot, we determined the dissociation constant of a monolayer of VCM (K_d) that is equal to 28.67 µM.

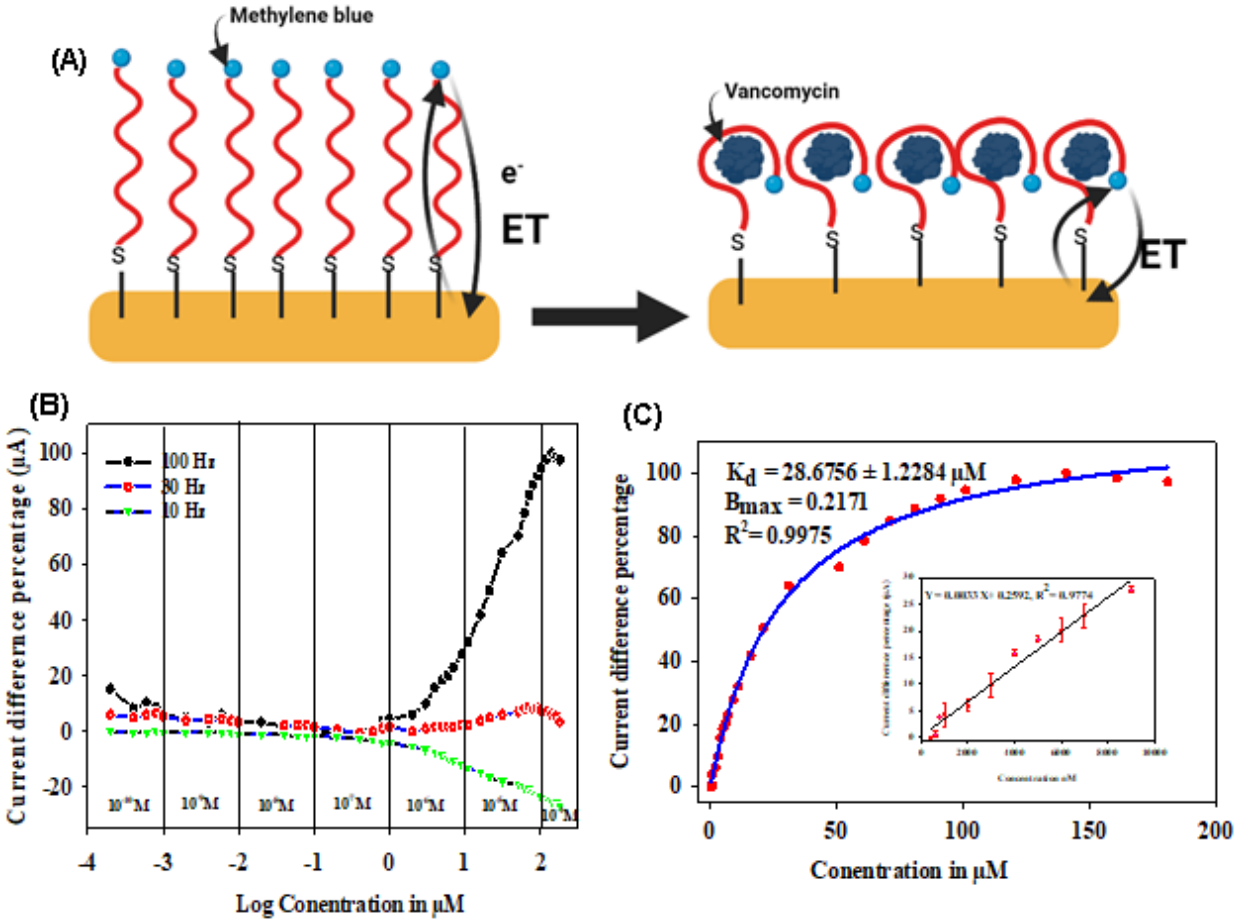

Figure 5.19 (A) illustrates the effect of VCM-aptamer binding on electron transfer rate. (B) concentration-signal response for the range of 2 x 10^{-4} µM to 200 µM, 100 Hz is considered to be the Signal-On frequency, 10 Hz is considered to be the Signal-Off frequency, and 30 Hz appears to be the non-response frequency. Calibration plot for gold electrode in PBS buffer solution containing VCM.

Then we utilized our flexible gold electrode that is shown in Figure 5.20A for in vitro measurements. After aptamer modification of the flexible electrode, the electrode was scanned in 10 mM potassium ferric cyanide $KFe(CN)_6$ with 100 mV/s in order to verify the attachment of the thiolated aptamer to our gold electrode, which is shown in 5.20B. From the behavior of the CVs, it was obvious that the negatively charged attached aptamer has reduced the redox peak currents of $KFe(CN)_6$ in comparison to the bare gold electrode. This is attributed to the electrostatic repulsion of $Fe(CN)_6^{3-}$ by the negatively charged aptamer molecules[59,60]. Utilizing the signal-on frequency that was proven using a gold electrode, that is 100 Hz for SWV, the graph in 5.20C concentration-response curve was obtained by scanning two flexible gold electrodes in various concentrations of VCM using SWV and plotting the signal change ratio over the concentration of VCM in micromolar. The plot was fitted using one site saturation fitting where the apparent equilibrium dissociation constant (K_d) was found to be 20.08 μM with an R^2 of 0.9547. The linearity of the concentration-response curve for the same two electrodes in PBS buffer was found to be 5- 40 μM with an R^2 of 0.9043 as in 5.20C inset. The selectivity of our flexible sensor for VCM detection was studied in the presence of abundant elements in the ISF that can interfere with the signal for VCM, including $MgCl_2$, ascorbic acid, uric acid, and glucose. Our 20 μM VCM solution in PBS was spiked with the normal levels of these elements and the impact of these compounds on the signal was shown against zero to show the percentage of change that showed to have a negligible impact over the current of the VCM signal, as in **Figure 2D.**

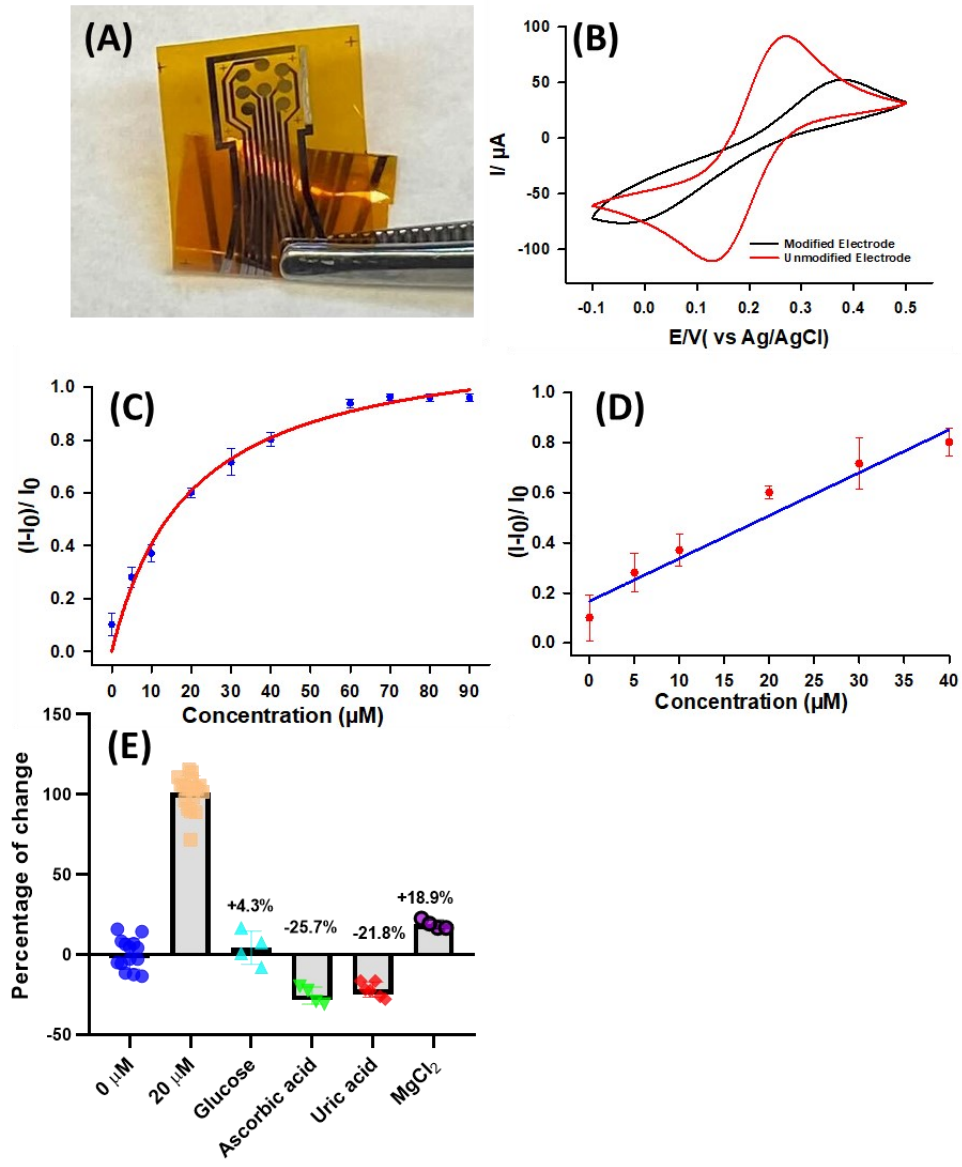

Figure 5.20 characterization of the flexible gold electrodes in vitro. (A) the flexible gold electrode consists of 8 gold working electrodes, a silver/ silver chloride reference electrode, and a gold counter electrode. (B) CV measurements of the VCM aptamer-modified electrode in 10 mM $Fe(CN)_6^{-3}$ / 0.1 M KCl shows higher redox peaks than the unmodified electrode. (C) the signal change ratio that indicates the signal-response curve of VCM aptamer in 1X PBS buffer containing 5-90 µM of VCM. The K_D was estimated to be 20.08 µM with an R^2 = 0.9562 and (D) the linearity range is from 5.0 µM to 40 µM. Means ± s.d. from two independent experiments. The slope and intercept of the dynamic orange are 0.0171 and 0.1669 respectively with an R^2 of 0.9043. (E) selectivity of our flexible gold modified electrode was studied by scanning the electrode in 20 µM VCM in 1X PBS solution containing one of the interfering elements of 0.5 mM $MgCl_2$,0.5 mM ascorbic acid, 0.5 mM uric acid, and 10 mM glucose. Means ± s.d. and each measurement were conducted at least five times.

5.3.2 Integrated assay for VCM detection using ex vivo skin model

The main goal of our VCM-Tracker which is composed of the flexible gold electrode and DAHA-MN is to determine vancomycin in human skin ISF with a minimally invasive and real-time procedure. Hence, we determined and optimized the detection of vancomycin electrochemically within *in vitro* and *ex vivo* models in skin-mimicking agarose phantom hydrogel module and porcine ear skin respectively. The agarose phantom gel was prepared using the protocol of our previous work[33], various concentrations were prepared (0- 35 μM) for the assessment of the VCM-Tracker. The DAHA microneedle is gently pushed against the skin and the aptamer-modified electrode is fixed on top of the microneedle using a transparent adhesive film dressing and left for 10 minutes to allow the flow of ISF into the DAHA MN. The electrode was scanned with the signal-on frequency, utilizing SWV scans in the voltage range from 0 V to -0.5 V. The concentration-response curve obtained showed a linear correlation between the concentration of vancomycin and the signal change ratio with an R^2 of 0.9 in the linear range of (5-35 μM), which covers the biological range of vancomycin and the overdose region, as shown in Figure 5.21.

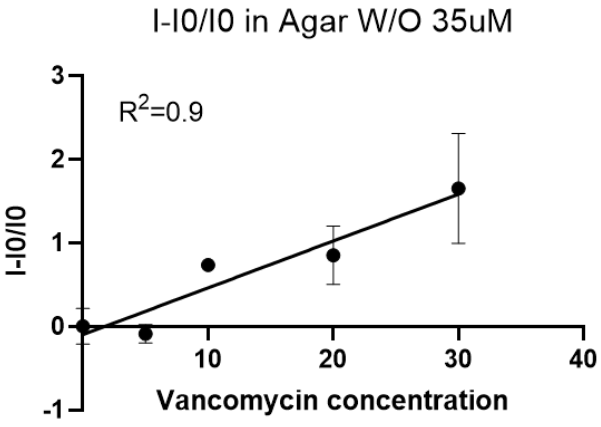

Figure 5.21 Characterization of VCM-Tracker in agarose phantom gel for the concentration range 0-30 μM

Porcine skin patches were dried with paper wipes to remove external moisture from the skin after being loaded with the required concentration of VCM. The scan is conducted after pushing the DAHA MN against the skin gently, positioning the aptamer-modified electrode on top of the microneedle, and fixing the whole setup with the same aforementioned dressing, as in Figure 5.22A. In order to exclude the external moisture effect of the skin that can be caused by perspiration, the electrode was first scanned against bare skin with zero and 20 μM of vancomycin without MNs. The results were compared to the presence of MN inside the skin patch with the same concentration as shown in Figure 5.22B. It was found that there was no signal recorded for the zero concentration in the absence of DAHA MN while the signal in the presence of MN had an average of 0.3581 μA in the presence of MN. For the 20 μM skin patches, the obtained result for the MN containing skin was nearly four times more than the signal obtained without skin, which demonstrates the necessity of our DAHA MN to absorb the ISF from the skin for vancomycin detection. Utilizing the signal-on frequency that was proven using gold electrode, that is 100 Hz for square wave voltammetry (SWV), the electrode was scanned between 0 and -0.5 V. The graph in Figure 5.22C concentration-response curve was obtained by scanning two electrodes in PBS buffer containing various concentrations of vancomycin using SWV. The plot was fitted using one site saturation fitting where the apparent equilibrium dissociation constant (K_d) was found to be 20.08 μM with R^2 of 0.9547. The linearity of the concentration-response curve for the same two electrodes in PBS buffer was found to be 5- 40 μM with an R^2 of 0.9043 as in Figure 5.22D inset.

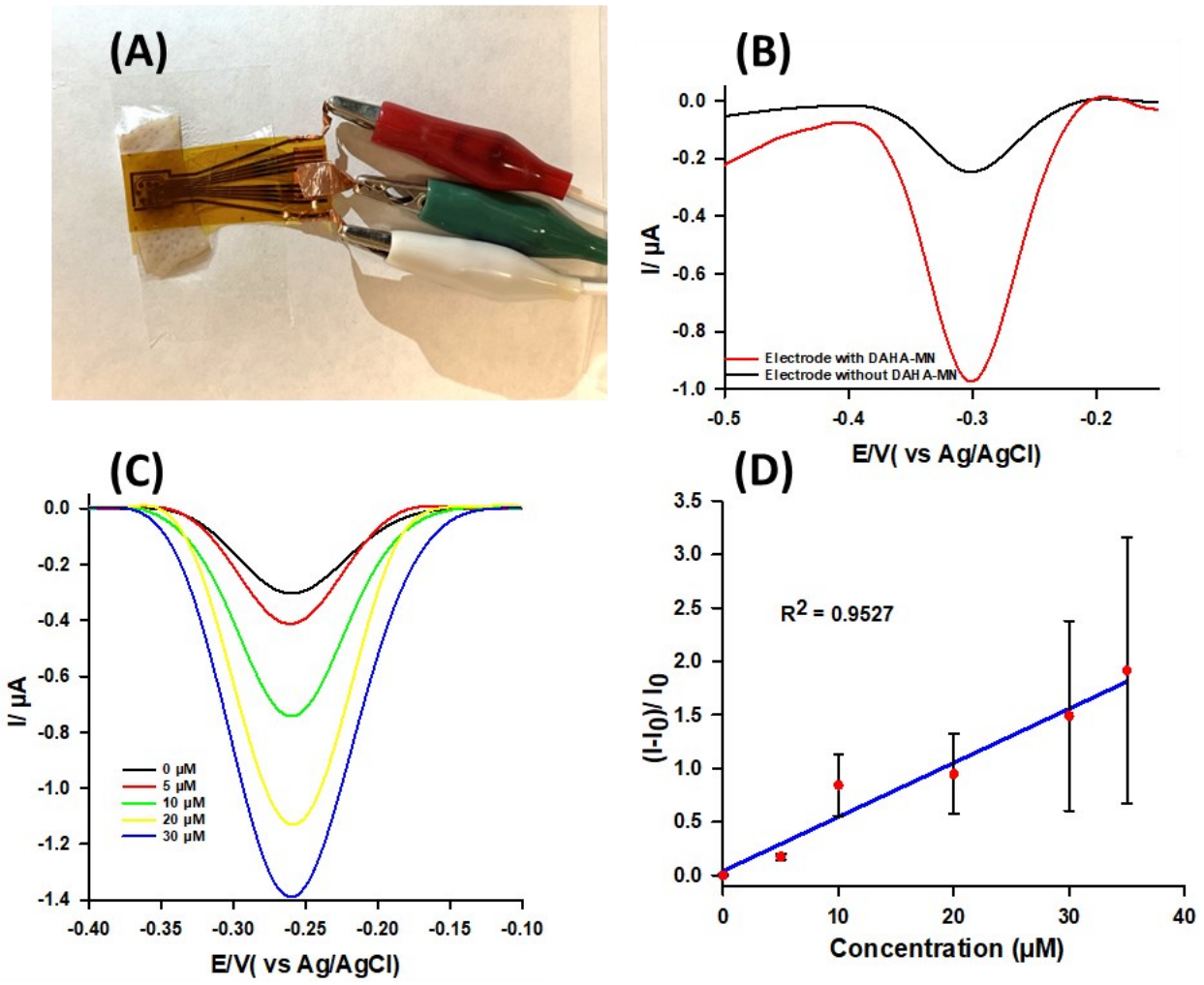

Figure 5.22 Characterization of VCM-Tracker in porcine skin. (A) the VCM-Tracker system consists of DAHA-MNs that penetrate the skin to absorb ISF, VCM aptamer-modified flexible gold electrode, and transparent adhesive film dressing. (B) SWVs of the response of VCM-Tracker on porcine skin containing 20 µM VCM with and without DAHA-MN in which the effect of adding DAHA-MN shows a significant increase in the signal. (C) SWVs of VCM tracker system in porcine skin. Curves were obtained by scanning from 0.1 V to -0.5 V with 100 Hz frequency, 0.025 V amplitude, and 0.001 step potential. The scans involved five concentrations including 0.0, 5.0, 10.0, 20.0, and 30.0 µM of VCM. (D) the linear range of VCM that is from 5.0 to 35 µM of VCM with an R^2 of 0.9527. Means ± s.e. three electrodes or more were involved for each concentration.

5.4 Chapter 6 Conclusion and Future Work

Despite their development as early as the 20th century, electrochemical sensors are still being widely used in many applications, due to their cost-effectiveness, capability of wireless detection, portability, and wide range of electrochemical active materials that are encountered in our lives and are essential to determine, including biomarkers, therapeutic agents, pesticides and toxins, heavy metals, and microorganisms, as discussed in the previous chapters. This thesis addressed different strategies that can enhance the detection of therapeutic agents. First, MnO_2-V_2O_5 nanorods were synthesized and used as a platform for the determination of CTL, an antiplatelet drug, in plasma and dosage forms. Second, NH_2-MIL-53(Al) MOF was fabricated and utilized as a catalyst for the determination of VLP in urine and plasma. Finally, VCM-Tracker aptasensors were manufactured and developed for the determination of VCM. In all of these studies, highly sensitive platforms were developed that were able to determine the levels of the targeted drugs in their normal levels in blood and detect overdoses.

In the future, this research can be an extension for other points, such as:

1- Testing the same system utilized in VCM-tracker for the detection of other therapeutic agents and biomarkers in the ISF
2- Testing NH_2-MIL-53(Al) MOF for other antiviral agents that are similar to VLP
3- Testing MnO_2-V_2O_5 nanorods in other applications of electrochemistry such as vanadium lithium batteries due to their spectacular electrochemical properties

References

(1) Gross, A. S. Best Practice in Therapeutic Drug Monitoring. *British Journal of Clinical Pharmacology* **1998**, *46* (2), 95. https://doi.org/10.1046/J.1365-2125.1998.00770.X.

(2) Touw, D. J.; Neef, C.; Thomson, A. H.; Vinks, A. A. Cost-Effectiveness of Therapeutic Drug Monitoring: A Systematic Review. *Ther Drug Monit* **2005**, *27* (1), 10–17. https://doi.org/10.1097/00007691-200502000-00004.

(3) Kang, J. S.; Lee, M. H. Overview of Therapeutic Drug Monitoring. *The Korean Journal of Internal Medicine* **2009**, *24* (1), 1. https://doi.org/10.3904/KJIM.2009.24.1.1.

(4) Birkett, D. J. *Pharmacokinetics Made Easy*; McGraw Hill Professional, 2002.

(5) Tange, S. M.; Grey, V. L.; Senécal, P. E. Therapeutic Drug Monitoring in Pediatrics: A Need for Improvement. *J Clin Pharmacol* **1994**, *34* (3), 200–214. https://doi.org/10.1002/J.1552-4604.1994.TB03987.X.

(6) Reed, M. D.; Blumer, J. L. Therapeutic Drug Monitoring in the Pediatric Intensive Care Unit. *Pediatr Clin North Am* **1994**, *41* (6), 1227–1243. https://doi.org/10.1016/S0031-3955(16)38870-8.

(7) Kearns, G. L.; Moss, M. M.; Clayton, B. D.; Hewett, D. D. Pharmacokinetics and Efficacy of Digoxin Specific Fab Fragments in a Child Following Massive Digoxin Overdose. *J Clin Pharmacol* **1989**, *29* (10), 901–908. https://doi.org/10.1002/J.1552-4604.1989.TB03252.X.

(8) Ohning, B. L. Neonatal Pharmacodynamics--Basic Principles. I: Drug Delivery. *Neonatal Network: NN* **1995**, *14* (2), 7–12.

(9) Momper, J. D.; Wagner, J. A. Therapeutic Drug Monitoring as a Component of Personalized Medicine: Applications in Pediatric Drug Development. *Clinical Pharmacology and Therapeutics* **2014**, *95* (2), 138–140. https://doi.org/10.1038/CLPT.2013.227.

(10) BUCHTHAL, F.; SVENSMARK, O. Aspects of the Pharmacology of Phenytoin (Dilantin) and Phenobarbital Relevant to Their Dosage in the Treatment of Epilepsy. *Epilepsia* **1960**, *1* (1–5), 373–384. https://doi.org/10.1111/J.1528-1157.1959.TB04274.X.

(11) Baastrup, P. C.; Mogens, S. Lithium as a Prophylactic Agents. Its Effect against Recurrent Depressions and Manic-Depressive Psychosis. *Arch Gen Psychiatry* **1967**, *16* (2), 162–172. https://doi.org/10.1001/ARCHPSYC.1967.01730200030005.

(12) Gross, A. S. Best Practice in Therapeutic Drug Monitoring. *British Journal of Clinical Pharmacology* **1998**, *46* (2), 95. https://doi.org/10.1046/J.1365-2125.1998.00770.X.

(13) Touw, D. J.; Neef, C.; Thomson, A. H.; Vinks, A. A.; Therapeutic, on behalf of the C.-E. of. Cost-Effectiveness of Therapeutic Drug Monitoring: A Systematic Review. *Therapeutic Drug Monitoring* **2005**, *27* (1).

(14) Ates, H. C.; Roberts, J. A.; Lipman, J.; Cass, A. E. G.; Urban, G. A.; Dincer, C. On-Site Therapeutic Drug Monitoring. *Trends in Biotechnology* **2020**, *38* (11), 1262–1277. https://doi.org/10.1016/J.TIBTECH.2020.03.001.

(15) Mollarasouli, F.; Bakirhan, N. K.; Ozkan, S. A. Introduction to Biomarkers. *The Detection of Biomarkers* **2022**, 1–22. https://doi.org/10.1016/B978-0-12-822859-3.00008-0.

(16) Strimbu, K.; Tavel, J. A. What Are Biomarkers? *Current Opinion in HIV and AIDS* **2010**, *5* (6), 463–466. https://doi.org/10.1097/COH.0B013E32833ED177.

(17) Hewitt, S. M.; Dear, J.; Star, R. A. Discovery of Protein Biomarkers for Renal Diseases. *Journal of the American Society of Nephrology* **2004**, *15* (7), 1677–1689. https://doi.org/10.1097/01.ASN.0000129114.92265.32.

(18) Bhalla, N.; Jolly, P.; Formisano, N.; Estrela, P. Introduction to Biosensors. *Essays in Biochemistry* **2016**, *60* (1), 1. https://doi.org/10.1042/EBC20150001.

(19) Cremer, M. *Über Die Ursache Der Elektromotorischen Eigenschaften Der Gewebe, Zugleich Ein Beitrag Zur Lehre von Den Polyphasischen Elektrolytketten*; R. Oldenbourg, 1906.

(20) Hughes, W. S. The Potential Difference between Glass and Electrolytes in Contact with the Glass. *J Am Chem Soc* **1922**, *44* (12), 2860–2867. https://doi.org/10.1021/JA01433A021/ASSET/JA01433A021.FP.PNG_V03.

(21) Griffin, E. G.; Nelson, J. M. The Influence of Certain Substances on the Activity of Invertase. *J Am Chem Soc* **1916**, *38* (3), 722–730. https://doi.org/10.1021/JA02260A027/ASSET/JA02260A027.FP.PNG_V03.

(22) Nelson, J. M.; Griffin, E. G. Adsorption of Invertase. *J Am Chem Soc* **1916**, *38* (5), 1109–1115. https://doi.org/10.1021/JA02262A018/ASSET/JA02262A018.FP.PNG_V03.

(23) Heineman, W. R.; Jensen, W. B. Leland C. Clark Jr. (1918–2005). *Biosensors and Bioelectronics* **2006**, *21* (8), 1403–1404. https://doi.org/10.1016/J.BIOS.2005.12.005.

(24) Guilbault, G. G.; Montalvo, J. G. A Urea-Specific Enzyme Electrode. *J Am Chem Soc* **1969**, *91* (8), 2164–2165. https://doi.org/10.1021/JA01036A083.

(25) Wang, Z.; Luan, J.; Seth, A.; Liu, L.; You, M.; Gupta, P.; Rathi, P.; Wang, Y.; Cao, S.; Jiang, Q.; Zhang, X.; Gupta, R.; Zhou, Q.; Morrissey, J. J.; Scheller, E. L.; Rudra, J. S.; Singamaneni, S. Microneedle Patch for the Ultrasensitive Quantification of Protein Biomarkers in Interstitial Fluid. *Nature Biomedical Engineering 2021 5:1* **2021**, *5* (1), 64–76. https://doi.org/10.1038/s41551-020-00672-y.

(26) He, R.; Niu, Y.; Li, Z.; Li, A.; Yang, H.; Xu, F.; Li, F. A Hydrogel Microneedle Patch for Point-of-Care Testing Based on Skin Interstitial Fluid. *Advanced Healthcare Materials* **2020**, *9* (4), 1901201. https://doi.org/10.1002/ADHM.201901201.

(27) Heikenfeld, J.; Jajack, A.; Feldman, B.; Granger, S. W.; Gaitonde, S.; Begtrup, G.; Katchman, B. A. Accessing Analytes in Biofluids for Peripheral Biochemical Monitoring. *Nat Biotechnol* **2019**, *37* (4), 407–419. https://doi.org/10.1038/S41587-019-0040-3.

(28) Tran, B. Q.; Miller, P. R.; Taylor, R. M.; Boyd, G.; Mach, P. M.; Rosenzweig, C. N.; Baca, J. T.; Polsky, R.; Glaros, T. Proteomic Characterization of Dermal Interstitial Fluid Extracted Using a Novel Microneedle-Assisted Technique. *J Proteome Res* **2018**, *17* (1), 479–485. https://doi.org/10.1021/ACS.JPROTEOME.7B00642.

(29) Müller, A. C.; Breitwieser, F. P.; Fischer, H.; Schuster, C.; Brandt, O.; Colinge, J.; Superti-Furga, G.; Stingl, G.; Elbe-Bürger, A.; Bennett, K. L. A Comparative Proteomic Study of Human Skin Suction Blister Fluid from Healthy Individuals Using Immunodepletion and ITRAQ Labeling. *J Proteome Res* **2012**, *11* (7), 3715–3727. https://doi.org/10.1021/PR3002035.

(30) Kool, J.; Reubsaet, L.; Wesseldijk, F.; Maravilha, R. T.; Pinkse, M. W.; D'Santos, C. S.; van Hilten, J. J.; Zijlstra, F. J.; Heck, A. J. R. Suction Blister Fluid as Potential Body Fluid for Biomarker Proteins. *Proteomics* **2007**, *7* (20), 3638–3650. https://doi.org/10.1002/PMIC.200600938.

(31) Samant, P. P.; Prausnitz, M. R. Mechanisms of Sampling Interstitial Fluid from Skin Using a Microneedle Patch. *Proc Natl Acad Sci U S A* **2018**, *115* (18), 4583–4588. https://doi.org/10.1073/PNAS.1716772115/SUPPL_FILE/PNAS.1716772115.SAPP.PDF.

(32) Liu, G. S.; Kong, Y.; Wang, Y.; Luo, Y.; Fan, X.; Xie, X.; Yang, B. R.; Wu, M. X. Microneedles for Transdermal Diagnostics: Recent Advances and New Horizons. *Biomaterials* **2019**, *232*, 119740–119740. https://doi.org/10.1016/J.BIOMATERIALS.2019.119740.

(33) Wu, Y.; Tehrani, F.; Teymourian, H.; Mack, J.; Shaver, A.; Reynoso, M.; Kavner, J.; Huang, N.; Furmidge, A.; Duvvuri, A.; Nie, Y.; Laffel, L. M.; Iii, F. J. D.; Patti, M.-E.; Dassau, E.; Wang, J.; Arroyo-Currás, N. Microneedle Aptamer-Based Sensors for Continuous, Real-Time Therapeutic Drug Monitoring. https://doi.org/10.1021/acs.analchem.2c00829.

(34) Martanto, W.; Moore, J. S.; Kashlan, O.; Kamath, R.; Wang, P. M.; O'Neal, J. M.; Prausnitz, M. R. Microinfusion Using Hollow Microneedles. *Pharmaceutical Research* **2006**, *23* (1), 104–113. https://doi.org/10.1007/S11095-005-8498-8/FIGURE S/10.

(35) Turner, J. G.; White, L. R.; Estrela, P.; Leese, H. S.; Turner, J. G.; White, L. R.; Leese, H. S.; Estrela, P. Hydrogel-Forming Microneedles: Current Advancements and Future Trends. *Macromolecular Bioscience* **2021**, *21* (2), 2000307. https://doi.org/10.1002/MABI.202000307.

(36) Miller, P. R.; Narayan, R. J.; Polsky, R. Microneedle-Based Sensors for Medical Diagnosis. *Journal of Materials Chemistry B* **2016**, *4* (8), 1379–1383. https://doi.org/10.1039/C5TB02421H.

(37) Stetter, J. R.; Penrose, W. R.; Yao, S. Sensors, Chemical Sensors, Electrochemical Sensors, and ECS. *Journal of The Electrochemical Society* **2003**, *150* (2), S11. https://doi.org/10.1149/1.1539051/XML.

(38) Naresh, V.; Lee, N. A Review on Biosensors and Recent Development of Nanostructured Materials-Enabled Biosensors. *Sensors 2021, Vol. 21, Page 1109* **2021**, *21* (4), 1109. https://doi.org/10.3390/S21041109.

(39) Vetelino, J. F.; Reghu, A. Introduction to Sensors. *Introduction to Sensors* **2017**, 1–180. https://doi.org/10.1201/9781315218274/INTRODUCTION-SENSORS-JOHN-VETELINO-ARAVIND-REGHU.

(40) Damborský, P.; Švitel, J.; Katrlík, J. Optical Biosensors. *Essays in Biochemistry* **2016**, *60* (1), 91–100. https://doi.org/10.1042/EBC20150010.

(41) Chen, Y. T.; Kolhatkar, A. G.; Zenasni, O.; Xu, S.; Lee, T. R. Biosensing Using Magnetic Particle Detection Techniques. *Sensors (Basel)* **2017**, *17* (10). https://doi.org/10.3390/S17102300.

(42) Pohanka, M. Overview of Piezoelectric Biosensors, Immunosensors and DNA Sensors and Their Applications. *Materials* **2018**, *11* (3). https://doi.org/10.3390/MA11030448.

(43) Ramanathan, K.; Danielsson, B. Principles and Applications of Thermal Biosensors. *Biosensors and Bioelectronics* **2001**, *16* (6), 417–423. https://doi.org/10.1016/S0956-5663(01)00124-5.

(44) Naresh, V.; Lee, N. A Review on Biosensors and Recent Development of Nanostructured Materials-Enabled Biosensors. *Sensors 2021, Vol. 21, Page 1109* **2021**, *21* (4), 1109. https://doi.org/10.3390/S21041109.

(45) Malhotra, B. D.; Ali, Md. A. Nanomaterials in Biosensors: Fundamentals and Applications. *Nanomaterials for Biosensors* **2018**, 1. https://doi.org/10.1016/B978-0-323-44923-6.00001-7.

(46) Low, I. M.; Dong, Y. Composite Materials: Manufacturing, Properties and Applications. **2021**.

(47) Elgrishi, N.; Rountree, K. J.; McCarthy, B. D.; Rountree, E. S.; Eisenhart, T. T.; Dempsey, J. L. A Practical Beginner's Guide to Cyclic Voltammetry. *Journal of Chemical Education* **2018**, *95* (2), 197–206. https://doi.org/10.1021/ACS.JCHEMED.7B00361/SUPPL_FILE/ED7B00361_SI_002.DOCX.

(48) Chaubey, A.; Malhotra, B. D. Mediated Biosensors. *Biosens Bioelectron* **2002**, *17* (6–7), 441–456. https://doi.org/10.1016/S0956-5663(01)00313-X.

(49) Mirsky, V. M.; Riepl, M.; Wolfbeis, O. S. Capacitive Monitoring of Protein Immobilization and Antigen-Antibody Reactions on Monomolecular Alkylthiol Films on Gold Electrodes.

Biosens Bioelectron **1997**, *12* (9–10), 977–989. https://doi.org/10.1016/S0956-5663(97)00053-5.

(50) Guiseppi-Elie, A.; Lingerfelt, L. Immobilisation of DNA on Chips I, Volume 260 of Topics in Current Chemistry. Springer-Verlag Berlin Berlin: 2005.

(51) Thévenot, D. R.; Toth, K.; Durst, R. A.; Wilson, G. S. Electrochemical Biosensors: Recommended Definitions and Classification. *Biosens Bioelectron* **2001**, *16* (1–2), 121–131. https://doi.org/10.1016/S0956-5663(01)00115-4.

(52) Luppa, P. B.; Sokoll, L. J.; Chan, D. W. Immunosensors--Principles and Applications to Clinical Chemistry. *Clin Chim Acta* **2001**, *314* (1–2), 1–26. https://doi.org/10.1016/S0009-8981(01)00629-5.

(53) Eggins, B. R. *Chemical Sensors and Biosensors*; John Wiley & Sons, 2002; Vol. 2.

(54) Thévenot, D. R.; Toth, K.; Durst, R. A.; Wilson, G. S. Electrochemical Biosensors: Recommended Definitions and Classification. *Biosens Bioelectron* **2001**, *16* (1–2), 121–131. https://doi.org/10.1016/S0956-5663(01)00115-4.

(55) Chaubey, A.; Malhotra, B. D. Mediated Biosensors. *Biosens Bioelectron* **2002**, *17* (6–7), 441–456. https://doi.org/10.1016/S0956-5663(01)00313-X.

(56) Wang, J. Analytical Electrochemistry, Third Edition. *Analytical Electrochemistry, Third Edition* **2006**, 1–250. https://doi.org/10.1002/0471790303.

(57) Nahir, T. M.; Buck, R. P. Modified Cottrell Behavior in Thin Layers: Applied Voltage Steps under Diffusion Control for Constant-Resistance Systems. *Journal of Electroanalytical Chemistry* **1992**, *341* (1–2), 1–14. https://doi.org/10.1016/0022-0728(92)80471-F.

(58) Bănică, F. G. Chemical Sensors and Biosensors: Fundamentals and Applications. *Chemical Sensors and Biosensors: Fundamentals and Applications* **2012**. https://doi.org/10.1002/9781118354162.

(59) Heyrovský, J. The Development of Polarographic Analysis. *Analyst* **1956**, *81* (961), 189–192.

(60) Eggins, B. R. *Chemical Sensors and Biosensors*; John Wiley & Sons, 2002; Vol. 2.

(61) Katz, E.; Willner, I. Probing Biomolecular Interactions at Conductive and Semiconductive Surfaces by Impedance Spectroscopy: Routes to Impedimetric Immunosensors, DNA-sensors, and Enzyme Biosensors. *Electroanalysis: An International Journal Devoted to Fundamental and Practical Aspects of Electroanalysis* **2003**, *15* (11), 913–947.

(62) Eggins, B. R. *Chemical Sensors and Biosensors*; John Wiley & Sons, 2002; Vol. 2.

(63) Chaubey, A.; Malhotra, B. D. Mediated Biosensors. *Biosens Bioelectron* **2002**, *17* (6–7), 441–456. https://doi.org/10.1016/S0956-5663(01)00313-X.

(64) D'Orazio, P. Biosensors in Clinical Chemistry. *Clin Chim Acta* **2003**, *334* (1–2), 41–69. https://doi.org/10.1016/S0009-8981(03)00241-9.

(65) Bakker, E.; Pretsch, E. Potentiometric Sensors for Trace-Level Analysis. *Trends Analyt Chem* **2005**, *24* (3), 199–207. https://doi.org/10.1016/J.TRAC.2005.01.003.

(66) Buerk, D. G. *Biosensors: Theory and Applications*; Crc Press, 2014.

(67) Grieshaber, D.; MacKenzie, R.; Vörös, J.; Reimhult, E. Electrochemical Biosensors - Sensor Principles and Architectures. *Sensors (Basel)* **2008**, *8* (3), 1400. https://doi.org/10.3390/S80314000.

(68) D'Orazio, P. Biosensors in Clinical Chemistry. *Clin Chim Acta* **2003**, *334* (1–2), 41–69. https://doi.org/10.1016/S0009-8981(03)00241-9.

(69) Thévenot, D. R.; Toth, K.; Durst, R. A.; Wilson, G. S. Electrochemical Biosensors: Recommended Definitions and Classification. *Biosens Bioelectron* **2001**, *16* (1–2), 121–131. https://doi.org/10.1016/S0956-5663(01)00115-4.

(70) Cullen, D. C.; Sethi, R. S.; Lowe, C. R. Multi-Analyte Miniature Conductance Biosensor. *Analytica Chimica Acta* **1990**, *231*, 33–40.

(71) Contractor, A. Q.; Sureshkumar, T. N.; Narayanan, R.; Sukeerthi, S.; Lal, R.; Srinivasa, R. S. Conducting Polymer-Based Biosensors. *Electrochimica Acta* **1994**, *39* (8–9), 1321–1324.

(72) Patolsky, F.; Zheng, G.; Lieber, C. M. Nanowire-Based Biosensors. *Anal Chem* **2006**, *78* (13), 4260–4269. https://doi.org/10.1021/AC069419J.

(73) Grieshaber, D.; MacKenzie, R.; Vörös, J.; Reimhult, E. Electrochemical Biosensors - Sensor Principles and Architectures. *Sensors (Basel)* **2008**, *8* (3), 1400. https://doi.org/10.3390/S80314000.

(74) Eggins, B. R. *Chemical Sensors and Biosensors*; John Wiley & Sons, 2002; Vol. 2.

(75) Yagiuda, K.; Hemmi, A.; Ito, S.; Asano, Y.; Fushinuki, Y.; Chen, C. Y.; Karube, I. Development of a Conductivity-Based Immunosensor for Sensitive Detection of Methamphetamine (Stimulant Drug) in Human Urine. *Biosens Bioelectron* **1996**, *11* (8), 703–707. https://doi.org/10.1016/0956-5663(96)85920-3.

(76) Chouteau, C.; Dzyadevych, S.; Chovelon, J. M.; Durrieu, C. Development of Novel Conductometric Biosensors Based on Immobilised Whole Cell Chlorella Vulgaris Microalgae. *Biosens Bioelectron* **2004**, *19* (9), 1089–1096. https://doi.org/10.1016/J.BIOS.2003.10.012.

(77) Lorenz, W.; Schulze, K. D. Application of Transform-Impedance Spectrometry. *Journal of Electroanalytical Chemistry* **1975**, *65* (1), 141–153.

(78) Willner, I.; Baron, R.; Willner, B. Integrated Nanoparticle–Biomolecule Systems for Biosensing and Bioelectronics. *Biosensors and Bioelectronics* **2007**, *22* (9–10), 1841–1852. https://doi.org/10.1016/J.BIOS.2006.09.018.

(79) Patolsky, F.; Zayats, M.; Katz, E.; Willner, I. Precipitation of an Insoluble Product on Enzyme Monolayer Electrodes for Biosensor Applications: Characterization by Faradaic Impedance Spectroscopy, Cyclic Voltammetry, and Microgravimetric Quartz Crystal Microbalance Analyses. *Anal Chem* **1999**, *71* (15), 3171–3180. https://doi.org/10.1021/AC9901541.

(80) Tlili, A.; Abdelghani, A.; Ameur, S.; Jaffrezic-Renault, N. Impedance Spectroscopy and Affinity Measurement of Specific Antibody–Antigen Interaction. *Materials Science and Engineering: C* **2006**, *26* (2–3), 546–550. https://doi.org/10.1016/J.MSEC.2005.10.007.

(81) Fernández-Sánchez, C.; McNeil, C. J.; Rawson, K. Electrochemical Impedance Spectroscopy Studies of Polymer Degradation: Application to Biosensor Development. *TrAC Trends in Analytical Chemistry* **2005**, *24* (1), 37–48. https://doi.org/10.1016/J.TRAC.2004.08.010.

(82) Sumner, C.; Sabot, A.; Turner, K.; Krause, S. A Transducer Based on Enzyme-Induced Degradation of Thin Polymer Films Monitored by Surface Plasmon Resonance. *Anal Chem* **2000**, *72* (21), 5225–5232. https://doi.org/10.1021/AC000411Y.

(83) Tong, Z.; Yuan, R.; Chai, Y.; Xie, Y.; Chen, S. A Novel and Simple Biomolecules Immobilization Method: Electro-Deposition ZrO2 Doped with HRP for Fabrication of Hydrogen Peroxide Biosensor. *J Biotechnol* **2007**, *128* (3), 567–575. https://doi.org/10.1016/J.JBIOTEC.2006.12.008.

(84) Bakker, E. Electrochemical Sensors. *Anal Chem* **2004**, *76* (12), 3285–3298. https://doi.org/10.1021/AC049580Z.

(85) Pei, R.; Cheng, Z.; Wang, E.; Yang, X. Amplification of Antigen-Antibody Interactions Based on Biotin Labeled Protein-Streptavidin Network Complex Using Impedance Spectroscopy. *Biosens Bioelectron* **2001**, *16* (6), 355–361. https://doi.org/10.1016/S0956-5663(01)00150-6.

(86) Luppa, P. B.; Sokoll, L. J.; Chan, D. W. Immunosensors--Principles and Applications to Clinical Chemistry. *Clin Chim Acta* **2001**, *314* (1–2), 1–26. https://doi.org/10.1016/S0009-8981(01)00629-5.

(87) Horenstein, M. N. *Microelectronic Circuits and Devices*; Prentice-Hall, Inc., 1990.

(88) Luo, X.; Morrin, A.; Killard, A. J.; Smyth, M. R. Application of Nanoparticles in Electrochemical Sensors and Biosensors. *Electroanalysis* **2006**, *18* (4), 319–326. https://doi.org/10.1002/ELAN.200503415.

(89) Gole, A.; Dash, C.; Ramakrishnan, V.; Sainkar, S. R.; Mandale, A. B.; Rao, M.; Sastry, M. Pepsin-Gold Colloid Conjugates: Preparation, Characterization, and Enzymatic Activity. *Langmuir* **2001**, *17* (5), 1674–1679. https://doi.org/10.1021/LA001164W.

(90) Gole, A.; Vyas, S.; Phadtare, S.; Lachke, A.; Sastry, M. Studies on the Formation of Bioconjugates of Endoglucanase with Colloidal Gold. *Colloids and Surfaces B: Biointerfaces* **2002**, *25* (2), 129–138. https://doi.org/10.1016/S0927-7765(01)00301-0.

(91) Li, Y.; Schluesener, H. J.; Xu, S. Gold Nanoparticle-Based Biosensors. *Gold Bulletin 2010 43:1* **2010**, *43* (1), 29–41. https://doi.org/10.1007/BF03214964.

(92) Yu, A.; Liang, Z.; Cho, J.; Caruso, F. Nanostructured Electrochemical Sensor Based on Dense Gold Nanoparticle Films. *Nano Letters* **2003**, *3* (9), 1203–1207. https://doi.org/10.1021/NL034363J/ASSET/IMAGES/LARGE/NL034363JF00006.JPEG.

(93) Raj, C. R.; Okajima, T.; Ohsaka, T. Gold Nanoparticle Arrays for the Voltammetric Sensing of Dopamine. *Journal of Electroanalytical Chemistry* **2003**, *543* (2), 127–133. https://doi.org/10.1016/S0022-0728(02)01481-X.

(94) Katz, E.; Willner, I.; Wang, J. Electroanalytical and Bioelectroanalytical Systems Based on Metal and Semiconductor Nanoparticles. *Electroanalysis* **2004**, *16* (1–2), 19–44. https://doi.org/10.1002/ELAN.200302930.

(95) Noah, N. M.; Ndangili, P. M. Current Trends of Nanobiosensors for Point-of-Care Diagnostics. *Journal of Analytical Methods in Chemistry* **2019**, *2019*. https://doi.org/10.1155/2019/2179718.

(96) Malekzad, H.; Sahandi Zangabad, P.; Mirshekari, H.; Karimi, M.; Hamblin, M. R. Noble Metal Nanoparticles in Biosensors: Recent Studies and Applications. *Nanotechnology Reviews* **2017**, *6* (3), 301–329. https://doi.org/10.1515/NTREV-2016-0014/ASSET/GRAPHIC/J_NTREV-2016-0014_FIG_002.JPG.

(97) Szeitner, Z.; András, J.; Gyurcsányi, R. E.; Mészáros, T. Is Less More? Lessons from Aptamer Selection Strategies. *Journal of Pharmaceutical and Biomedical Analysis* **2014**, *101*, 58–65. https://doi.org/10.1016/J.JPBA.2014.04.018.

(98) Fritea, L.; Haddache, F.; Reuillard, B.; le Goff, A.; Gorgy, K.; Gondran, C.; Holzinger, M.; Săndulescu, R.; Cosnier, S. Electrochemical Nanopatterning of an Electrogenerated Photosensitive Poly-[Trisbipyridinyl-Pyrrole Ruthenium(II)] Metallopolymer by Nanosphere Lithography. *Electrochemistry Communications* **2014**, *46*, 75–78. https://doi.org/10.1016/J.ELECOM.2014.06.012.

(99) Bounegru, A. V.; Apetrei, C. Carbonaceous Nanomaterials Employed in the Development of Electrochemical Sensors Based on Screen-Printing Technique—A Review. *Catalysts 2020, Vol. 10, Page 680* **2020**, *10* (6), 680. https://doi.org/10.3390/CATAL10060680.

(100) Zeng, Z.; Fang, X.; Miao, W.; Liu, Y.; Maiyalagan, T.; Mao, S. Electrochemically Sensing of Trichloroacetic Acid with Iron(II) Phthalocyanine and Zn-Based Metal Organic Framework Nanocomposites. *ACS Sensors* **2019**, *4* (7), 1934–1941. https://doi.org/10.1021/ACSSENSORS.9B00894/ASSET/IMAGES/LARGE/SE-2019-008949_0006.JPEG.

(101) Labib, M.; Sargent, E. H.; Kelley, S. O. Electrochemical Methods for the Analysis of Clinically Relevant Biomolecules. *Chemical Reviews* **2016**, *116* (16), 9001–9090. https://doi.org/10.1021/ACS.CHEMREV.6B00220/ASSET/IMAGES/MEDIUM/CR-2016-00220G_0047.GIF.

(102) Kajal, N.; Singh, V.; Gupta, R.; Gautam, S. Metal Organic Frameworks for Electrochemical Sensor Applications: A Review. *Environmental Research* **2022**, *204*, 112320. https://doi.org/10.1016/J.ENVRES.2021.112320.

(103) Toropov, N.; Vartanyan, T. Noble Metal Nanoparticles: Synthesis and Optical Properties. *Comprehensive Nanoscience and Nanotechnology* **2019**, *1–5*, 61–88. https://doi.org/10.1016/B978-0-12-803581-8.00585-3.

(104) Fritea, L.; Banica, F.; Costea, T. O.; Moldovan, L.; Dobjanschi, L.; Muresan, M.; Cavalu, S. Metal Nanoparticles and Carbon-Based Nanomaterials for Improved Performances of Electrochemical (Bio)Sensors with Biomedical Applications. *Materials 2021, Vol. 14, Page 6319* **2021**, *14* (21), 6319. https://doi.org/10.3390/MA14216319.

(105) Saha, K.; Agasti, S. S.; Kim, C.; Li, X.; Rotello, V. M. Gold Nanoparticles in Chemical and Biological Sensing. *Chem Rev* **2012**, *112* (5), 2739. https://doi.org/10.1021/CR2001178.

(106) Wilson, R. The Use of Gold Nanoparticles in Diagnostics and Detection. *Chem Soc Rev* **2008**, *37* (9), 2028–2045. https://doi.org/10.1039/B712179M.

(107) Liu, X.; Zeng, X.; Mai, N.; Liu, Y.; Kong, B.; Li, Y.; Wei, W.; Luo, S. Amperometric Glucose Biosensor with Remarkable Acid Stability Based on Glucose Oxidase Entrapped in Colloidal Gold-Modified Carbon Ionic Liquid Electrode. *Biosens Bioelectron* **2010**, *25* (12), 2675–2679. https://doi.org/10.1016/J.BIOS.2010.04.045.

(108) Chen, M.; Diao, G. Electrochemical Study of Mono-6-Thio-Beta-Cyclodextrin/Ferrocene Capped on Gold Nanoparticles: Characterization and Application to the Design of Glucose Amperometric Biosensor. *Talanta* **2009**, *80* (2), 815–820. https://doi.org/10.1016/J.TALANTA.2009.07.068.

(109) Sun, Y.; Bai, Y.; Yang, W.; Sun, C. Controlled Multilayer Films of Sulfonate-Capped Gold Nanoparticles/Thionine Used for Construction of a Reagentless Bienzymatic Glucose Biosensor. *Electrochimica Acta* **2007**, *52* (25), 7352–7361. https://doi.org/10.1016/J.ELECTACTA.2007.06.007.

(110) Jena, B. K.; Raj, C. R. Enzyme-Free Amperometric Sensing of Glucose by Using Gold Nanoparticles. *Chemistry – A European Journal* **2006**, *12* (10), 2702–2708. https://doi.org/10.1002/CHEM.200501051.

(111) Li, Y.; Song, Y. Y.; Yang, C.; Xia, X. H. Hydrogen Bubble Dynamic Template Synthesis of Porous Gold for Nonenzymatic Electrochemical Detection of Glucose. *Electrochemistry Communications* **2007**, *9* (5), 981–988. https://doi.org/10.1016/J.ELECOM.2006.11.035.

(112) Kurniawan, F.; Tsakova, V.; Mirsky, V. M. Gold Nanoparticles in Nonenzymatic Electrochemical Detection of Sugars. *Electroanalysis* **2006**, *18* (19–20), 1937–1942. https://doi.org/10.1002/ELAN.200603607.

(113) Zheng, B.; Qian, L.; Yuan, H.; Xiao, D.; Yang, X.; Paau, M. C.; Choi, M. M. F. Preparation of Gold Nanoparticles on Eggshell Membrane and Their Biosensing Application. *Talanta* **2010**, *82* (1), 177–183. https://doi.org/10.1016/J.TALANTA.2010.04.014.

(114) Huang, X.; Li, Y.; Wang, P.; Wang, L. Sensitive Determination of Dopamine and Uric Acid by the Use of a Glassy Carbon Electrode Modified with Poly(3-Methylthiophene)/Gold Nanoparticle Composites. *Anal Sci* **2008**, *24* (12), 1563–1568. https://doi.org/10.2116/ANALSCI.24.1563.

(115) Li, M.; Gao, F.; Yang, P.; Wang, L.; Fang, B. Conveniently Assembling Dithiocarbamate and Gold Nanoparticles onto the Gold Electrode: A New Type of Electrochemical Sensors for Biomolecule Detection. *Surface Science* **2008**, *602* (1), 151–155. https://doi.org/10.1016/J.SUSC.2007.10.006.

(116) Raj, C. R.; Okajima, T.; Ohsaka, T. Gold Nanoparticle Arrays for the Voltammetric Sensing of Dopamine. *Journal of Electroanalytical Chemistry* **2003**, *543* (2), 127–133. https://doi.org/10.1016/S0022-0728(02)01481-X.

(117) Hu, G. Z.; Zhang, D. P.; Wu, W. L.; Yang, Z. S. Selective Determination of Dopamine in the Presence of High Concentration of Ascorbic Acid Using Nano-Au Self-Assembly Glassy Carbon Electrode. *Colloids Surf B Biointerfaces* **2008**, *62* (2), 199–205. https://doi.org/10.1016/J.COLSURFB.2007.10.001.

(118) Zhang, L.; Jiang, X. Attachment of Gold Nanoparticles to Glassy Carbon Electrode and Its Application for the Voltammetric Resolution of Ascorbic Acid and Dopamine. *Journal of Electroanalytical Chemistry* **2005**, *583* (2), 292–299. https://doi.org/10.1016/J.JELECHEM.2005.06.014.

(119) Li, J.; Lin, X. Simultaneous Determination of Dopamine and Serotonin on Gold Nanocluster/Overoxidized-Polypyrrole Composite Modified Glassy Carbon Electrode. *Sensors and Actuators B: Chemical* **2007**, *124* (2), 486–493. https://doi.org/10.1016/J.SNB.2007.01.021.

(120) Hu, G.; Ma, Y.; Guo, Y.; Shao, S. Electrocatalytic Oxidation and Simultaneous Determination of Uric Acid and Ascorbic Acid on the Gold Nanoparticles-Modified Glassy Carbon Electrode. *Electrochimica Acta* **2008**, *53* (22), 6610–6615. https://doi.org/10.1016/J.ELECTACTA.2008.04.054.

(121) Zhang, S.; Xu, M.; Zhang, Y. Simultaneous Voltammetric Detection of Salsolinol and Uric Acid in the Presence of High Concentration of Ascorbic Acid with Gold Nanoparticles/Functionalized Multiwalled Carbon Nanotubes Composite Film Modified Electrode. *Electroanalysis* **2009**, *21* (23), 2607–2610. https://doi.org/10.1002/ELAN.200900228.

(122) Raj, C. R.; Ohsaka, T. Voltammetric Detection of Uric Acid in the Presence of Ascorbic Acid at a Gold Electrode Modified with a Self-Assembled Monolayer of Heteroaromatic Thiol. *Journal of Electroanalytical Chemistry* **2003**, *540*, 69–77. https://doi.org/10.1016/S0022-0728(02)01285-8.

(123) Li, J.; Lin, X. Q. Electrodeposition of Gold Nanoclusters on Overoxidized Polypyrrole Film Modified Glassy Carbon Electrode and Its Application for the Simultaneous Determination of Epinephrine and Uric Acid under Coexistence of Ascorbic Acid. *Anal Chim Acta* **2007**, *596* (2), 222–230. https://doi.org/10.1016/J.ACA.2007.05.057.

(124) Lu, L.; Lin, X. Glassy Carbon Electrode Modified with Gold Nanoparticles and DNA for the Simultaneous Determination of Uric Acid and Norepinephrine under Coexistence of Ascorbic Acid. *Anal Sci* **2004**, *20* (3), 527–530. https://doi.org/10.2116/ANALSCI.20.527.

(125) Kalimuthu, P.; John, S. A. Size Dependent Electrocatalytic Activity of Gold Nanoparticles Immobilized onto Three Dimensional Sol–Gel Network. *Journal of Electroanalytical Chemistry* **2008**, *617* (2), 164–170. https://doi.org/10.1016/J.JELECHEM.2008.02.012.

(126) Kannan, P.; John, S. A. Determination of Nanomolar Uric and Ascorbic Acids Using Enlarged Gold Nanoparticles Modified Electrode. *Anal Biochem* **2009**, *386* (1), 65–72. https://doi.org/10.1016/J.AB.2008.11.043.

(127) Yin, H.; Zhou, Y.; Ai, S.; Han, R.; Tang, T.; Zhu, L. Electrochemical Behavior of Bisphenol A at Glassy Carbon Electrode Modified with Gold Nanoparticles, Silk Fibroin, and PAMAM Dendrimers. *Microchimica Acta* **2010**, *170* (1), 99–105. https://doi.org/10.1007/s00604-010-0396-z.

(128) Li, J. Electrocatalytic Oxidation of Nitrite at Gold Nanoparticle- Polypyrrole Nanowire Modified Glassy Carbon Electrode. *Chinese Journal of Chemistry* **2009**, *27* (12), 2373–2378. https://doi.org/10.1002/CJOC.201090011.

(129) Liu, Y.; Gu, H. Y. Amperometric Detection of Nitrite Using a Nanometer-Sized Gold Colloid Modified Pretreated Glassy Carbon Electrode. *Microchimica Acta 2008 162:1* **2008**, *162* (1), 101–106. https://doi.org/10.1007/S00604-007-0946-9.

(130) Jiang, Y. N.; Luo, H. Q.; Li, N. B. Determination of Nitrite with a Nano-Gold Modified Glassy Carbon Electrode by Cyclic Voltammetry. *http://dx.doi.org/10.1080/03067310601079582* **2007**, *87* (4), 295–306. https://doi.org/10.1080/03067310601079582.

(131) Łuczak, T. Comparison of Electrochemical Oxidation of Epinephrine in the Presence of Interfering Ascorbic and Uric Acids on Gold Electrodes Modified with S-Functionalized Compounds and Gold Nanoparticles. *Electrochimica Acta* **2009**, *54* (24), 5863–5870. https://doi.org/10.1016/J.ELECTACTA.2009.05.047.

(132) Wang, L.; Bai, J.; Huang, P.; Wang, H.; Zhang, L.; Zhao, Y. Self-Assembly of Gold Nanoparticles for the Voltammetric Sensing of Epinephrine. *Electrochemistry Communications* **2006**, *8* (6), 1035–1040. https://doi.org/10.1016/J.ELECOM.2006.04.012.

(133) Jin, B.; Zhang, H. NANO-GOLD MODIFIED GLASSY CARBON ELECTRODE FOR SELECTIVE DETERMINATION OF EPINEPHRINE IN THE PRESENCE OF ASCORBIC ACID. *http://dx.doi.org/10.1081/AL-120014282* **2007**, *35* (12), 1907–1918. https://doi.org/10.1081/AL-120014282.

(134) Li, J.; Lin, X. Q. Electrodeposition of Gold Nanoclusters on Overoxidized Polypyrrole Film Modified Glassy Carbon Electrode and Its Application for the Simultaneous Determination of Epinephrine and Uric Acid under Coexistence of Ascorbic Acid. *Anal Chim Acta* **2007**, *596* (2), 222–230. https://doi.org/10.1016/J.ACA.2007.05.057.

(135) B, B. P.; D, J.; MP, T. A Dual-Template Imprinted Polymer-Modified Carbon Ceramic Electrode for Ultra Trace Simultaneous Analysis of Ascorbic Acid and Dopamine. *Biosens Bioelectron* **2013**, *50*, 19–27. https://doi.org/10.1016/J.BIOS.2013.05.062.

(136) Nair, S. S.; John, S. A.; Sagara, T. Simultaneous Determination of Paracetamol and Ascorbic Acid Using Tetraoctylammonium Bromide Capped Gold Nanoparticles Immobilized on 1,6-Hexanedithiol Modified Au Electrode. *Electrochimica Acta* **2009**, *54* (27), 6837–6843. https://doi.org/10.1016/J.ELECTACTA.2009.06.077.

(137) Ragupathy, D.; Gopalan, A. I.; Lee, K. P. Electrocatalytic Oxidation and Determination of Ascorbic Acid in the Presence of Dopamine at Multiwalled Carbon Nanotube–Silica Network–Gold Nanoparticles Based Nanohybrid Modified Electrode. *Sensors and Actuators B: Chemical* **2010**, *143* (2), 696–703. https://doi.org/10.1016/J.SNB.2009.10.026.

(138) Sivanesan, A.; Kannan, P.; Abraham John, S. Electrocatalytic Oxidation of Ascorbic Acid Using a Single Layer of Gold Nanoparticles Immobilized on 1,6-Hexanedithiol Modified Gold Electrode. *Electrochimica Acta* **2007**, *52* (28), 8118–8124. https://doi.org/10.1016/J.ELECTACTA.2007.07.020.

(139) Wang, J.; Wang, F.; Zou, X.; Xu, Z.; Dong, S. Surface Plasmon Resonance and Electrochemistry for Detection of Small Molecules Using Catalyzed Deposition of Metal Ions on Gold Substrate. *Electrochemistry Communications* **2007**, *9* (2), 343–347. https://doi.org/10.1016/J.ELECOM.2006.09.011.

(140) Mehmandoust, M.; Erk, N.; Karaman, C.; Karimi, F.; Salmanpour, S. Sensitive and Selective Electrochemical Detection of Epirubicin as Anticancer Drug Based on Nickel Ferrite Decorated with Gold Nanoparticles. *Micromachines (Basel)* **2021**, *12* (11), 1334. https://doi.org/10.3390/MI12111334/S1.

(141) Mehrabi, A.; Rahimnejad, M.; Mohammadi, M.; Pourali, M. Electrochemical Detection of Flutamide as an Anticancer Drug with Gold Nanoparticles Modified Glassy Carbon Electrode in the Presence of Prostate Cancer Cells. *Journal of Applied Electrochemistry* **2021**, *51* (4), 597–606. https://doi.org/10.1007/S10800-020-01519-9/FIGURE S/11.

(142) Karthik, R.; Karikalan, N.; Chen, S. M.; Gnanaprakasam, P.; Karuppiah, C. Voltammetric Determination of the Anti-Cancer Drug Nilutamide Using a Screen-Printed

Carbon Electrode Modified with a Composite Prepared from β-Cyclodextrin, Gold Nanoparticles and Graphene Oxide. *Microchimica Acta* **2017**, *184* (2), 507–514. https://doi.org/10.1007/S00604-016-2037-7/TABLES/2.

(143) Ibrahim, H.; Temerk, Y. Gold Nanoparticles Anchored Graphitized Carbon Nanofibers Ionic Liquid Electrode for Ultrasensitive and Selective Electrochemical Sensing of Anticancer Drug Irinotecan. *Microchimica Acta* **2020**, *187* (10), 1–11. https://doi.org/10.1007/S00604-020-04560-9/FIGURE S/5.

(144) Ibrahim, M.; Ibrahim, H.; Almandil, N. B.; Kawde, A. N. A Novel Nanocomposite Based on Gold Nanoparticles Loaded on Acetylene Black for Electrochemical Sensing of the Anticancer Drug Topotecan in the Presence of High Concentration of Uric Acid. *Journal of Electroanalytical Chemistry* **2018**, *824*, 22–31. https://doi.org/10.1016/J.JELECHEM.2018.07.031.

(145) Afkhami, A.; Bahiraei, A.; Madrakian, T. Gold Nanoparticle/Multi-Walled Carbon Nanotube Modified Glassy Carbon Electrode as a Sensitive Voltammetric Sensor for the Determination of Diclofenac Sodium. *Materials Science and Engineering: C* **2016**, *59*, 168–176. https://doi.org/10.1016/J.MSEC.2015.09.097.

(146) Nasiri, F.; Rounaghi, G. H.; Ashraf, N.; Deiminiat, B. A New Electrochemical Sensing Platform for Quantitative Determination of Diclofenac Based on Gold Nanoparticles Decorated Multiwalled Carbon Nanotubes/Graphene Oxide Nanocomposite Film. *International Journal of Environmental Analytical Chemistry* **2021**, *101* (2), 153–166. https://doi.org/10.1080/03067319.2019.1661396/SUPPL_FILE/GEAC_A_1661396_SM1973.DOCX.

(147) Wang, C.; Jiang, T.; Zhao, K.; Deng, A.; Li, J. A Novel Electrochemiluminescent Immunoassay for Diclofenac Using Conductive Polymer Functionalized Graphene Oxide as Labels and Gold Nanorods as Signal Enhancers. *Talanta* **2019**, *193*, 184–191. https://doi.org/https://doi.org/10.1016/j.talanta.2018.09.103.

(148) *A Sensitive Simultaneous Determination of Uric Acid, Norepinephrine and Indomethacin using a Cadmium Sulfide Nanoparticles/Multi-Walled Carbon Nanotubes Modified Gold Electrode*. http://www.abechem.com/article_39217.html (accessed 2022-06-14).

(149) Diouf, A.; Moufid, M.; Bouyahya, D.; Österlund, L.; el Bari, N.; Bouchikhi, B. An Electrochemical Sensor Based on Chitosan Capped with Gold Nanoparticles Combined with a Voltammetric Electronic Tongue for Quantitative Aspirin Detection in Human Physiological Fluids and Tablets. *Materials Science and Engineering: C* **2020**, *110*, 110665. https://doi.org/10.1016/J.MSEC.2020.110665.

(150) Ying, J.; Zheng, Y.; Zhang, H.; Fu, L. Room Temperature Biosynthesis of Gold Nanoparticles with Lycoris Aurea Leaf Extract for the Electrochemical Determination of Aspirin. *Revista Mexicana de Ingeniería Química* **2020**, *19* (2), 585–592. https://doi.org/10.24275/RMIQ/MAT741.

(151) Ţuchiu, B. M.; Stefan-van Staden, R. I.; van Staden, J. (Koos) F. Recent Trends in Ibuprofen and Ketoprofen Electrochemical Quantification – A Review. *https://doi.org/10.1080/10408347.2022.2050348* **2022**. https://doi.org/10.1080/10408347.2022.2050348.

(152) Hassan, S. S.; Nafady, A.; Sirajuddin; Solangi, A. R.; Kalhoro, M. S.; Abro, M. I.; Sherazi, S. T. H. Ultra-Trace Level Electrochemical Sensor for Methylene Blue Dye Based on Nafion Stabilized Ibuprofen Derived Gold Nanoparticles. *Sensors and Actuators B: Chemical* **2015**, *208*, 320–326. https://doi.org/10.1016/J.SNB.2014.11.021.

(153) Mehdi Ghoreishi, S.; Behpour, M.; Sadeghzadeh, S.; Golestaneh, M. Electrochemical Determination of Acetaminophen in Different Pharmaceutical Forms with Gold Nanoparticles Carbon Paste Electrode. *Acta Chim. Slov* **2011**, *58*, 69–74.

(154) Galhardo, K. S.; Dadamos, T. R. L.; Bettencourt da Silva, R. J. N.; Machado, S. A. S. Development and Validation of an Advanced Electrochemical Sensor for the Fast and Cheap Determination of Hydrochlorothiazide in Urine Samples Using the Monte-Carlo Method for Uncertainty Evaluation. *Talanta* **2020**, *215*, 120883. https://doi.org/10.1016/J.TALANTA.2020.120883.

(155) Stoiljković, Z.; Avramov Ivić, M.; Petrović, S. D.; Mijin, D.; Stevanović, S.; Lačnjevac, U.; Marinković, A. D. Voltammetric and Square-Wave Anodic Stripping Determination of Amlodipine Besylate on Gold Electrode. *International Journal of electrochemical science* **2012**, *7* (3), 2288–2303.

(156) Norouzi, P.; Ganjali, M. R.; Sepehri, A.; Ghorbani, M. Novel Method for Fast Determination of Ultra Trace Amounts of Timolol Maleate by Continuous Cyclic Voltammetry at Au Microelectrode in Flowing Injection Systems. *Sensors and Actuators B: Chemical* **2005**, *110* (2), 239–245. https://doi.org/10.1016/J.SNB.2005.02.001.

(157) Roushani, M.; Jalilian, Z.; Nezhadali, A. A Novel Electrochemical Sensor Based on Electrode Modified with Gold Nanoparticles and Molecularly Imprinted Polymer for Rapid Determination of Trazosin. *Colloids and Surfaces B: Biointerfaces* **2018**, *172*, 594–600. https://doi.org/10.1016/J.COLSURFB.2018.09.015.

(158) Atta, N. F.; Galal, A.; Azab, S. M. Gold Nanoparticles Modified Electrode for the Determination of an Antihypertensive Drug. *Electroanalysis* **2012**, *24* (6), 1431–1440. https://doi.org/10.1002/ELAN.201200169.

(159) Shahbakhsh, M.; Hashemzaei, Z.; Narouie, S.; Shahbakhsh, Y.; Noroozifar, M. Gold Nanoparticles/Biphenol–Biphenoquinone for Ultra-Trace Voltammetric Determination of Captopril. *Electroanalysis* **2021**, *33* (3), 713–722. https://doi.org/10.1002/ELAN.202060352.

(160) Goyal, R. N.; Gupta, V. K.; Oyama, M.; Bachheti, N. Differential Pulse Voltammetric Determination of Atenolol in Pharmaceutical Formulations and Urine Using Nanogold

Modified Indium Tin Oxide Electrode. *Electrochemistry Communications* **2006**, *8* (1), 65–70. https://doi.org/10.1016/J.ELECOM.2005.10.011.

(161) Roushani, M.; Jalilian, Z.; Nezhadali, A. Screen Printed Carbon Electrode Sensor with Thiol Graphene Quantum Dots and Gold Nanoparticles for Voltammetric Determination of Solatol. *Heliyon* **2019**, *5* (6), e01984. https://doi.org/10.1016/J.HELIYON.2019.E01984.

(162) Ghoreishi, S. M.; Behpour, M.; Khoobi, A. Central Composite Rotatable Design in the Development of a New Method for Optimization, Voltammetric Determination and Electrochemical Behavior of Betaxolol in the Presence of Acetaminophen Based on a Gold Nanoparticle Modified Electrode. *Analytical Methods* **2012**, *4* (8), 2475–2485. https://doi.org/10.1039/C2AY25268F.

(163) Sanghavi, B. J.; Srivastava, A. K. Simultaneous Voltammetric Determination of Acetaminophen and Tramadol Using Dowex50wx2 and Gold Nanoparticles Modified Glassy Carbon Paste Electrode. *Analytica Chimica Acta* **2011**, *706* (2), 246–254. https://doi.org/10.1016/J.ACA.2011.08.040.

(164) Kolahi-Ahari, S.; Deiminiat, B.; Rounaghi, G. H. Modification of a Pencil Graphite Electrode with Multiwalled Carbon Nanotubes Capped Gold Nanoparticles for Electrochemical Determination of Tramadol. *Journal of Electroanalytical Chemistry* **2020**, *862*, 113996. https://doi.org/10.1016/J.JELECHEM.2020.113996.

(165) Hojjati-Najafabadi, A.; Salmanpour, S.; Sen, F.; Asrami, P. N.; Mahdavian, M.; Khalilzadeh, M. A. A Tramadol Drug Electrochemical Sensor Amplified by Biosynthesized Au Nanoparticle Using Mentha Aquatic Extract and Ionic Liquid. *Topics in Catalysis* **2022**, *65* (5–6), 587–594. https://doi.org/10.1007/S11244-021-01498-X/TABLES/2.

(166) Atta, N. F.; Ahmed, R. A.; Amin, H. M. A.; Galal, A. Monodispersed Gold Nanoparticles Decorated Carbon Nanotubes as an Enhanced Sensing Platform for Nanomolar Detection of Tramadol. *Electroanalysis* **2012**, *24* (11), 2135–2146. https://doi.org/10.1002/ELAN.201200344.

(167) Khairy, M. A Synergetic Effect of Cerium Oxide Nanocubes and Gold Nanoparticles for Developing a New Photoelectrochemical Sensor of Codeine Drug. *Journal of Electroanalytical Chemistry* **2021**, *895*, 115517. https://doi.org/10.1016/J.JELECHEM.2021.115517.

(168) Afkhami, A.; Khoshsafar, H.; Bagheri, H.; Madrakian, T. Facile Simultaneous Electrochemical Determination of Codeine and Acetaminophen in Pharmaceutical Samples and Biological Fluids by Graphene–CoFe2O4 Nancomposite Modified Carbon Paste Electrode. *Sensors and Actuators B: Chemical* **2014**, *203*, 909–918. https://doi.org/10.1016/J.SNB.2014.07.031.

(169) Niu, X.; Huang, L.; Zhao, J.; Yin, M.; Luo, D.; Yang, Y. An Ultrasensitive Aptamer Biosensor for the Detection of Codeine Based on a Au Nanoparticle/Polyamidoamine

Dendrimer-Modified Screen-Printed Carbon Electrode. *Analytical Methods* **2016**, *8* (5), 1091–1095. https://doi.org/10.1039/C5AY01747E.

(170) Atta, N. F.; Galal, A.; Azab, S. M. Determination of Morphine at Gold Nanoparticles / Nafion ® Carbon Paste Modified Sensor Electrode. *Analyst* **2011**, *136* (22), 4682–4691. https://doi.org/10.1039/C1AN15423K.

(171) Atta, N. F.; Galal, A.; Wassel, A. A.; Ibrahim, A. H. Sensitive Electrochemical Determination of Morphine Using Gold Nanoparticles-Ferrocene Modified Carbon Paste Electrode. *Int. J. Electrochem. Sci* **2012**, *7*, 10501–10518.

(172) Zhao, Y.; Wu, Y.; Zhang, Y.; Chen, Z.; Cao, X.; Di, J.; Yang, J. Electrocatalytic Behavior and Amperometric Detection of Morphine on ITO Electrode Modified with Directly Electrodeposited Gold Nanoparticles. *Electroanalysis* **2009**, *21* (8), 939–943. https://doi.org/10.1002/ELAN.200804495.

(173) Deshmukh, M. A.; Kang, B. C.; Ha, T. J. Non-Enzymatic Electrochemical Glucose Sensors Based on Polyaniline/Reduced-Graphene-Oxide Nanocomposites Functionalized with Silver Nanoparticles. *Journal of Materials Chemistry C* **2020**, *8* (15), 5112–5123. https://doi.org/10.1039/C9TC06836H.

(174) Ensafi, A. A.; Zandi-Atashbar, N.; Rezaei, B.; Ghiaci, M.; Taghizadeh, M. Silver Nanoparticles Decorated Carboxylate Functionalized SiO2, New Nanocomposites for Non-Enzymatic Detection of Glucose and Hydrogen Peroxide. *Electrochimica Acta* **2016**, *214*, 208–216. https://doi.org/10.1016/J.ELECTACTA.2016.08.047.

(175) Lin, J.; He, C.; Zhao, Y.; Zhang, S. One-Step Synthesis of Silver Nanoparticles/Carbon Nanotubes/Chitosan Film and Its Application in Glucose Biosensor. *Sensors and Actuators B: Chemical* **2009**, *137* (2), 768–773. https://doi.org/10.1016/J.SNB.2009.01.033.

(176) Quan, H.; Park, S. U.; Park, J. Electrochemical Oxidation of Glucose on Silver Nanoparticle-Modified Composite Electrodes. *Electrochimica Acta* **2010**, *55* (7), 2232–2237. https://doi.org/10.1016/J.ELECTACTA.2009.11.074.

(177) Poletti Papi, M. A.; Caetano, F. R.; Bergamini, M. F.; Marcolino-Junior, L. H. Facile Synthesis of a Silver Nanoparticles/Polypyrrole Nanocomposite for Non-Enzymatic Glucose Determination. *Materials Science and Engineering: C* **2017**, *75*, 88–94. https://doi.org/10.1016/J.MSEC.2017.02.026.

(178) Org, W. E.; Rad, A. S.; Mirabi, A.; Binaian, E.; Tayebi, H. ELECTROCHEMICAL SCIENCE A Review on Glucose and Hydrogen Peroxide Biosensor Based on Modified Electrode Included Silver Nanoparticles. *Int. J. Electrochem. Sci* **2011**, *6*, 3671–3683.

(179) Ensafi, A. A.; Zandi-Atashbar, N.; Rezaei, B.; Ghiaci, M.; Chermahini, M. E.; Moshiri, P. Non-Enzymatic Glucose Electrochemical Sensor Based on Silver Nanoparticle Decorated Organic Functionalized Multiwall Carbon Nanotubes. *RSC Advances* **2016**, *6* (65), 60926–60932. https://doi.org/10.1039/C6RA10698F.

(180) Khalifa, Z.; Zahran, M.; A-H Zahran, M.; Azzem, M. A. Mucilage-Capped Silver Nanoparticles for Glucose Electrochemical Sensing and Fuel Cell Applications. *RSC Advances* **2020**, *10* (62), 37675–37682. https://doi.org/10.1039/D0RA07359H.

(181) Yusoff, N.; Rameshkumar, P.; Mehmood, M. S.; Pandikumar, A.; Lee, H. W.; Huang, N. M. Ternary Nanohybrid of Reduced Graphene Oxide-Nafion@silver Nanoparticles for Boosting the Sensor Performance in Non-Enzymatic Amperometric Detection of Hydrogen Peroxide. *Biosensors and Bioelectronics* **2017**, *87*, 1020–1028. https://doi.org/10.1016/J.BIOS.2016.09.045.

(182) Dodevska, T.; Vasileva, I.; Denev, P.; Karashanova, D.; Georgieva, B.; Kovacheva, D.; Yantcheva, N.; Slavov, A. Rosa Damascena Waste Mediated Synthesis of Silver Nanoparticles: Characteristics and Application for an Electrochemical Sensing of Hydrogen Peroxide and Vanillin. *Materials Chemistry and Physics* **2019**, *231*, 335–343. https://doi.org/10.1016/J.MATCHEMPHYS.2019.04.030.

(183) Welch, C. M.; Banks, C. E.; Simm, A. O.; Compton, R. G. Silver Nanoparticle Assemblies Supported on Glassy-Carbon Electrodes for the Electro-Analytical Detection of Hydrogen Peroxide. *Analytical and Bioanalytical Chemistry* **2005**, *382* (1), 12–21. https://doi.org/10.1007/S00216-005-3205-5/TABLES/1.

(184) Yadav, D. K.; Gupta, R.; Ganesan, V.; Sonkar, P. K.; Rastogi, P. K. Electrochemical Sensing Platform for Hydrogen Peroxide Determination at Low Reduction Potential Using Silver Nanoparticle-Incorporated Bentonite Clay. *Journal of Applied Electrochemistry* **2016**, *46* (1), 103–112. https://doi.org/10.1007/S10800-015-0904-2/TABLES/2.

(185) Shi, Y.; Liu, Z.; Zhao, B.; Sun, Y.; Xu, F.; Zhang, Y.; Wen, Z.; Yang, H.; Li, Z. Carbon Nanotube Decorated with Silver Nanoparticles via Noncovalent Interaction for a Novel Nonenzymatic Sensor towards Hydrogen Peroxide Reduction. *Journal of Electroanalytical Chemistry* **2011**, *656* (1–2), 29–33. https://doi.org/10.1016/J.JELECHEM.2011.01.036.

(186) Kumar, V.; Gupta, R. K.; Gundampati, R. K.; Singh, D. K.; Mohan, S.; Hasan, S. H.; Malviya, M. Enhanced Electron Transfer Mediated Detection of Hydrogen Peroxide Using a Silver Nanoparticle–Reduced Graphene Oxide–Polyaniline Fabricated Electrochemical Sensor. *RSC Advances* **2018**, *8* (2), 619–631. https://doi.org/10.1039/C7RA11466D.

(187) Yang, Z.; Qi, C.; Zheng, X.; Zheng, J. Sensing Hydrogen Peroxide with a Glassy Carbon Electrode Modified with Silver Nanoparticles, AlOOH and Reduced Graphene Oxide. *Microchimica Acta* **2016**, *183* (3), 1131–1136. https://doi.org/10.1007/S00604-016-1743-5/FIGURE S/6.

(188) Zhan, B.; Liu, C.; Shi, H.; Li, C.; Wang, L.; Huang, W.; Dong, X. A Hydrogen Peroxide Electrochemical Sensor Based on Silver Nanoparticles Decorated Three-Dimensional Graphene. *Applied Physics Letters* **2014**, *104* (24), 243704. https://doi.org/10.1063/1.4884418.

(189) Maduraiveeran, G.; Kundu, M.; Sasidharan, M. Electrochemical Detection of Hydrogen Peroxide Based on Silver Nanoparticles via Amplified Electron Transfer Process. *Journal of Materials Science* **2018**, *53* (11), 8328–8338. https://doi.org/10.1007/S10853-018-2141-7/TABLES/1.

(190) Tian, Y.; Wang, F.; Liu, Y.; Pang, F.; Zhang, X. Green Synthesis of Silver Nanoparticles on Nitrogen-Doped Graphene for Hydrogen Peroxide Detection. *Electrochimica Acta* **2014**, *146*, 646–653. https://doi.org/10.1016/J.ELECTACTA.2014.08.133.

(191) Yin, J.; Qi, X.; Yang, L.; Hao, G.; Li, J.; Zhong, J. A Hydrogen Peroxide Electrochemical Sensor Based on Silver Nanoparticles Decorated Silicon Nanowire Arrays. *Electrochimica Acta* **2011**, *56* (11), 3884–3889. https://doi.org/10.1016/J.ELECTACTA.2011.02.033.

(192) Ghanbari, K.; Hajheidari, N. Simultaneous Electrochemical Determination of Dopamine, Uric Acid and Ascorbic Acid Using Silver Nanoparticles Deposited on Polypyrrole Nanofibers. *Journal of Polymer Research* **2015**, *22* (8), 1–9. https://doi.org/10.1007/S10965-015-0797-0/TABLES/3.

(193) Sookhakian, M.; Basirun, W. J.; Goh, B. T.; Woi, P. M.; Alias, Y. Molybdenum Disulfide Nanosheet Decorated with Silver Nanoparticles for Selective Detection of Dopamine. *Colloids and Surfaces B: Biointerfaces* **2019**, *176*, 80–86. https://doi.org/10.1016/J.COLSURFB.2018.12.058.

(194) Saha, S.; Sarkar, P.; Turner, A. P. F. Interference-Free Electrochemical Detection of Nanomolar Dopamine Using Doped Polypyrrole and Silver Nanoparticles. *Electroanalysis* **2014**, *26* (10), 2197–2206. https://doi.org/10.1002/ELAN.201400332.

(195) Shin, J. W.; Kim, K. J.; Yoon, J.; Jo, J.; El-Said, W. A.; Choi, J. W. Silver Nanoparticle Modified Electrode Covered by Graphene Oxide for the Enhanced Electrochemical Detection of Dopamine. *Sensors 2017, Vol. 17, Page 2771* **2017**, *17* (12), 2771. https://doi.org/10.3390/S17122771.

(196) Sreenivasulu, V.; Siva Kumar, N.; Suguna, M.; Asif, M.; Al-Ghurabi, E. H.; Huang, Z. X.; Zhen, Z. ELECTROCHEMICAL SCIENCE Biosynthesis of Silver Nanoparticles Using Mimosa Pudica Plant Root Extract: Characterization, Antibacterial Activity and Electrochemical Detection of Dopamine. *Int. J. Electrochem. Sci* **2016**, *11*, 9959–9971. https://doi.org/10.20964/2016.12.69.

(197) Cincotto, F. H.; Canevari, T. C.; Campos, A. M.; Landers, R.; Machado, S. A. S. Simultaneous Determination of Epinephrine and Dopamine by Electrochemical Reduction on the Hybrid Material SiO 2 /Graphene Oxide Decorated with Ag Nanoparticles. *Analyst* **2014**, *139* (18), 4634–4640. https://doi.org/10.1039/C4AN00580E.

(198) Cesarino, I.; Galesco, H. v.; Machado, S. A. S. Determination of Serotonin on Platinum Electrode Modified with Carbon Nanotubes/Polypyrrole/Silver Nanoparticles Nanohybrid. *Materials Science and Engineering: C* **2014**, *40*, 49–54. https://doi.org/10.1016/J.MSEC.2014.03.030.

(199) Ehsani, M.; Soleymani, J.; Mohammadalizadeh, P.; Hasanzadeh, M.; Jouyban, A.; Khoubnasabjafari, M.; Vaez-Gharamaleki, Y. Low Potential Detection of Doxorubicin Using a Sensitive Electrochemical Sensor Based on Glassy Carbon Electrode Modified with Silver Nanoparticles-Supported Poly(Chitosan): A New Platform in Pharmaceutical Analysis. *Microchemical Journal* **2021**, *165*, 106101. https://doi.org/10.1016/J.MICROC.2021.106101.

(200) Zhang, K.; Zhang, Y. Electrochemical Behavior of Adriamycin at an Electrode Modified with Silver Nanoparticles and Multi-Walled Carbon Nanotubes, and Its Application. *Microchimica Acta* **2010**, *169* (1), 161–165. https://doi.org/10.1007/S00604-010-0331-3/FIGURE S/5.

(201) Ahmadi, F.; Raoof, J. B.; Ojani, R.; Baghayeri, M.; Lakouraj, M. M.; Tashakkorian, H. Synthesis of Ag Nanoparticles for the Electrochemical Detection of Anticancer Drug Flutamide. *Chinese Journal of Catalysis* **2015**, *36* (3), 439–445. https://doi.org/10.1016/S1872-2067(14)60209-6.

(202) Wu, Z.; Liu, J.; Liang, M.; Zheng, H.; Zhu, C.; Wang, Y. Detection of Imatinib Based on Electrochemical Sensor Constructed Using Biosynthesized Graphene-Silver Nanocomposite. *Frontiers in Chemistry* **2021**, *9*, 208. https://doi.org/10.3389/FCHEM.2021.670074/BIBTEX.

(203) Shams, A.; Yari, A. A New Sensor Consisting of Ag-MWCNT Nanocomposite as the Sensing Element for Electrochemical Determination of Epirubicin. *Sensors and Actuators B: Chemical* **2019**, *286*, 131–138. https://doi.org/10.1016/J.SNB.2019.01.128.

(204) Zahed, F. M.; Hatamluyi, B.; Lorestani, F.; Es'haghi, Z. Silver Nanoparticles Decorated Polyaniline Nanocomposite Based Electrochemical Sensor for the Determination of Anticancer Drug 5-Fluorouracil. *Journal of Pharmaceutical and Biomedical Analysis* **2018**, *161*, 12–19. https://doi.org/10.1016/J.JPBA.2018.08.004.

(205) Manea, F.; Motoc, S.; Pop, A.; Remes, A.; Schoonman, J. Silver-Functionalized Carbon Nanofiber Composite Electrodes for Ibuprofen Detection. *Nanoscale Research Letters* **2012**, *7* (1), 1–4. https://doi.org/10.1186/1556-276X-7-331/FIGURE S/3.

(206) Motoc, S.; Manea, F.; Pop, A.; Pode, R.; Burtica, G. Determination of Ibuprofen in Water Using Ag-Doped Zeolite-Expanded Graphite Composite Electrode. *Advanced Science, Engineering and Medicine* **2012**, *3* (1), 7–12. https://doi.org/10.1166/ASEM.2011.1084.

(207) Motoc, S.; Remes, A.; Pop, A.; Manea, F.; Schoonman, J. Electrochemical Detection and Degradation of Ibuprofen from Water on Multi-Walled Carbon Nanotubes-Epoxy Composite Electrode. *Journal of Environmental Sciences* **2013**, *25* (4), 838–847. https://doi.org/10.1016/S1001-0742(12)60068-0.

(208) Manea, F.; Motoc, S.; Pop, A.; Remes, A.; Schoonman, J. Silver-Functionalized Carbon Nanofiber Composite Electrodes for Ibuprofen Detection. *Nanoscale Research Letters* **2012**, *7* (1), 1–4. https://doi.org/10.1186/1556-276X-7-331/FIGURE S/3.

(209) Naz, S.; Nisar, A.; Qian, L.; Hussain, S.; Karim, S.; Hussain, S. Z.; Liu, Y.; Sun, H.; Atta-Ur-Rahman, A. U. R.; Ahmad, M. Graphene Oxide Functionalized with Silver Nanoparticles and ZnO Synergic Nanocomposite as an Efficient Electrochemical Sensor for Diclofenac Sodium. *https://doi.org/10.1142/S1793292021501393* **2021**, *16* (12). https://doi.org/10.1142/S1793292021501393.

(210) Gowthaman, N. S. K.; Lim, H. N.; Shankar, S. Electrochemical Scaffold Based on Silver Phosphate Nanoparticles for the Quantification of Acetaminophen in Body Fluids and Pharmaceutical Formulations. *ACS Applied Nano Materials* **2020**, *3* (2), 1213–1222. https://doi.org/10.1021/ACSANM.9B01959/SUPPL_FILE/AN9B01959_SI_001.PDF.

(211) Dou, N.; Zhang, S.; Qu, J. Simultaneous Detection of Acetaminophen and 4-Aminophenol with an Electrochemical Sensor Based on Silver–Palladium Bimetal Nanoparticles and Reduced Graphene Oxide. *RSC Advances* **2019**, *9* (54), 31440–31446. https://doi.org/10.1039/C9RA05987C.

(212) Riggin, R. M.; Schmidt, A. L.; Kissinger, P. T. Determination of Acetaminophen in Pharmaceutical Preparations and Body Fluids by High-Performance Liquid Chromatography with Electrochemical Detection. *Journal of Pharmaceutical Sciences* **1975**, *64* (4), 680–683. https://doi.org/10.1002/JPS.2600640423.

(213) Keerthi, M.; Boopathy, G.; Chen, S.-M.; Chen, T.-W.; Rwei, S.-P.; Liu, X. An Efficient Electrochemical Sensor Based on Ag Nanoparticle Decorated MnO 2 /Reduced Graphene Oxide Ternary Nanocomposite for Detection of Acetaminophen in Human Urine Sample. *Int. J. Electrochem. Sci* **2019**, *14*, 346–358. https://doi.org/10.20964/2019.01.59.

(214) Santos, A. M.; Wong, A.; Fatibello-Filho, O. Simultaneous Determination of Salbutamol and Propranolol in Biological Fluid Samples Using an Electrochemical Sensor Based on Functionalized-Graphene, Ionic Liquid and Silver Nanoparticles. *Journal of Electroanalytical Chemistry* **2018**, *824*, 1–8. https://doi.org/10.1016/J.JELECHEM.2018.07.018.

(215) George, J. M.; Antony, A.; Mathew, B. Metal Oxide Nanoparticles in Electrochemical Sensing and Biosensing: A Review. *Microchimica Acta 2018 185:7* **2018**, *185* (7), 1–26. https://doi.org/10.1007/S00604-018-2894-3.

(216) Agnihotri, A. S.; Varghese, A.; M, N. Transition Metal Oxides in Electrochemical and Bio Sensing: A State-of-Art Review. *Applied Surface Science Advances* **2021**, *4*, 100072. https://doi.org/10.1016/J.APSADV.2021.100072.

(217) Younes Jomma, E.; Ding, S.-N.; Lei, Y.; Tiwari, A.; Liu, H. One-Pot Hydrothermal Synthesis of Magnetite Prussian Blue Nano-Composites and Their Application to Fabricate Glucose Biosensor. *Sensors 2016, Vol. 16, Page 243* **2016**, *16* (2), 243. https://doi.org/10.3390/S16020243.

(218) Jędrzak, A.; Kuznowicz, M.; Rębiś, T.; Jesionowski, T. Portable Glucose Biosensor Based on Polynorepinephrine@magnetite Nanomaterial Integrated with a Smartphone Analyzer

for Point-of-Care Application. *Bioelectrochemistry* **2022**, *145*, 108071. https://doi.org/10.1016/J.BIOELECHEM.2022.108071.

(219) Kavitha, A. L.; Gurumallesh Prabu, H.; Ananda Babu, S.; Suja, S. K. Magnetite Nanoparticles-Chitosan Composite Containing Carbon Paste Electrode for Glucose Biosensor Application. *Journal of Nanoscience and Nanotechnology* **2013**, *13* (1), 98–104. https://doi.org/10.1166/JNN.2013.6720.

(220) Kuznowicz, M.; Jędrzak, A.; Rębiś, T.; Jesionowski, T. Biomimetic Magnetite/Polydopamine/β-Cyclodextrins Nanocomposite for Long-Term Glucose Measurements. *Biochemical Engineering Journal* **2021**, *174*, 108127. https://doi.org/10.1016/J.BEJ.2021.108127.

(221) Batool, R.; Akhtar, M. A.; Hayat, A.; Han, D.; Niu, L.; Ahmad, M. A.; Nawaz, M. H. A Nanocomposite Prepared from Magnetite Nanoparticles, Polyaniline and Carboxy-Modified Graphene Oxide for Non-Enzymatic Sensing of Glucose. *Microchimica Acta* **2019**, *186* (5), 1–10. https://doi.org/10.1007/S00604-019-3364-2/TABLES/2.

(222) Jaime, J.; Rangel, G.; Muñoz-Bonilla, A.; Mayoral, A.; Herrasti, P. Magnetite as a Platform Material in the Detection of Glucose, Ethanol and Cholesterol. *Sensors and Actuators B: Chemical* **2017**, *238*, 693–701. https://doi.org/10.1016/J.SNB.2016.07.059.

(223) Salamon, J.; Sathishkumar, Y.; Ramachandran, K.; Lee, Y. S.; Yoo, D. J.; Kim, A. R.; GnanaKumar, G. One-Pot Synthesis of Magnetite Nanorods/Graphene Composites and Its Catalytic Activity toward Electrochemical Detection of Dopamine. *Biosensors and Bioelectronics* **2015**, *64*, 269–276. https://doi.org/10.1016/J.BIOS.2014.08.085.

(224) Ognjanović, M.; Stanković, D. M.; Jaćimović, Ž. K.; Kosović-Perutović, M.; Dojčinović, B.; Antić, B. The Effect of Surface-Modifier of Magnetite Nanoparticles on Electrochemical Detection of Dopamine and Heating Efficiency in Magnetic Hyperthermia. *Journal of Alloys and Compounds* **2021**, *884*, 161075. https://doi.org/10.1016/J.JALLCOM.2021.161075.

(225) He, Q.; Liu, J.; Liu, X.; Li, G.; Chen, D.; Deng, P.; Liang, J. Fabrication of Amine-Modified Magnetite-Electrochemically Reduced Graphene Oxide Nanocomposite Modified Glassy Carbon Electrode for Sensitive Dopamine Determination. *Nanomaterials 2018, Vol. 8, Page 194* **2018**, *8* (4), 194. https://doi.org/10.3390/NANO8040194.

(226) Rosli, A. R. M.; Noorashikin, M. S.; Yusoff, F. Electrochemical Sensor Based on Reduced Graphene Oxide Incorporated with Magnetite and Silver Nanoparticles Composite Electrode for Determination of Dopamine. *Journal of The Electrochemical Society* **2021**, *168* (8), 087512. https://doi.org/10.1149/1945-7111/AC1DCE.

(227) Hosseini, M.; Aghazadeh, M.; Reza Ganjali, M. A Facile One-Pot Synthesis of Cobalt-Doped Magnetite/Graphene Nanocomposite as Peroxidase Mimetics in Dopamine Detection. *New Journal of Chemistry* **2017**, *41* (21), 12678–12684. https://doi.org/10.1039/C7NJ02082A.

(228) Molodtsova, T.; Gorshenkov, M.; Saliev, A.; Vanyushin, V.; Goncharov, I.; Smirnova, N. One-Step Synthesis of γ-Fe2O3/Fe3O4 Nanocomposite for Sensitive Electrochemical Detection of Hydrogen Peroxide. *Electrochimica Acta* **2021**, *370*, 137723. https://doi.org/10.1016/J.ELECTACTA.2021.137723.

(229) Bencsik, G.; Janáky, C.; Endrdi, B.; Visy, C. Electrocatalytic Properties of the Polypyrrole/Magnetite Hybrid Modified Electrode towards the Reduction of Hydrogen Peroxide in the Presence of Dissolved Oxygen. *Electrochimica Acta* **2012**, *73*, 53–58. https://doi.org/10.1016/J.ELECTACTA.2011.10.100.

(230) Venosta, L.; Bracamonte, M. v.; Rodríguez, M. C.; Jacobo, S. E.; Bercoff, P. G. Comparative Studies of Hybrid Functional Materials Based on Different Carbon Structures Decorated with Nano-Magnetite. Suitable Application as Platforms for Enzyme-Free Electrochemical Sensing of Hydrogen Peroxide. *Sensors and Actuators B: Chemical* **2017**, *248*, 460–469. https://doi.org/10.1016/J.SNB.2017.03.159.

(231) Gabunada, J. C.; Vinothkannan, M.; Kim, D. H.; Kim, A. R.; Yoo, D. J. Magnetite Nanorods Stabilized by Polyaniline/Reduced Graphene Oxide as a Sensing Platform for Selective and Sensitive Non-Enzymatic Hydrogen Peroxide Detection. *Electroanalysis* **2019**, *31* (8), 1507–1516. https://doi.org/10.1002/ELAN.201900134.

(232) Munshi, A. M.; Ho, D.; Saunders, M.; Agarwal, V.; Raston, C. L.; Iyer, K. S. Influence of Aspect Ratio of Magnetite Coated Gold Nanorods in Hydrogen Peroxide Sensing. *Sensors and Actuators B: Chemical* **2016**, *235*, 492–497. https://doi.org/10.1016/J.SNB.2016.05.090.

(233) Urçuk, A.; Yıldız, C.; Eskiköy Bayraktepe, D.; Yazan, Z. Highly Sensitive and Disposable Electrochemical Nano Sensor for Simultaneous Analysis of Caffeic Acid and Uric Acid Based on Halloysite Nanotubes and Magnetite Nanoparticles. *Microchemical Journal* **2022**, *181*, 107695. https://doi.org/10.1016/J.MICROC.2022.107695.

(234) Weng, Y. K.; Rashidah, A.; Rosli, M.; Yusoff, F. Magnetite Graphene for Electrochemical Determination of Uric Acid. *Malaysian Journal of Analytical Sciences* **2019**, *23*, 407–422. https://doi.org/10.17576/mjas-2019-2303-05.

(235) Qiu, H.; Luo, C.; Sun, M.; Lu, F.; Fan, L.; Li, X. A Chemiluminescence Sensor for Determination of Epinephrine Using Graphene Oxide–Magnetite-Molecularly Imprinted Polymers. *Carbon N Y* **2012**, *50* (11), 4052–4060. https://doi.org/10.1016/J.CARBON.2012.04.052.

(236) Mattioli, I. A.; Cervini, P.; Cavalheiro, É. T. G. Screen-Printed Disposable Electrodes Using Graphite-Polyurethane Composites Modified with Magnetite and Chitosan-Coated Magnetite Nanoparticles for Voltammetric Epinephrine Sensing: A Comparative Study. *Microchimica Acta* **2020**, *187* (6), 1–12. https://doi.org/10.1007/S00604-020-04259-X/TABLES/3.

(237) Bonyani, M.; Mirzaei, A.; Leonardi, S. G.; Bonavita, A.; Neri, G. Electrochemical Properties of Ag@iron Oxide Nanocomposite for Application as Nitrate Sensor. *Electroanalysis* **2015**, *27* (11), 2654–2662. https://doi.org/10.1002/ELAN.201500240.

(238) Mirzajani, R.; Karimi, S. Preparation of γ-Fe2O3/Hydroxyapatite/Cu(II) Magnetic Nanocomposite and Its Application for Electrochemical Detection of Metformin in Urine and Pharmaceutical Samples. *Sensors and Actuators B: Chemical* **2018**, *270*, 405–416. https://doi.org/10.1016/J.SNB.2018.05.032.

(239) Zia Mohammadi, S.; Tajik, S.; Tashakkorian, H.; Zhang, K.; van Le, Q.; Saeidi, S.; Won Jang, H.; Shokouhimehr, M.; Peng, W. Voltammetric Determination of Antidiabetic Drug Gliclazide in the Presence of Glibenclamide in Real Samples. *Int. J. Electrochem. Sci* **2020**, *15*, 2020. https://doi.org/10.20964/2020.09.49.

(240) Haghshenas, E.; Madrakian, T.; Afkhami, A. Electrochemically Oxidized Multiwalled Carbon Nanotube/Glassy Carbon Electrode as a Probe for Simultaneous Determination of Dopamine and Doxorubicin in Biological Samples. *Analytical and Bioanalytical Chemistry* **2016**, *408* (10), 2577–2586. https://doi.org/10.1007/S00216-016-9361-Y/TABLES/2.

(241) Tajik, S.; Afshar, A. A.; Shamsaddini, S.; Askari, M. B.; Dourandish, Z.; Garkani Nejad, F.; Beitollahi, H.; di Bartolomeo, A. Fe3O4@MoS2/RGO Nanocomposite/Ionic Liquid Modified Carbon Paste Electrode for Electrochemical Sensing of Dasatinib in the Presence of Doxorubicin. *Industrial and Engineering Chemistry Research* **2022**. https://doi.org/10.1021/ACS.IECR.2C00370/ASSET/IMAGES/LARGE/IE2C00370_0008.JPEG.

(242) Hashemi, S. A.; Mousavi, S. M.; Bahrani, S.; Gholami, A.; Chiang, W. H.; Yousefi, K.; Omidifar, N.; Rao, N. V.; Ramakrishna, S.; Babapoor, A.; Lai, C. W. Bio-Enhanced Polyrhodanine/Graphene Oxide/Fe3O4 Nanocomposite with Kombucha Solvent Supernatant as Ultra-Sensitive Biosensor for Detection of Doxorubicin Hydrochloride in Biological Fluids. *Materials Chemistry and Physics* **2022**, *279*, 125743. https://doi.org/10.1016/J.MATCHEMPHYS.2022.125743.

(243) Madrakian, T.; Asl, K. D.; Ahmadi, M.; Afkhami, A. Fe 3 O 4 @Pt/MWCNT/Carbon Paste Electrode for Determination of a Doxorubicin Anticancer Drug in a Human Urine Sample. *RSC Advances* **2016**, *6* (76), 72803–72809. https://doi.org/10.1039/C6RA13935C.

(244) Tajik, S.; Beitollahi, H.; Shahsavari, S.; Nejad, F. G. Simultaneous and Selective Electrochemical Sensing of Methotrexate and Folic Acid in Biological Fluids and Pharmaceutical Samples Using Fe3O4/Ppy/Pd Nanocomposite Modified Screen Printed Graphite Electrode. *Chemosphere* **2022**, *291*, 132736. https://doi.org/10.1016/J.CHEMOSPHERE.2021.132736.

(245) Ghalkhani, M.; Sohouli, E. Synthesis of the Decorated Carbon Nano Onions with Aminated MCM-41/Fe3O4 NPs: Morphology and Electrochemical Sensing Performance for Methotrexate Analysis. *Microporous and Mesoporous Materials* **2022**, *331*, 111658. https://doi.org/10.1016/J.MICROMESO.2021.111658.

(246) El-Said, W. A.; Abdel-Rahman, M. A.; Sayed, E. M.; Abdel-Wahab, A. M. A. Electrochemical Monitoring of Methotrexate Anticancer Drug in Human Blood Serum by Using in Situ Solvothermal Synthesized Fe3O4/ITO Electrode. *Electroanalysis* **2019**, *31* (5), 829–837. https://doi.org/10.1002/ELAN.201800798.

(247) El-Said, W. A.; Abdel-Rahman, M. A.; Sayed, E. M.; Abdel-Wahab, A. M. A. Electrochemical Monitoring of Methotrexate Anticancer Drug in Human Blood Serum by Using in Situ Solvothermal Synthesized Fe3O4/ITO Electrode. *Electroanalysis* **2019**, *31* (5), 829–837. https://doi.org/10.1002/ELAN.201800798.

(248) Shalali, F.; Cheraghi, S.; Taher, M. A. A Sensitive Electrochemical Sensor Amplified with Ionic Liquid and N-CQD/Fe3O4 Nanoparticles for Detection of Raloxifene in the Presence of Tamoxifen as Two Essentials Anticancer Drugs. *Materials Chemistry and Physics* **2022**, *278*, 125658. https://doi.org/10.1016/J.MATCHEMPHYS.2021.125658.

(249) Pourzamani, H.; Hajizadeh, Y.; Mengelizadeh, N. Application of Three-Dimensional Electrofenton Process Using MWCNTs-Fe3O4 Nanocomposite for Removal of Diclofenac. *Process Safety and Environmental Protection* **2018**, *119*, 271–284. https://doi.org/10.1016/J.PSEP.2018.08.014.

(250) Arvand, M.; Hassannezhad, M. Square Wave Voltammetric Determination of Uric Acid and Diclofenac on Multi-Walled Carbon Nanotubes Decorated with Magnetic Core-Shell Fe3O4@SiO2 Nanoparticles as an Enhanced Sensing Interface. *Ionics (Kiel)* **2015**, *21* (12), 3245–3256. https://doi.org/10.1007/S11581-015-1514-Z/TABLES/5.

(251) Huaccallo-Aguilar, Y.; Diaz de Tuesta, J. L.; Álvarez-Torrellas, S.; Gomes, H. T.; Larriba, M.; Ovejero, G.; García, J. New Insights on the Removal of Diclofenac and Ibuprofen by CWPO Using a Magnetite-Based Catalyst in an up-Flow Fixed-Bed Reactor. *Journal of Environmental Management* **2021**, *281*, 111913. https://doi.org/10.1016/J.JENVMAN.2020.111913.

(252) Azadbakht, A.; Beirnvand, S. Voltammetric Aptamer-Based Switch Probes for Sensing Diclofenac Using a Glassy Carbon Electrode Modified with a Composite Prepared from Gold Nanoparticles, Carbon Nanotubes and Amino-Functionalized Fe3O4 Nanoparticles. *Microchimica Acta* **2017**, *184* (8), 2825–2835. https://doi.org/10.1007/S00604-017-2285-1/FIGURE S/7.

(253) Hadi Beitollahi; Fariba Garkani Nejad. A Carbon Paste Electrode Modified by Graphene Oxide/Fe3O4@SiO2/Ionic Liquid Nanocomposite for Voltammetric Determination of Acetaminophen in the Presence of Tyrosine. *Russian Journal of Electrochemistry* **2019**, *55* (12), 1162–1170. https://doi.org/10.1134/S1023193519120024/TABLES/2.

(254) Singh, B. P.; Kumar, A.; Duarte, A. P.; Rojas, S. J.; Crespo-Medina, M.; Areizaga-Martinez, H. I.; Vega-Olivencia, C. A.; Tomar, M. S. Synthesis, Characterization, and Electrochemical Response of Iron Oxide Nanoparticles for Sensing Acetaminophen. *Materials Research Express* **2016**, *3* (10), 106105. https://doi.org/10.1088/2053-1591/3/10/106105.

(255) Raimbault, N.; Grisafi, A.; Ceriotti, M.; -, al; Leitner, J.; Sedmidubský, D.; Andawiyah, atul; Mulyasuryani, A.; Sulistyarti, H. Voltammetric Determination of Paracetamol Using Polyvinyl Alcohol (PVA)-Fe3O4 Modified Glassy Carbon Electrode. *IOP Conference Series: Materials Science and Engineering* **2020**, *833* (1), 012059. https://doi.org/10.1088/1757-899X/833/1/012059.

(256) Chokkareddy, R.; Thondavada, N.; Bhajanthri, N. K.; Redhi, G. G. An Amino Functionalized Magnetite Nanoparticle and Ionic Liquid Based Electrochemical Sensor for the Detection of Acetaminophen. *Analytical Methods* **2019**, *11* (48), 6204–6212. https://doi.org/10.1039/C9AY01743G.

(257) Atta, N. F.; Galal, A.; El-Ads, E. H.; Galal, A. E. New Insight in Fabrication of a Sensitive Nano-Magnetite/Glutamine/Carbon Based Electrochemical Sensor for Determination of Aspirin and Omeprazole. *Journal of The Electrochemical Society* **2019**, *166* (2), B161–B172. https://doi.org/10.1149/2.1241902JES/XML.

(258) Bamoulid, L.; Maurette, M. T.; de Caro, D.; Guenbour, A.; ben Bachir, A.; Aries, L.; el Hajjaji, S.; Benoît-Marquié, F.; Ansart, F. An Efficient Protection of Stainless Steel against Corrosion: Combination of a Conversion Layer and Titanium Dioxide Deposit. *Surface and Coatings Technology* **2008**, *202* (20), 5020–5026. https://doi.org/10.1016/J.SURFCOAT.2008.05.011.

(259) He, X.; Hu, C. Building Three-Dimensional Pt Catalysts on TiO2 Nanorod Arrays for Effective Ethanol Electrooxidation. *Journal of Power Sources* **2011**, *196* (6), 3119–3123. https://doi.org/10.1016/J.JPOWSOUR.2010.12.001.

(260) Liao, J.; Lin, S.; Yang, Y.; Liu, K.; Du, W. Highly Selective and Sensitive Glucose Sensors Based on Organic Electrochemical Transistors Using TiO2 Nanotube Arrays-Based Gate Electrodes. *Sensors and Actuators B: Chemical* **2015**, *208*, 457–463. https://doi.org/10.1016/J.SNB.2014.11.038.

(261) Luo, Z.; Ma, X.; Yang, D.; Yuwen, L.; Zhu, X.; Weng, L.; Wang, L. Synthesis of Highly Dispersed Titanium Dioxide Nanoclusters on Reduced Graphene Oxide for Increased Glucose Sensing. *Carbon N Y* **2013**, *57*, 470–476. https://doi.org/10.1016/J.CARBON.2013.02.020.

(262) AL-Mokaram, A. M. A. A. A.; Yahya, R.; Abdi, M. M.; Mahmud, H. N. M. E. The Development of Non-Enzymatic Glucose Biosensors Based on Electrochemically Prepared Polypyrrole–Chitosan–Titanium Dioxide Nanocomposite Films. *Nanomaterials 2017, Vol. 7, Page 129* **2017**, *7* (6), 129. https://doi.org/10.3390/NANO7060129.

(263) Muthuchamy, N.; Gopalan, A.; Lee, K. P. Highly Selective Non-Enzymatic Electrochemical Sensor Based on a Titanium Dioxide Nanowire–Poly(3-Aminophenyl Boronic Acid)–Gold Nanoparticle Ternary Nanocomposite. *RSC Advances* **2018**, *8* (4), 2138–2147. https://doi.org/10.1039/C7RA09097H.

(264) Siavash Moakhar, R.; Flynn, S. E.; Jalali, M.; del Real Mata, C.; Mahshid, S. S.; Mahshid, S. A Non-Enzymatic Photoelectrochemical Sensor Based on Co-Pi Modified One-Dimensional Titanium Oxide Embedded Microscale Reactor. *Biosensors and Bioelectronics: X* **2022**, *11*, 100157. https://doi.org/10.1016/J.BIOSX.2022.100157.

(265) Dong, Q.; Ryu, H.; Lei, Y. Metal Oxide Based Non-Enzymatic Electrochemical Sensors for Glucose Detection. *Electrochimica Acta* **2021**, *370*, 137744. https://doi.org/10.1016/J.ELECTACTA.2021.137744.

(266) Grochowska, K.; Ryl, J.; Karczewski, J.; Śliwiński, G.; Cenian, A.; Siuzdak, K. Non-Enzymatic Flexible Glucose Sensing Platform Based on Nanostructured TiO2 – Au Composite. *Journal of Electroanalytical Chemistry* **2019**, *837*, 230–239. https://doi.org/10.1016/J.JELECHEM.2019.02.040.

(267) Hovancová, J.; Šišoláková, I.; Vanýsek, P.; Oriňaková, R.; Shepa, I.; Kaňuchová, M.; Király, N.; Vojtko, M.; Čudek, P.; Oriňak, A. Ligand-to-Metal Charge Transfer (LMCT) Complex: New Approach to Non-Enzymatic Glucose Sensors Based on TiO2. *Journal of Electroanalytical Chemistry* **2020**, *878*, 114589. https://doi.org/10.1016/J.JELECHEM.2020.114589.

(268) Li, X.; Yao, J.; Liu, F.; He, H.; Zhou, M.; Mao, N.; Xiao, P.; Zhang, Y. Nickel/Copper Nanoparticles Modified TiO2 Nanotubes for Non-Enzymatic Glucose Biosensors. *Sensors and Actuators B: Chemical* **2013**, *181*, 501–508. https://doi.org/10.1016/J.SNB.2013.02.035.

(269) Jeong, H.; Yoo, J.; Park, S.; Lu, J.; Park, S.; Lee, J. Non-Enzymatic Glucose Biosensor Based on Highly Pure TiO2 Nanoparticles. *Biosensors 2021, Vol. 11, Page 149* **2021**, *11* (5), 149. https://doi.org/10.3390/BIOS11050149.

(270) Gao, A.; Zhang, X.; Peng, X.; Wu, H.; Bai, L.; Jin, W.; Wu, G.; Hang, R.; Chu, P. K. In Situ Synthesis of Ni(OH)2/TiO2 Composite Film on NiTi Alloy for Non-Enzymatic Glucose Sensing. *Sensors and Actuators B: Chemical* **2016**, *232*, 150–157. https://doi.org/10.1016/J.SNB.2016.03.122.

(271) Batra, B.; Narwal, V.; Sumit; Ahlawat, J.; Sharma, M. An Amperometric Cholesterol Biosensor Based on Immobilization of Cholesterol Oxidase onto Titanium Dioxide Nanoparticles. *Sensors International* **2021**, *2*, 100111. https://doi.org/10.1016/J.SINTL.2021.100111.

(272) Azahar Ali, M.; Srivastava, S.; Solanki, P. R.; Varun Agrawal, V.; John, R.; Malhotra, B. D. Nanostructured Anatase-Titanium Dioxide Based Platform for Application to Microfluidics Cholesterol Biosensor. *Applied Physics Letters* **2012**, *101* (8), 084105. https://doi.org/10.1063/1.4747714.

(273) Khaliq, N.; Rasheed, M. A.; Cha, G.; Khan, M.; Karim, S.; Schmuki, P.; Ali, G. Development of Non-Enzymatic Cholesterol Bio-Sensor Based on TiO2 Nanotubes

Decorated with Cu2O Nanoparticles. *Sensors and Actuators B: Chemical* **2020**, *302*, 127200. https://doi.org/10.1016/J.SNB.2019.127200.

(274) Komathi, S.; Muthuchamy, N.; Lee, K. P.; Gopalan, A. I. Fabrication of a Novel Dual Mode Cholesterol Biosensor Using Titanium Dioxide Nanowire Bridged 3D Graphene Nanostacks. *Biosensors and Bioelectronics* **2016**, *84*, 64–71. https://doi.org/10.1016/J.BIOS.2015.11.042.

(275) Wu, H. P.; Cheng, T. L.; Tseng, W. L. Phosphate-Modified TiO2 Nanoparticles for Selective Detection of Dopamine, Levodopa, Adrenaline, and Catechol Based on Fluorescence Quenching. *Langmuir* **2007**, *23* (14), 7880–7885. https://doi.org/10.1021/LA700555Y/SUPPL_FILE/LA700555Y-FILE002.PDF.

(276) Rajeshwari, V.; Vedhi, C.; Fernando, J. Dopamine Sensor Based on Coreshell Poly Paraphenylene Diamine/ Titanium Dioxide/ Multiwalled Carbon Nanotube Nanocomposite. *Materials Today: Proceedings* **2022**. https://doi.org/10.1016/J.MATPR.2022.05.179.

(277) Güngör, Ö.; Özgül, O.; Aksoy, B.; Okuşluk, F.; Köytepe, S. Titanium Dioxide-Multiwalled Carbon Nanotube/Polyimide Composite Film Modified Electrodes for Simultaneous Voltammetric Detection of Ascorbic Acid, Uric Acid and Dopamine as Biomarker Molecules. *Polymer Bulletin* **2022**, 1–27. https://doi.org/10.1007/S00289-022-04077-6/FIGURE S/20.

(278) Lv, C.-Z.; Chen, D.; Cao, Z.; Liu, F.; Cao, X.-M.; He, J.-L.; Zhao, W.-Y. Highly Sensitive and Selective Determination of Dopamine Based on Ionic Liquid-Titanium Dioxide/Graphene Oxide Nanocomposite Modified Electrode. *Int. J. Electrochem. Sci* **2016**, *11*, 10107–10122. https://doi.org/10.20964/2016.12.01.

(279) Patel, B. R.; Imran, S.; Ye, W.; Weng, H.; Noroozifar, M.; Kerman, K. Simultaneous Voltammetric Detection of Six Biomolecules Using a Nanocomposite of Titanium Dioxide Nanorods with Multi-Walled Carbon Nanotubes. *Electrochimica Acta* **2020**, *362*, 137094. https://doi.org/10.1016/J.ELECTACTA.2020.137094.

(280) Josephine, D. S. R.; Babu, K. J.; Gnana kumar, G. peter; Sethuraman, K. Titanium Dioxide Anchored Graphene Oxide Nanosheets for Highly Selective Voltammetric Sensing of Dopamine. *Microchimica Acta* **2017**, *184* (3), 781–790. https://doi.org/10.1007/S00604-016-2015-0/TABLES/1.

(281) Nishan, U.; Sabba, U.; Rahim, A.; Asad, M.; Shah, M.; Iqbal, A.; Iqbal, J.; Muhammad, N. Ionic Liquid Tuned Titanium Dioxide Nanostructures as an Efficient Colorimetric Sensing Platform for Dopamine Detection. *Materials Chemistry and Physics* **2021**, *262*, 124289. https://doi.org/10.1016/J.MATCHEMPHYS.2021.124289.

(282) How, G. T. S.; Pandikumar, A.; Ming, H. N.; Ngee, L. H. Highly Exposed {001} Facets of Titanium Dioxide Modified with Reduced Graphene Oxide for Dopamine Sensing. *Scientific Reports 2014 4:1* **2014**, *4* (1), 1–8. https://doi.org/10.1038/srep05044.

(283) Patel, B. R.; Imran, S.; Ye, W.; Weng, H.; Noroozifar, M.; Kerman, K. Simultaneous Voltammetric Detection of Six Biomolecules Using a Nanocomposite of Titanium Dioxide Nanorods with Multi-Walled Carbon Nanotubes. *Electrochimica Acta* **2020**, *362*, 137094. https://doi.org/10.1016/J.ELECTACTA.2020.137094.

(284) Güngör, Ö.; Özgül, O.; Aksoy, B.; Okuşluk, F.; Köytepe, S. Titanium Dioxide-Multiwalled Carbon Nanotube/Polyimide Composite Film Modified Electrodes for Simultaneous Voltammetric Detection of Ascorbic Acid, Uric Acid and Dopamine as Biomarker Molecules. *Polymer Bulletin* **2022**, 1–27. https://doi.org/10.1007/S00289-022-04077-6/FIGURE S/20.

(285) Zenasni, M.; Quintero-Jaime, A.; Salinas-Torres, D.; Benyoucef, A.; Morallón, E. Electrochemical Synthesis of Composite Materials Based on Titanium Carbide and Titanium Dioxide with Poly(N-Phenyl-o-Phenylenediamine) for Selective Detection of Uric Acid. *Journal of Electroanalytical Chemistry* **2021**, *895*, 115481. https://doi.org/10.1016/J.JELECHEM.2021.115481.

(286) Biswas, S.; Pradhan, S.; Naskar, H.; Bandyopadhyay, R.; Pramanik, P. Sol-Gel Synthesis of Cubic Titanium Dioxide Nanoparticle Using Poly(Ethylene Glycol) as a Capping Agent: Voltammetric Simultaneous Determination of Uric Acid and Guanine. *Microchimica Acta* **2018**, *185* (11), 1–10. https://doi.org/10.1007/S00604-018-3042-9/TABLES/2.

(287) Hosseini, M. G.; Faraji, M.; Momeni, M. M. Application of Titanium Oxide Nanotube Films Containing Gold Nanoparticles for the Electroanalytical Determination of Ascorbic Acid. *Thin Solid Films* **2011**, *519* (11), 3457–3461. https://doi.org/10.1016/J.TSF.2010.12.239.

(288) Chavhan, P. M.; Reddy, V.; Kim, C. Nanostructured Titanium Oxide Platform for Application to Ascorbic Acid Detection. *Int. J. Electrochem. Sci* **2012**, *7*, 5420–5428.

(289) Hoffmann, A. A.; Dias, S. L. P.; Rodrigues, J. R.; Pavan, F. A.; Benvenutti, E. v.; Lima, E. C. Methylene Blue Immobilized on Cellulose Acetate with Titanium Dioxide: An Application as Sensor for Ascorbic Acid. *J Braz Chem Soc* **2008**, *19* (5), 943–949. https://doi.org/10.1590/S0103-50532008000500020.

(290) Li, H.; Li, M.; Guo, W.; Di, H.; Fang, C.; Yang, B. Electrochemical Application of Titanium Dioxide Nanoparticle/Gold Nanoparticle/Multiwalled Carbon Nanotube Nanocomposites for Nonenzymatic Detection of Ascorbic Acid. *Journal of Solid State Electrochemistry* **2014**, *18* (2), 477–485. https://doi.org/10.1007/S10008-013-2277-Y/TABLES/1.

(291) Veerapandi, G.; Meenakshi, S.; Anitta, S.; Arul, C.; Ashokkumar, P.; Sekar, C. Precise and Quick Detection of Ascorbic Acid and Eugenol in Fruits, Pharmaceuticals and Medicinal Herbs Using Hydroxyapatite-Titanium Dioxide Nanocomposite-Based Electrode. *Food Chemistry* **2022**, *382*, 132251. https://doi.org/10.1016/J.FOODCHEM.2022.132251.

(292) Güngör, Ö.; Özgül, O.; Aksoy, B.; Okuşluk, F.; Köytepe, S. Titanium Dioxide-Multiwalled Carbon Nanotube/Polyimide Composite Film Modified Electrodes for Simultaneous Voltammetric Detection of Ascorbic Acid, Uric Acid and Dopamine as Biomarker

Molecules. *Polymer Bulletin* **2022**, 1–27. https://doi.org/10.1007/S00289-022-04077-6/FIGURE S/20.

(293) Ganchimeg, P.; Tan, W. T.; Yusof, N. A.; Goh, J. K. Voltammetric Oxidation of Ascorbic Acid Mediated by Multi-Walled Carbon Nanotubes/Titanium Dioxide Composite Modified Glassy Carbon Electrode. *Journal of Applied Sciences* **2011**, *11* (5), 848–854. https://doi.org/10.3923/JAS.2011.848.854.

(294) Li, J.; Han, T.; Wei, N.; Du, J.; Zhao, X. Three-Dimensionally Ordered Macroporous (3DOM) Gold-Nanoparticle-Doped Titanium Dioxide (GTD) Photonic Crystals Modified Electrodes for Hydrogen Peroxide Biosensor. *Biosensors and Bioelectronics* **2009**, *25* (4), 773–777. https://doi.org/10.1016/J.BIOS.2009.08.026.

(295) Halim, N. H. A.; Lee, Y. H.; Marugan, R. S. P. M.; Hashim, U. Mediatorless Impedance Studies with Titanium Dioxide Conjugated Gold Nanoparticles for Hydrogen Peroxide Detection. *Biosensors 2017, Vol. 7, Page 38* **2017**, *7* (3), 38. https://doi.org/10.3390/BIOS7030038.

(296) Hamtak, M.; Fotouhi, L.; Hosseini, M.; Reza Ganjali, M. Sensitive Nonenzymatic Electrochemiluminescence Determination of Hydrogen Peroxide in Dental Products Using a Polypyrrole/Polyluminol/Titanium Dioxide Nanocomposite. *https://doi.org/10.1080/00032719.2018.1483940* **2018**, *52* (4), 633–648. https://doi.org/10.1080/00032719.2018.1483940.

(297) Li, J.; Wang, X.; Duan, H.; Wang, Y.; Luo, C. Ultra-Sensitive Determination of Epinephrine Based on TiO2-Au Nanoclusters Supported on Reduced Graphene Oxide and Carbon Nanotube Hybrid Nanocomposites. *Materials Science and Engineering: C* **2016**, *64*, 391–398. https://doi.org/10.1016/J.MSEC.2016.04.003.

(298) Huang, X.; Wei, S.; Yao, S.; Zhang, H.; He, C.; Cao, J. Development of Molecularly Imprinted Electrochemical Sensor with Reduced Graphene Oxide and Titanium Dioxide Enhanced Performance for the Detection of Toltrazuril in Chicken Muscle and Egg. *Journal of Pharmaceutical and Biomedical Analysis* **2019**, *164*, 607–614. https://doi.org/10.1016/J.JPBA.2018.11.020.

(299) Tsele, T. P.; Adekunle, A. S.; Fayemi, O. E.; Ebenso, E. E. Electrochemical Detection of Epinephrine Using Polyaniline Nanocomposite Films Doped with TiO2 and RuO2 Nanoparticles on Multi-Walled Carbon Nanotube. *Electrochimica Acta* **2017**, *243*, 331–348. https://doi.org/10.1016/J.ELECTACTA.2017.05.031.

(300) Joseph, T.; Thomas, N. A Facile Electrochemical Sensor Based on Titanium Oxide (TiO2)/Reduced Graphene Oxide (RGO) Nano Composite Modified Carbon Paste Electrode for Sensitive Detection of Epinephrine (EP) from Ternary Mixture. *Materials Today: Proceedings* **2021**, *41*, 606–609. https://doi.org/10.1016/J.MATPR.2020.05.257.

(301) Mazloum-Ardakani, M.; Ahmadi, S. H.; Mahmoudabadi, Z. S.; Khoshroo, A.; Heydar, K. T. Electrochemical and Catalytic Investigations of Epinephrine, Acetaminophen and Folic

Acid at the Surface of Titanium Dioxide Nanoparticle-Modified Carbon Paste Electrode. *Ionics (Kiel)* **2014**, *20* (12), 1757–1765. https://doi.org/10.1007/S11581-014-1068-5/TABLES/2.

(302) Mazloum-Ardakani, M.; Khoshroo, A. Electrocatalytic Properties of Functionalized Carbon Nanotubes with Titanium Dioxide and Benzofuran Derivative/Ionic Liquid for Simultaneous Determination of Isoproterenol and Serotonin. *Electrochimica Acta* **2014**, *130*, 634–641. https://doi.org/10.1016/J.ELECTACTA.2014.03.063.

(303) Mazloum-Ardakani, M.; Khoshroo, A. Electrocatalytic Properties of Functionalized Carbon Nanotubes with Titanium Dioxide and Benzofuran Derivative/Ionic Liquid for Simultaneous Determination of Isoproterenol and Serotonin. *Electrochimica Acta* **2014**, *130*, 634–641. https://doi.org/10.1016/J.ELECTACTA.2014.03.063.

(304) Mehmandoust, M.; Çakar, S.; Özacar, M.; Erk, N. The Determination of Timolol Maleate Using Silver/Tannic Acid/Titanium Oxide Nanocomposite as an Electrochemical Sensor in Real Samples. *Electroanalysis* **2022**, *34* (7), 1150–1162. https://doi.org/10.1002/ELAN.202100363.

(305) Dehnavi, A.; Soleymanpour, A. Titanium Dioxide/Multi-Walled Carbon Nanotubes Composite Modified Pencil Graphite Sensor for Sensitive Voltammetric Determination of Propranolol in Real Samples. *Electroanalysis* **2021**, *33* (2), 355–364. https://doi.org/10.1002/ELAN.202060132.

(306) Manjunatha, K. G.; Swamy, B. E. K.; Madhuchandra, H. D.; Vishnumurthy, K. A. Synthesis, Characterization and Electrochemical Studies of Titanium Oxide Nanoparticle Modified Carbon Paste Electrode for the Determination of Paracetamol in Presence of Adrenaline. *Chemical Data Collections* **2021**, *31*, 100604. https://doi.org/10.1016/J.CDC.2020.100604.

(307) Pollap, A.; Baran, K.; Kuszewska, N.; Kochana, J. Electrochemical Sensing of Ciprofloxacin and Paracetamol in Environmental Water Using Titanium Sol Based Sensor. *Journal of Electroanalytical Chemistry* **2020**, *878*, 114574. https://doi.org/10.1016/J.JELECHEM.2020.114574.

(308) Demir, N.; Atacan, K.; Ozmen, M.; Bas, S. Z. Design of a New Electrochemical Sensing System Based on MoS 2 –TiO 2 /Reduced Graphene Oxide Nanocomposite for the Detection of Paracetamol. *New Journal of Chemistry* **2020**, *44* (27), 11759–11767. https://doi.org/10.1039/D0NJ02298E.

(309) Mazloum-Ardakani, M.; Ahmadi, S. H.; Mahmoudabadi, Z. S.; Khoshroo, A.; Heydar, K. T. Electrochemical and Catalytic Investigations of Epinephrine, Acetaminophen and Folic Acid at the Surface of Titanium Dioxide Nanoparticle-Modified Carbon Paste Electrode. *Ionics (Kiel)* **2014**, *20* (12), 1757–1765. https://doi.org/10.1007/S11581-014-1068-5/TABLES/2.

(310) Murugan, E.; Kumar, K. Fabrication of SnS/TiO 2 @GO Composite Coated Glassy Carbon Electrode for Concomitant Determination of Paracetamol, Tryptophan, and Caffeine in Pharmaceutical Formulations. *Analytical Chemistry* **2019**, *91* (9), 5667–5676. https://doi.org/10.1021/ACS.ANALCHEM.8B05531/ASSET/IMAGES/LARGE/AC-2018-055313_0014.JPEG.

(311) Killedar, L.; Ilager, D.; Shetti, N. P.; Aminabhavi, T. M.; Raghava Reddy, K. Synthesis of Ruthenium Doped Titanium Dioxide Nanoparticles for the Electrochemical Detection of Diclofenac Sodium. *Journal of Molecular Liquids* **2021**, *340*, 116891. https://doi.org/10.1016/J.MOLLIQ.2021.116891.

(312) Farghali, R. A.; Farghali, R. A.; Ahmed, R. A.; Alharthi, A. A. Synthesis and Characterization of Electrochemical Sensor Based on Polymeric /TiO2Nanocomposite Modified with Imidizolium Ionic Liquid for Determination of Diclofenac. *International Journal of Int. J. Electrochem. Sci* **2018**, *13*, 10390–10414. https://doi.org/10.20964/2018.11.16.

(313) Sadeghi, M.; Shabani-Nooshabadi, M. High Sensitive Titanium/Chitosan-Coated Nanoporous Gold Film Electrode for Electrochemical Determination of Acetaminophen in the Presence of Piroxicam. *Progress in Organic Coatings* **2021**, *151*, 106100. https://doi.org/10.1016/J.PORGCOAT.2020.106100.

(314) Song, M.; Zhang, R.; Wang, X. Nano-Titanium Dioxide Enhanced Biosensing of the Interaction of Dacarbazine with DNA and DNA Bases. *Materials Letters* **2006**, *60* (17–18), 2143–2147. https://doi.org/10.1016/J.MATLET.2005.12.100.

(315) Liu, C. sen; Li, J.; Pang, H. Metal-Organic Framework-Based Materials as an Emerging Platform for Advanced Electrochemical Sensing. *Coordination Chemistry Reviews* **2020**, *410*, 213222. https://doi.org/10.1016/J.CCR.2020.213222.

(316) Yuan, S.; Feng, L.; Wang, K.; Pang, J.; Bosch, M.; Lollar, C.; Sun, Y.; Qin, J.; Yang, X.; Zhang, P.; Wang, Q.; Zou, L.; Zhang, Y.; Zhang, L.; Fang, Y.; Li, J.; Zhou, H.-C.; Yuan, S.; Feng, L.; Wang, K.; Pang, J.; Bosch, M.; Lollar, C.; Sun, Y.; Qin, J.; Yang, X.; Zhang, P.; Wang, Q.; Zou, L.; Zhang, Y.; Zhang, L.; Fang, Y.; Li, J.; Zhou, H. Stable Metal–Organic Frameworks: Design, Synthesis, and Applications. *Advanced Materials* **2018**, *30* (37), 1704303. https://doi.org/10.1002/ADMA.201704303.

(317) Katoch, A.; Goyal, N.; Gautam, S. Applications and Advances in Coordination Cages: Metal-Organic Frameworks. *Vacuum* **2019**, *167*, 287–300. https://doi.org/10.1016/J.VACUUM.2019.03.038.

(318) Li, H.; Li, L.; Lin, R.-B.; Zhou, W.; Zhang, Z.; Xiang, S.; Chen, B. Porous Metal-Organic Frameworks for Gas Storage and Separation: Status and Challenges. *EnergyChem* **2019**, *1* (1), 100006. https://doi.org/10.1016/J.ENCHEM.2019.100006.

(319) Katoch, A.; Bhardwaj, R.; Goyal, N.; Gautam, S. Synthesis, Structural and Optical Study of Ni-Doped Metal-Organic Framework for Adsorption Based Chemical Sensor

Application. *Vacuum* **2018**, *158*, 249–256. https://doi.org/10.1016/J.VACUUM.2018.09.019.

(320) Cao, J.; Li, X.; Tian, H. Metal-Organic Framework (MOF)-Based Drug Delivery. *Current Medicinal Chemistry* **2019**, *27* (35), 5949–5969. https://doi.org/10.2174/0929867326666190618152518.

(321) Kang, Y. S.; Lu, Y.; Chen, K.; Zhao, Y.; Wang, P.; Sun, W. Y. Metal–Organic Frameworks with Catalytic Centers: From Synthesis to Catalytic Application. *Coordination Chemistry Reviews* **2019**, *378*, 262–280. https://doi.org/10.1016/J.CCR.2018.02.009.

(322) Li, D.; Kassymova, M.; Cai, X.; Zang, S. Q.; Jiang, H. L. Photocatalytic CO2 Reduction over Metal-Organic Framework-Based Materials. *Coordination Chemistry Reviews* **2020**, *412*, 213262. https://doi.org/10.1016/J.CCR.2020.213262.

(323) Zheng, S.; Guo, X.; Xue, H.; Pan, K.; Liu, C.; Pang, H. Facile One-Pot Generation of Metal Oxide/Hydroxide@metal–Organic Framework Composites: Highly Efficient Bifunctional Electrocatalysts for Overall Water Splitting. *Chemical Communications* **2019**, *55* (73), 10904–10907. https://doi.org/10.1039/C9CC06113D.

(324) Shi, L.; Zhu, X.; Liu, T.; Zhao, H.; Lan, M. Encapsulating Cu Nanoparticles into Metal-Organic Frameworks for Nonenzymatic Glucose Sensing. *Sensors and Actuators B: Chemical* **2016**, *227*, 583–590. https://doi.org/10.1016/J.SNB.2015.12.092.

(325) Kim, S. eun; Muthurasu, A. Metal-Organic Framework–Assisted Bimetallic Ni@Cu Microsphere for Enzyme-Free Electrochemical Sensing of Glucose. *Journal of Electroanalytical Chemistry* **2020**, *873*, 114356. https://doi.org/10.1016/J.JELECHEM.2020.114356.

(326) Wang, M. Q.; Zhang, Y.; Bao, S. J.; Yu, Y. N.; Ye, C. Ni(II)-Based Metal-Organic Framework Anchored on Carbon Nanotubes for Highly Sensitive Non-Enzymatic Hydrogen Peroxide Sensing. *Electrochimica Acta* **2016**, *190*, 365–370. https://doi.org/10.1016/J.ELECTACTA.2015.12.199.

(327) Wang, Q.; Yang, Y.; Gao, F.; Ni, J.; Zhang, Y.; Lin, Z. Graphene Oxide Directed One-Step Synthesis of Flowerlike Graphene@HKUST-1 for Enzyme-Free Detection of Hydrogen Peroxide in Biological Samples. *ACS Applied Materials and Interfaces* **2016**, *8* (47), 32477–32487. https://doi.org/10.1021/ACSAMI.6B11965/ASSET/IMAGES/LARGE/AM-2016-119656_0008.JPEG.

(328) Yang, J.; Ye, H.; Zhao, F.; Zeng, B. A Novel CuxO Nanoparticles@ZIF-8 Composite Derived from Core-Shell Metal-Organic Frameworks for Highly Selective Electrochemical Sensing of Hydrogen Peroxide. *ACS Applied Materials and Interfaces* **2016**, *8* (31), 20407–20414. https://doi.org/10.1021/ACSAMI.6B06436/ASSET/IMAGES/LARGE/AM-2016-06436J_0005.JPEG.

(329) Liu, L.; Liu, L.; Wang, Y.; Ye, B. C. A Novel Electrochemical Sensor Based on Bimetallic Metal–Organic Framework-Derived Porous Carbon for Detection of Uric Acid. *Talanta* **2019**, *199*, 478–484. https://doi.org/10.1016/J.TALANTA.2019.03.008.

(330) Azizpour Moallem, Q.; Beitollahi, H. Electrochemical Sensor for Simultaneous Detection of Dopamine and Uric Acid Based on a Carbon Paste Electrode Modified with Nanostructured Cu-Based Metal-Organic Frameworks. *Microchemical Journal* **2022**, *177*, 107261. https://doi.org/10.1016/J.MICROC.2022.107261.

(331) Krishnan, S.; Tong, L.; Liu, S.; Xing, R. A Mesoporous Silver-Doped TiO2-SnO2 Nanocomposite on g-C3N4 Nanosheets and Decorated with a Hierarchical Core−shell Metal-Organic Framework for Simultaneous Voltammetric Determination of Ascorbic Acid, Dopamine and Uric Acid. *Microchimica Acta* **2020**, *187* (1), 1–9. https://doi.org/10.1007/S00604-019-4045-X/TABLES/2.

(332) Huang, Z.; Zhang, L.; Cao, P.; Wang, N.; Lin, M. Electrochemical Sensing of Dopamine Using a Ni-Based Metal-Organic Framework Modified Electrode. *Ionics (Kiel)* **2021**, *27* (3), 1339–1345. https://doi.org/10.1007/S11581-020-03857-2/TABLES/2.

(333) Silva Vasconcelos, W.; da Silva, G. G.; Alves Junior, S.; dos Anjos, J. V.; da Cunha Areias, M. C. Voltammetric Determination of Captopril on a Glassy Carbon Electrode Modified with Copper Metal-Organic Framework. *Electroanalysis* **2017**, *29* (11), 2572–2578. https://doi.org/10.1002/ELAN.201700384.

(334) da Silva, D. M.; Carneiro da Cunha Areias, M. Voltammetric Detection of Captopril in a Commercial Drug Using a Gold-Copper Metal-Organic Framework Nanocomposite Modified Electrode. *Electroanalysis* **2021**, *33* (5), 1255–1263. https://doi.org/10.1002/ELAN.202060271.

(335) Rajpurohit, A. S.; Bora, D. K.; Srivastava, A. K. Simultaneous Determination of Amlodipine and Losartan Using an Iron Metal–Organic Framework/Mesoporous Carbon Nanocomposite-Modified Glassy Carbon Electrode by Differential Pulse Voltammetry. *Analytical Methods* **2018**, *10* (45), 5423–5438. https://doi.org/10.1039/C8AY01553H.

(336) Haghighi, M.; Shahlaei, M.; Bahrami, K.; Targhan, H. Reduced Graphene Oxide Supported Ti-Based Metal–Organic Framework as a Novel Electrochemical Sensor for Electro-Oxidation of Propranolol. *Journal of Materials Science: Materials in Electronics* **2021**, *32* (7), 8396–8409. https://doi.org/10.1007/S10854-021-05439-Y/TABLES/2.

(337) Liu, Y.; Peng, J.; Zhuge, W.; Huang, Q.; Xiang, G.; Wei, L. Phthalocyanine-Based Two-Dimensional Conductive Metal–Organic Framework as Electrochemical Sensor for Highly Sensitive Detection of Nifedipine. *Journal of The Electrochemical Society* **2022**, *169* (4), 046502. https://doi.org/10.1149/1945-7111/AC60EC.

(338) Yao, W.; Guo, H.; Liu, H.; Li, Q.; Xue, R.; Wu, N.; Li, L.; Wang, M.; Yang, W. Simultaneous Electrochemical Determination of Acetaminophen and Dopamine Based on Metal-Organic Framework/Multiwalled Carbon Nanotubes-Au@Ag Nanocomposites.

Journal of The Electrochemical Society **2019**, *166* (14), B1258–B1267. https://doi.org/10.1149/2.0101914JES/XML.

(339) Liang, W.; Ren, H.; Li, Y.; Qiu, H.; Ye, B. C. A Robust Electrochemical Sensing Based on Bimetallic Metal-Organic Framework Mediated Mo2C for Simultaneous Determination of Acetaminophen and Isoniazid. *Analytica Chimica Acta* **2020**, *1136*, 99–105. https://doi.org/10.1016/J.ACA.2020.08.044.

(340) Guo, L.; Hao, L.; Zhang, Y.; Yang, X.; Wang, Q.; Wang, Z.; Wang, C. Metal-Organic Framework Precursors Derived Ni-Doping Porous Carbon Spheres for Sensitive Electrochemical Detection of Acetaminophen. *Talanta* **2021**, *228*, 122228. https://doi.org/10.1016/J.TALANTA.2021.122228.

(341) Motoc, S.; Manea, F.; Iacob, A.; Martinez-Joaristi, A.; Gascon, J.; Pop, A.; Schoonman, J. Electrochemical Selective and Simultaneous Detection of Diclofenac and Ibuprofen in Aqueous Solution Using HKUST-1 Metal-Organic Framework-Carbon Nanofiber Composite Electrode. *Sensors 2016, Vol. 16, Page 1719* **2016**, *16* (10), 1719. https://doi.org/10.3390/S16101719.

(342) Dehdashtian, S.; Hashemi, B.; Chegeni, mahdieh; Aeenmehr, A. The Application of Perlite/Cobalt Oxide/Reduced Graphene Oxide (PC-RGO)/Metal Organic Framework (MOF) Composite as Electrode Modifier for Direct Sensing of Anticancer Drug Idarubicin. *IEEE Sensors Journal* **2019**, *19* (24), 11739–11745. https://doi.org/10.1109/JSEN.2019.2937400.

(343) Rong, S.; Zou, L.; Meng, L.; Yang, X.; Dai, J.; Wu, M.; Qiu, R.; Tian, Y.; Feng, X.; Ren, X.; Jia, L.; Jiang, L.; Hang, Y.; Ma, H.; Pan, H. Dual Function Metal-Organic Frameworks Based Ratiometric Electrochemical Sensor for Detection of Doxorubicin. *Analytica Chimica Acta* **2022**, *1196*, 339545. https://doi.org/10.1016/J.ACA.2022.339545.

(344) Rezvani Jalal, N.; Madrakian, T.; Afkhami, A.; Ghoorchian, A. In Situ Growth of Metal-Organic Framework HKUST-1 on Graphene Oxide Nanoribbons with High Electrochemical Sensing Performance in Imatinib Determination. *ACS Applied Materials and Interfaces* **2020**, *12* (4), 4859–4869. https://doi.org/10.1021/ACSAMI.9B18097/ASSET/IMAGES/LARGE/AM9B18097_0005.JPEG.

(345) Akhter, S.; Mohd Zain, N. K.; Shalauddin, M.; Singh, V. K.; Misnon, I. I.; Sharma, R. K.; Das, S.; Basirun, W. J.; Johan, M. R.; Jose, R. Tri-Metallic Co-Ni-Cu Based Metal Organic Framework Nanostructures for the Detection of an Anticancer Drug Nilutamide. *Sensors and Actuators A: Physical* **2021**, *325*, 112711. https://doi.org/10.1016/J.SNA.2021.112711.

(346) Florea, A.; Guo, Z.; Cristea, C.; Bessueille, F.; Vocanson, F.; Goutaland, F.; Dzyadevych, S.; Səndulescu, R.; Jaffrezic-Renault, N. Anticancer Drug Detection Using a Highly Sensitive Molecularly Imprinted Electrochemical Sensor Based on an Electropolymerized Microporous Metal Organic Framework. *Talanta* **2015**, *138*, 71–76. https://doi.org/10.1016/J.TALANTA.2015.01.013.

(347) Bhalla, N.; Jolly, P.; Formisano, N.; Estrela, P. Introduction to Biosensors. *Essays Biochem* **2016**, *60* (1), 1–8. https://doi.org/10.1042/EBC20150001.

(348) Zeng, X.; Shen, Z.; Mernaugh, R. Recombinant Antibodies and Their Use in Biosensors. *Analytical and Bioanalytical Chemistry* **2012**, *402* (10), 3027–3038. https://doi.org/10.1007/S00216-011-5569-Z/FIGURE S/8.

(349) Veloso, A. J.; Chow, A. M.; Ganesh, H. V. S.; Li, N.; Dhar, D.; Wu, D. C. H.; Mikhaylichenko, S.; Brown, I. R.; Kerman, K. Electrochemical Immunosensors for Effective Evaluation of Amyloid-Beta Modulators on Oligomeric and Fibrillar Aggregation Processes. *Analytical Chemistry* **2014**, *86* (10), 4901–4909. https://doi.org/10.1021/AC500424T/SUPPL_FILE/AC500424T_SI_001.PDF.

(350) Rama, E. C.; González-García, M. B.; Costa-García, A. Competitive Electrochemical Immunosensor for Amyloid-Beta 1-42 Detection Based on Gold Nanostructurated Screen-Printed Carbon Electrodes. *Sensors and Actuators B: Chemical* **2014**, *201*, 567–571. https://doi.org/10.1016/J.SNB.2014.05.044.

(351) Kaushik, A.; Shah, P.; Vabbina, P. K.; Jayant, R. D.; Tiwari, S.; Vashist, A.; Yndart, A.; Nair, M. A Label-Free Electrochemical Immunosensor for Beta-Amyloid Detection. *Analytical Methods* **2016**, *8* (31), 6115–6120. https://doi.org/10.1039/C6AY01910B.

(352) Abbasi, H. Y.; Tehrani, Z.; Devadoss, A.; Ali, M. M.; Moradi-Bachiller, S.; Albani, D.; Guy, O. J. Graphene Based Electrochemical Immunosensor for the Ultra-Sensitive Label Free Detection of Alzheimer's Beta Amyloid Peptides Aβ(1–42). *Nanoscale Advances* **2021**, *3* (8), 2295–2304. https://doi.org/10.1039/D0NA00801J.

(353) Carneiro, P.; Loureiro, J.; Delerue-Matos, C.; Morais, S.; do Carmo Pereira, M. Alzheimer's Disease: Development of a Sensitive Label-Free Electrochemical Immunosensor for Detection of Amyloid Beta Peptide. *Sensors and Actuators B: Chemical* **2017**, *239*, 157–165. https://doi.org/10.1016/J.SNB.2016.07.181.

(354) Palla, G.; Malecka, K.; Dehaen, W.; Radecki, J.; Radecka, H. Immunosensor Incorporating Half-Antibody Fragment for Electrochemical Monitoring of Amyloid-β Fibrils in Artificial Blood Plasma. *Bioelectrochemistry* **2021**, *137*, 107643. https://doi.org/10.1016/J.BIOELECHEM.2020.107643.

(355) Devi, R.; Gogoi, S.; Dutta, H. S.; Bordoloi, M.; Sanghi, S. K.; Khan, R. Au/NiFe 2 O 4 Nanoparticle-Decorated Graphene Oxide Nanosheets for Electrochemical Immunosensing of Amyloid Beta Peptide. *Nanoscale Advances* **2020**, *2* (1), 239–248. https://doi.org/10.1039/C9NA00578A.

(356) Miao, J.; Li, X.; Li, Y.; Dong, X.; Zhao, G.; Fang, J.; Wei, Q.; Cao, W. Dual-Signal Sandwich Electrochemical Immunosensor for Amyloid β-Protein Detection Based on Cu–Al2O3-g–C3N4–Pd and UiO-66@PANI-MB. *Analytica Chimica Acta* **2019**, *1089*, 48–55. https://doi.org/10.1016/J.ACA.2019.09.017.

(357) Razzino, C. A.; Serafín, V.; Gamella, M.; Pedrero, M.; Montero-Calle, A.; Barderas, R.; Calero, M.; Lobo, A. O.; Yáñez-Sedeño, P.; Campuzano, S.; Pingarrón, J. M. An Electrochemical Immunosensor Using Gold Nanoparticles-PAMAM-Nanostructured Screen-Printed Carbon Electrodes for Tau Protein Determination in Plasma and Brain Tissues from Alzheimer Patients. *Biosensors and Bioelectronics* **2020**, *163*, 112238. https://doi.org/10.1016/J.BIOS.2020.112238.

(358) Carlin, N.; Martic-Milne, S. Anti-Tau Antibodies Based Electrochemical Sensor for Detection of Tau Protein Biomarkers. *Journal of The Electrochemical Society* **2018**, *165* (12), G3018–G3025. https://doi.org/10.1149/2.0041812JES/XML.

(359) Yola, B. B.; Karaman, C.; Özcan, N.; Atar, N.; Polat, İ.; Yola, M. L. Electrochemical Tau Protein Immunosensor Based on MnS/GO/PANI and Magnetite-Incorporated Gold Nanoparticles. *Electroanalysis* **2022**. https://doi.org/10.1002/ELAN.202200159.

(360) Singh, V.; Krishnan, S. Voltammetric Immunosensor Assembled on Carbon-Pyrenyl Nanostructures for Clinical Diagnosis of Type of Diabetes. *Analytical Chemistry* **2015**, *87* (5), 2648–2654. https://doi.org/10.1021/ACS.ANALCHEM.5B00016/SUPPL_FILE/AC5B00016_SI_001.PDF.

(361) Li, Y.; Tian, L.; Liu, L.; Khan, M. S.; Zhao, G.; Fan, D.; Cao, W.; Wei, Q. Dual-Responsive Electrochemical Immunosensor for Detection of Insulin Based on Dual-Functional Zinc Silicate Spheres-Palladium Nanoparticles. *Talanta* **2018**, *179*, 420–425. https://doi.org/10.1016/J.TALANTA.2017.11.037.

(362) Rezaei, B.; Majidi, N.; Rahmani, H.; Khayamian, T. Electrochemical Impedimetric Immunosensor for Insulin like Growth Factor-1 Using Specific Monoclonal Antibody-Nanogold Modified Electrode. *Biosensors and Bioelectronics* **2011**, *26* (5), 2130–2134. https://doi.org/10.1016/J.BIOS.2010.09.020.

(363) Gao, Z.; Li, Y.; Zhang, C.; Zhang, S.; Li, F.; Wang, P.; Wang, H.; Wei, Q. Label-Free Electrochemical Immunosensor for Insulin Detection by High-Efficiency Synergy Strategy of Pd NPs@3D MoSx towards H2O2. *Biosensors and Bioelectronics* **2019**, *126*, 108–114. https://doi.org/10.1016/J.BIOS.2018.10.017.

(364) Zhu, C.; Yang, G.; Li, H.; Du, D.; Lin, Y. Electrochemical Sensors and Biosensors Based on Nanomaterials and Nanostructures. *Analytical Chemistry* **2015**, *87* (1), 230–249. https://doi.org/10.1021/AC5039863/ASSET/IMAGES/LARGE/AC-2014-039863_0006.JPEG.

(365) Rocchitta, G.; Spanu, A.; Babudieri, S.; Latte, G.; Madeddu, G.; Galleri, G.; Nuvoli, S.; Bagella, P.; Demartis, M. I.; Fiore, V.; Manetti, R.; Serra, P. A. Enzyme Biosensors for Biomedical Applications: Strategies for Safeguarding Analytical Performances in Biological Fluids. *Sensors (Basel)* **2016**, *16* (6). https://doi.org/10.3390/S16060780.

(366) Rocchitta, G.; Secchi, O.; Alvau, M. D.; Farina, D.; Bazzu, G.; Calia, G.; Migheli, R.; Desole, M. S.; O'Neill, R. D.; Serra, P. A. Simultaneous Telemetric Monitoring of Brain Glucose and Lactate and Motion in Freely Moving Rats. *Anal Chem* **2013**, *85* (21), 10282–10288. https://doi.org/10.1021/AC402071W.

(367) Devasenathipathy, R.; Mani, V.; Chen, S. M.; Huang, S. T.; Huang, T. T.; Lin, C. M.; Hwa, K. Y.; Chen, T. Y.; Chen, B. J. Glucose Biosensor Based on Glucose Oxidase Immobilized at Gold Nanoparticles Decorated Graphene-Carbon Nanotubes. *Enzyme Microb Technol* **2015**, *78*, 40–45. https://doi.org/10.1016/J.ENZMICTEC.2015.06.006.

(368) Saɨlam, Ö.; KIzIlkaya, B.; Uysal, H.; Dilgin, Y. Biosensing of Glucose in Flow Injection Analysis System Based on Glucose Oxidase-Quantum Dot Modified Pencil Graphite Electrode. *Talanta* **2016**, *147*, 315–321. https://doi.org/10.1016/J.TALANTA.2015.09.050.

(369) Hossain, M. F.; Park, J. Y. Plain to Point Network Reduced Graphene Oxide-Activated Carbon Composites Decorated with Platinum Nanoparticles for Urine Glucose Detection. *Sci Rep* **2016**, *6*. https://doi.org/10.1038/SREP21009.

(370) Gaffney, E. M.; Lim, K.; Minteer, S. D. Breath Biosensing: Using Electrochemical Enzymatic Sensors for Detection of Biomarkers in Human Breath. *Current Opinion in Electrochemistry* **2020**, *23*, 26–30. https://doi.org/10.1016/J.COELEC.2020.02.014.

(371) Romero, M. R.; Garay, F.; Baruzzi, A. M. Design and Optimization of a Lactate Amperometric Biosensor Based on Lactate Oxidase Cross-Linked with Polymeric Matrixes. *Sensors and Actuators B: Chemical* **2008**, *131* (2), 590–595. https://doi.org/10.1016/J.SNB.2007.12.044.

(372) Kuretake, T.; Kawahara, S.; Motooka, M.; Uno, S. An Electrochemical Gas Biosensor Based on Enzymes Immobilized on Chromatography Paper for Ethanol Vapor Detection. *Sensors 2017, Vol. 17, Page 281* **2017**, *17* (2), 281. https://doi.org/10.3390/S17020281.

(373) Adhikari, B. R.; Schraft, H.; Chen, A. A High-Performance Enzyme Entrapment Platform Facilitated by a Cationic Polymer for the Efficient Electrochemical Sensing of Ethanol. *Analyst* **2017**, *142* (14), 2595–2602. https://doi.org/10.1039/C7AN00594F.

(374) Makovos, E. B.; Liu, C. C. Measurements of Lactate Concentration Using Lactate Oxidase and an Electrochemical Oxygen Sensor. *Biotechnology and Bioengineering* **1985**, *27* (2), 167–170. https://doi.org/10.1002/BIT.260270210.

(375) Goran, J. M.; Lyon, J. L.; Stevenson, K. J. Amperometric Detection of L-Lactate Using Nitrogen-Doped Carbon Nanotubes Modified with Lactate Oxidase. *Analytical Chemistry* **2011**, *83* (21), 8123–8129. https://doi.org/10.1021/AC2016272/SUPPL_FILE/AC2016272_SI_001.PDF.

(376) Ibupoto, Z. H.; Shah, S. M. U. A.; Khun, K.; Willander, M. Electrochemical L-Lactic Acid Sensor Based on Immobilized ZnO Nanorods with Lactate Oxidase. *Sensors 2012, Vol. 12, Pages 2456-2466* **2012**, *12* (3), 2456–2466. https://doi.org/10.3390/S120302456.

(377) Teymourian, H.; Moonla, C.; Tehrani, F.; Vargas, E.; Aghavali, R.; Barfidokht, A.; Tangkuaram, T.; Mercier, P. P.; Dassau, E.; Wang, J. Microneedle-Based Detection of Ketone Bodies along with Glucose and Lactate: Toward Real-Time Continuous Interstitial Fluid Monitoring of Diabetic Ketosis and Ketoacidosis. *Analytical Chemistry* **2020**, *92* (2), 2291–2300. https://doi.org/10.1021/ACS.ANALCHEM.9B05109/ASSET/IMAGES/LARGE/AC9B05109_0004.JPEG.

(378) Rocchitta, G.; Spanu, A.; Babudieri, S.; Latte, G.; Madeddu, G.; Galleri, G.; Nuvoli, S.; Bagella, P.; Demartis, M. I.; Fiore, V.; Manetti, R.; Serra, P. A. Enzyme Biosensors for Biomedical Applications: Strategies for Safeguarding Analytical Performances in Biological Fluids. *Sensors (Basel)* **2016**, *16* (6). https://doi.org/10.3390/S16060780.

(379) Ikebukuro, K.; Kiyohara, C.; Sode, K. Electrochemical Detection of Protein Using a Double Aptamer Sandwich. *http://dx.doi.org/10.1081/AL-200035778* **2007**, *37* (14), 2901–2909. https://doi.org/10.1081/AL-200035778.

(380) Cho, E. J.; Lee, J. W.; Ellington, A. D. Applications of Aptamers as Sensors. *http://dx.doi.org/10.1146/annurev.anchem.1.031207.112851* **2009**, *2*, 241–264. https://doi.org/10.1146/ANNUREV.ANCHEM.1.031207.112851.

(381) Moreno, M. Aptasensor. *Encyclopedia of Astrobiology* **2015**, 114–115. https://doi.org/10.1007/978-3-662-44185-5_5167.

(382) Ziu, I.; Laryea, E. T.; Alashkar, F.; Wu, C. G.; Martic, S. A Dip-and-Read Optical Aptasensor for Detection of Tau Protein. *Analytical and Bioanalytical Chemistry* **2020**, *412* (5), 1193–1201. https://doi.org/10.1007/S00216-019-02350-8/TABLES/1.

(383) Tao, D.; Shui, B.; Gu, Y.; Cheng, J.; Zhang, W.; Jaffrezic-Renault, N.; Song, S.; Guo, Z. Development of a Label-Free Electrochemical Aptasensor for the Detection of Tau381 and Its Preliminary Application in AD and Non-AD Patients' Sera. *Biosensors (Basel)* **2019**, *9* (3). https://doi.org/10.3390/BIOS9030084.

(384) Negahdary, M.; Heli, H. An Ultrasensitive Electrochemical Aptasensor for Early Diagnosis of Alzheimer's Disease, Using a Fern Leaves-like Gold Nanostructure. *Talanta* **2019**, *198*, 510–517. https://doi.org/10.1016/J.TALANTA.2019.01.109.

(385) Wang, X.; Gu, X.; Li, L.; Yu, B.; Lv, L.; Chen, Q.; Xu, M. An Excellent Electrochemical Aptasensor for Amyloid-β Oligomers Based on a Triple-Helix Aptamer Switch via Target-Triggered Signal Transduction DNA Displacement Events. *Analytical and Bioanalytical Chemistry* **2021**, *413* (14), 3707–3716. https://doi.org/10.1007/S00216-021-03319-2/TABLES/3.

(386) Zhang, Y.; Figueroa-Miranda, G.; Lyu, Z.; Zafiu, C.; Willbold, D.; Offenhäusser, A.; Mayer, D. Monitoring Amyloid-β Proteins Aggregation Based on Label-Free Aptasensor. *Sensors and Actuators B: Chemical* **2019**, *288*, 535–542. https://doi.org/10.1016/J.SNB.2019.03.049.

(387) Yin, L.; Wang, Y.; Tan, R.; Li, H.; Tu, Y. Determination of β-Amyloid Oligomer Using Electrochemiluminescent Aptasensor with Signal Enhancement by AuNP/MOF Nanocomposite. *Microchimica Acta* **2021**, *188* (2), 1–8. https://doi.org/10.1007/S00604-021-04710-7/TABLES/2.

(388) Zhou, Y.; Li, C.; Li, X.; Zhu, X.; Ye, B.; Xu, M. A Sensitive Aptasensor for the Detection of β-Amyloid Oligomers Based on Metal–Organic Frameworks as Electrochemical Signal Probes. *Analytical Methods* **2018**, *10* (36), 4430–4437. https://doi.org/10.1039/C8AY00736E.

(389) Liu, D.; Lu, X.; Yang, Y.; Zhai, Y.; Zhang, J.; Li, L. A Novel Fluorescent Aptasensor for the Highly Sensitive and Selective Detection of Cardiac Troponin I Based on a Graphene Oxide Platform. *Analytical and Bioanalytical Chemistry* **2018**, *410* (18), 4285–4291. https://doi.org/10.1007/S00216-018-1076-9/TABLES/2.

(390) Jo, H.; Gu, H.; Jeon, W.; Youn, H.; Her, J.; Kim, S. K.; Lee, J.; Shin, J. H.; Ban, C. Electrochemical Aptasensor of Cardiac Troponin i for the Early Diagnosis of Acute Myocardial Infarction. *Analytical Chemistry* **2015**, *87* (19), 9869–9875. https://doi.org/10.1021/ACS.ANALCHEM.5B02312/ASSET/IMAGES/LARGE/AC-2015-02312K_0006.JPEG.

(391) Lopa, N. S.; Rahman, M. M.; Ahmed, F.; Ryu, T.; Sutradhar, S. C.; Lei, J.; Kim, J.; Kim, D. H.; Lee, Y. H.; Kim, W. Simple, Low-Cost, Sensitive and Label-Free Aptasensor for the Detection of Cardiac Troponin I Based on a Gold Nanoparticles Modified Titanium Foil. *Biosensors and Bioelectronics* **2019**, *126*, 381–388. https://doi.org/10.1016/J.BIOS.2018.11.012.

(392) Mi, X.; Li, H.; Tan, R.; Tu, Y. Dual-Modular Aptasensor for Detection of Cardiac Troponin i Based on Mesoporous Silica Films by Electrochemiluminescence/Electrochemical Impedance Spectroscopy. *Analytical Chemistry* **2020**, *92* (21), 14640–14647. https://doi.org/10.1021/ACS.ANALCHEM.0C03130/ASSET/IMAGES/LARGE/AC0C03130_0006.JPEG.

(393) Han, Y.; Su, X.; Fan, L.; Liu, Z.; Guo, Y. Electrochemical Aptasensor for Sensitive Detection of Cardiac Troponin I Based on CuNWs/MoS2/RGO Nanocomposite. *Microchemical Journal* **2021**, *169*, 106598. https://doi.org/10.1016/J.MICROC.2021.106598.

(394) Hui, R.; Kim, D.-J.; Tabrizi, M. A.; Acedo, P. Highly Sensitive RNA-Based Electrochemical Aptasensor for the Determination of C-Reactive Protein Using Carbon Nanofiber-Chitosan Modified Screen-Printed Electrode. *Nanomaterials 2022, Vol. 12, Page 415* **2022**, *12* (3), 415. https://doi.org/10.3390/NANO12030415.

(395) Mahyari, M.; Hooshmand, S. E.; Sepahvand, H.; Gholami, S.; Rezayan, A. H.; Zarei, M. A. Gold Nanoparticles Anchored onto Covalent Poly Deep Eutectic Solvent Functionalized Graphene: An Electrochemical Aptasensor for the Detection of C-Reactive Protein.

Materials Chemistry and Physics **2021**, *269*, 124730. https://doi.org/10.1016/J.MATCHEMPHYS.2021.124730.

(396) Wang, J.; Guo, J.; Zhang, J.; Zhang, W.; Zhang, Y. RNA Aptamer-Based Electrochemical Aptasensor for C-Reactive Protein Detection Using Functionalized Silica Microspheres as Immunoprobes. *Biosensors and Bioelectronics* **2017**, *95*, 100–105. https://doi.org/10.1016/J.BIOS.2017.04.014.

(397) Jarczewska, M.; Rębiś, J.; Górski, Ł.; Malinowska, E. Development of DNA Aptamer-Based Sensor for Electrochemical Detection of C-Reactive Protein. *Talanta* **2018**, *189*, 45–54. https://doi.org/10.1016/J.TALANTA.2018.06.035.

(398) Wang, Y.; Sun, S.; Luo, J.; Xiong, Y.; Ming, T.; Liu, J.; Ma, Y.; Yan, S.; Yang, Y.; Yang, Z.; Reboud, J.; Yin, H.; Cooper, J. M.; Cai, X. Low Sample Volume Origami-Paper-Based Graphene-Modified Aptasensors for Label-Free Electrochemical Detection of Cancer Biomarker-EGFR. *Microsystems & Nanoengineering 2020 6:1* **2020**, *6* (1), 1–9. https://doi.org/10.1038/s41378-020-0146-2.

(399) Song, Y.; He, L.; Chen, K.; Wang, M.; Yang, L.; He, L.; Guo, C.; Jia, Q.; Zhang, Z. Quantification of EGFR and EGFR-Overexpressed Cancer Cells Based on Carbon Dots@bimetallic CuCo Prussian Blue Analogue. *RSC Advances* **2020**, *10* (47), 28355–28364. https://doi.org/10.1039/D0RA01439G.

(400) Guo, C.; Li, Z.; Duan, F.; Zhang, Z.; Marchetti, F.; Du, M. Semiconducting Cu x Ni 3−x (Hexahydroxytriphenylene) 2 Framework for Electrochemical Aptasensing of C6 Glioma Cells and Epidermal Growth Factor Receptor. *Journal of Materials Chemistry B* **2020**, *8* (43), 9951–9960. https://doi.org/10.1039/D0TB01910K.

(401) Derikvand, H.; Roushani, M.; Abbasi, A. R.; Derikvand, Z.; Azadbakht, A. Design of Folding-Based Impedimetric Aptasensor for Determination of the Nonsteroidal Anti-Inflammatory Drug. *Analytical Biochemistry* **2016**, *513*, 77–86. https://doi.org/10.1016/J.AB.2016.06.013.

(402) Du, Y.; Chen, C.; Yin, J.; Li, B.; Zhou, M.; Dong, S.; Wang, E. Solid-State Probe Based Electrochemical Aptasensor for Cocaine: A Potentially Convenient, Sensitive, Repeatable, and Integrated Sensing Platform for Drugs. *Analytical Chemistry* **2010**, *82* (4), 1556–1563. https://doi.org/10.1021/AC902566U/ASSET/IMAGES/LARGE/AC-2009-02566U_0001.JPEG.

(403) Chen, D.; Yao, D.; Xie, C.; Liu, D. Development of an Aptasensor for Electrochemical Detection of Tetracycline. *Food Control* **2014**, *42*, 109–115. https://doi.org/10.1016/J.FOODCONT.2014.01.018.

(404) Dauphin-Ducharme, P.; Yang, K.; Arroyo-Currás, N.; Ploense, K. L.; Zhang, Y.; Gerson, J.; Kurnik, M.; Kippin, T. E.; Stojanovic, M. N.; Plaxco, K. W. Electrochemical Aptamer-Based Sensors for Improved Therapeutic Drug Monitoring and High-Precision, Feedback-

Controlled Drug Delivery. *ACS Sens* **2019**, *4* (10), 2832. https://doi.org/10.1021/ACSSENSORS.9B01616.

(405) Guan, Y.; Xia, M.; Wang, X.; Cao, W.; Marchetti, A. Water-Based Preparation of Nano-Sized NH2-MIL-53(Al) Frameworks for Enhanced Dye Removal. *Inorganica Chimica Acta* **2019**, *484*, 180–184. https://doi.org/10.1016/j.ica.2018.09.036.

(406) Vogel, A. I. *Text Book of Practical Organic Chemistry, ELBS and Longman. P London*; 1978.

(407) Shahat, A.; Elsalam, S. A.; Herrero-Martínez, J. M.; Simó-Alfonso, E. F.; Ramis-Ramos, G. Optical Recognition and Removal of Hg(II) Using a New Self-Chemosensor Based on a Modified Amino-Functionalized Al-MOF. *Sensors and Actuators, B: Chemical* **2017**, *253*, 164–172. https://doi.org/10.1016/j.snb.2017.06.125.

(408) Liu, L.; Tai, X.; Zhou, X.; Liu, L. Synthesis, Post-Modification and Catalytic Properties of Metal-Organic Framework NH2-MIL-53(Al). *Chemical Research in Chinese Universities* **2017**, *33* (2), 231–238. https://doi.org/10.1007/s40242-017-6420-7.

(409) Häfeli, U. O.; Ensom, M. H. H.; Kiang, T. K. L.; Stoeber, B.; Chua, B. A.; Pudek, M.; Schmitt, V. Comparison of Vancomycin Concentrations in Blood and Interstitial Fl Uid: A Possible Model for Less Invasive Therapeutic Drug Monitoring. *Clinical Chemistry and Laboratory Medicine* **2011**, *49* (12), 2123–2125. https://doi.org/10.1515/CCLM.2011.727.

(410) Samant, P. P.; Niedzwiecki, M. M.; Raviele, N.; Tran, V.; Mena-Lapaix, J.; Walker, D. I.; Felner, E. I.; Jones, D. P.; Miller, G. W.; Prausnitz, M. R. Sampling Interstitial Fluid from Human Skin Using a Microneedle Patch. *Sci Transl Med* **2020**, *12* (571). https://doi.org/10.1126/SCITRANSLMED.AAW0285.

(411) Kim, S.; Lee, M. S.; Yang, H. S.; Jung, J. H. Enhanced Extraction of Skin Interstitial Fluid Using a 3D Printed Device Enabling Tilted Microneedle Penetration. *Scientific Reports 2021 11:1* **2021**, *11* (1), 1–11. https://doi.org/10.1038/s41598-021-93235-3.

(412) Xiao, Y.; Lai, R. Y.; Plaxco, K. W. Preparation of Electrode-Immobilized, Redox-Modified Oligonucleotides for Electrochemical DNA and Aptamer-Based Sensing. *Nature Protocols 2007 2:11* **2007**, *2* (11), 2875–2880. https://doi.org/10.1038/nprot.2007.413.

(413) Dauphin-Ducharme, P.; Yang, K.; Arroyo-Currás, N.; Ploense, K. L.; Zhang, Y.; Gerson, J.; Kurnik, M.; Kippin, T. E.; Stojanovic, M. N.; Plaxco, K. W. Electrochemical Aptamer-Based Sensors for Improved Therapeutic Drug Monitoring and High-Precision, Feedback-Controlled Drug Delivery. *ACS Sens* **2019**, *4* (10), 2832–2837. https://doi.org/10.1021/ACSSENSORS.9B01616.

(414) Vigil, J. A.; Lambert, T. N.; Duay, J.; Delker, C. J.; Beechem, T. E.; Swartzentruber, B. S. Nanoscale Carbon Modified α-MnO2Nanowires: Highly Active and Stable Oxygen Reduction Electrocatalysts with Low Carbon Content. *ACS Applied Materials and Interfaces* **2018**, *10* (2), 2040–2050. https://doi.org/10.1021/acsami.7b16576.

(415) Ghosh, D.; Bhandari, S.; Khastgir, D. Synthesis of MnO2 Nanoparticles and Their Effective Utilization as UV Protectors for Outdoor High Voltage Polymeric Insulators Used in Power Transmission Lines. *Physical Chemistry Chemical Physics* **2016**, *18* (48), 32876–32890. https://doi.org/10.1039/C6CP06611A.

(416) Compton, R. G.; Banks, C. E. Cyclic Voltammetry at Macroelectrodes. In *Understanding Voltammetry*; WORLD SCIENTIFIC, 2007; pp 107–151. https://doi.org/10.1142/9789812779809_0004.

(417) Compton, R. G.; Banks, C. E. Cyclic Voltammetry at Macroelectrodes. In *Understanding Voltammetry*; WORLD SCIENTIFIC, 2007; pp 107–151. https://doi.org/10.1142/9789812779809_0004.

(418) Mohammed, M. A.; Attia, A. K.; Elwy, H. M. Electrochemical Sensor Based on Multiwalled Carbon Nanotube, Alizarine Red S and Chitosan for Simultaneous Determination of Oxomemazine Hydrochloride, Paracetamol and Guaifenesin. *Electroanalysis* **2017**, *29* (2), 506–513. https://doi.org/10.1002/elan.201600311.

(419) Ziyatdinova, G.; Ziganshina, E.; Budnikov, H. Electrochemical Reduction and Quantification of Menadione in Sodium Dodecyl Sulfate Micellar Media. *Journal of Solid State Electrochemistry* **2013**, *17* (10), 2679–2685. https://doi.org/10.1007/s10008-013-2170-8.

(420) Laviron, E.; Roullier, L.; Degrand, C. A Multilayer Model for the Study of Space Distributed Redox Modified Electrodes. *Journal of Electroanalytical Chemistry and Interfacial Electrochemistry* **1980**, *112* (1), 11–23. https://doi.org/10.1016/S0022-0728(80)80003-9.

(421) Laviron, E.; Roullier, L.; Degrand, C. A Multilayer Model for the Study of Space Distributed Redox Modified Electrodes. *Journal of Electroanalytical Chemistry and Interfacial Electrochemistry* **1980**, *112* (1), 11–23. https://doi.org/10.1016/S0022-0728(80)80003-9.

(422) Karimi-Maleh, H.; Tahernejad-Javazmi, F.; Ensafi, A. A.; Moradi, R.; Mallakpour, S.; Beitollahi, H. A High Sensitive Biosensor Based on FePt/CNTs Nanocomposite/N-(4-Hydroxyphenyl)-3,5-Dinitrobenzamide Modified Carbon Paste Electrode for Simultaneous Determination of Glutathione and Piroxicam. *Biosensors and Bioelectronics* **2014**, *60*, 1–7. https://doi.org/10.1016/j.bios.2014.03.055.

(423) Pan, T.-M.; Mondal, S. Structural Properties and Sensing Characteristics of Sensing Materials. In *Comprehensive Materials Processing*; Elsevier, 2014; Vol. 13, pp 179–203. https://doi.org/10.1016/B978-0-08-096532-1.01306-6.

(424) Samui, A.; Sahu, S. K. One-Pot Synthesis of Microporous Nanoscale Metal Organic Frameworks Conjugated with Laccase as a Promising Biocatalyst. *New Journal of Chemistry* **2018**, *42* (6), 4192–4200. https://doi.org/10.1039/c7nj03619a.

(425) Cheng, X.; Zhang, A.; Hou, K.; Liu, M.; Wang, Y.; Song, C.; Zhang, G.; Guo, X. Size- and Morphology-Controlled NH2-MIL-53(Al) Prepared in DMF-Water Mixed Solvents. *Dalton Transactions* **2013**, *42* (37), 13698–13705. https://doi.org/10.1039/c3dt51322j.

(426) Sánchez-Sánchez, M.; Getachew, N.; Díaz, K.; Díaz-García, M.; Chebude, Y.; Díaz, I. Synthesis of Metal-Organic Frameworks in Water at Room Temperature: Salts as Linker Sources. *Green Chemistry* **2015**, *17* (3), 1500–1509. https://doi.org/10.1039/c4gc01861c.

(427) Zhang, L.; Hu, Y. H. A Systematic Investigation of Decomposition of Nano Zn4O(C 8H4O4)3 Metal-Organic Framework. *Journal of Physical Chemistry C* **2010**, *114* (6), 2566–2572. https://doi.org/10.1021/jp911043r.

(428) Chang, L.; Li, J.; Duan, X.; Liu, W. Porous Carbon Derived from Metal-Organic Framework (MOF) for Capacitive Deionization Electrode. *Electrochimica Acta* **2015**, *176*, 956–964. https://doi.org/10.1016/j.electacta.2015.07.130.

(429) Zhang, W.; Wu, Z. Y.; Jiang, H. L.; Yu, S. H. Nanowire-Directed Templating Synthesis of Metal-Organic Framework Nanofibers and Their Derived Porous Doped Carbon Nanofibers for Enhanced Electrocatalysis. *Journal of the American Chemical Society* **2014**, *136* (41), 14385–14388. https://doi.org/10.1021/ja5084128.

(430) Liu, R. L.; Ji, W. J.; He, T.; Zhang, Z. Q.; Zhang, J.; Dang, F. Q. Fabrication of Nitrogen-Doped Hierarchically Porous Carbons through a Hybrid Dual-Template Route for CO2 Capture and Haemoperfusion. *Carbon* **2014**, *76*, 84–95. https://doi.org/10.1016/j.carbon.2014.04.052.

(431) Lu, T.; Zhang, L.; Sun, M.; Deng, D.; Su, Y.; Lv, Y. Amino-Functionalized Metal-Organic Frameworks Nanoplates-Based Energy Transfer Probe for Highly Selective Fluorescence Detection of Free Chlorine. *Analytical Chemistry* **2016**, *88* (6), 3413–3420. https://doi.org/10.1021/acs.analchem.6b00253.

(432) Ahmadi Feijani, E.; Tavasoli, A.; Mahdavi, H. Improving Gas Separation Performance of Poly(Vinylidene Fluoride) Based Mixed Matrix Membranes Containing Metal-Organic Frameworks by Chemical Modification. *Industrial and Engineering Chemistry Research* **2015**, *54* (48), 12124–12134. https://doi.org/10.1021/acs.iecr.5b02549.

Publications out of this work

1- **MA Saleh**, MM Taha, MA Mohamed, NK Allam, A novel and ultrasensitive electrochemical biosensor based on MnO_2-V_2O_5 nanorods for the detection of the antiplatelet prodrug agent Cilostazol in pharmaceutical formulations, *Microchemical Journal* 164, 105946, 2021.

2- **MA Saleh**, MA Mohamed, A Shahat, NK Allam, Sensitive determination of SARS-COV-2 and anti-hepatitis C virus agent Velpatasvir enabled by novel metal-organic frameworks, *ACS Omega* 6 (40), 26791-26798, 2021.

3- VCM-Tracker apta-sensor in the detection of vancomycin, in preparation.